NASA CONTRACTOR REPORT

NASA CR-589

NASA CR-589

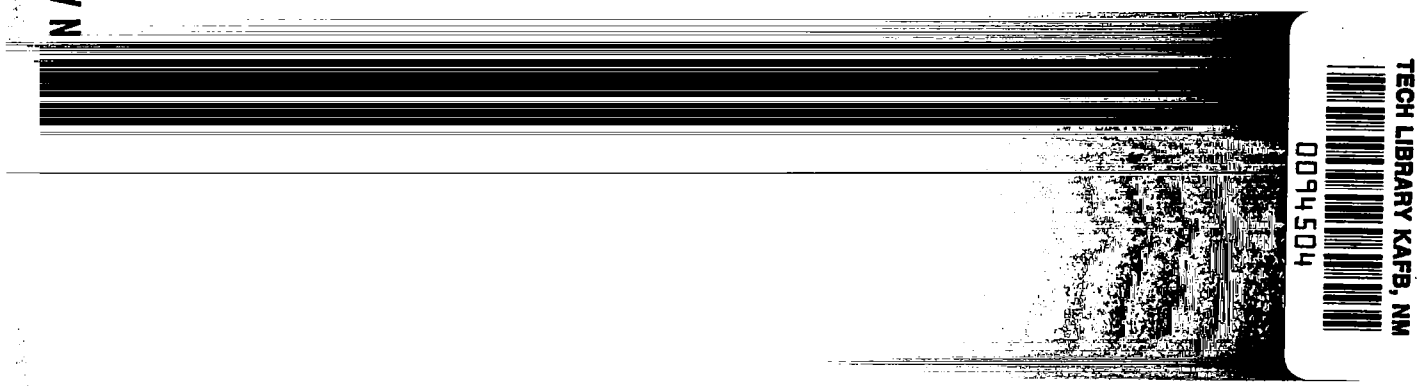

LOW-FREQUENCY NOISE REDUCTION OF SPACECRAFT STRUCTURES

by R. H. Lyon, C. W. Dietrich, E. E. Ungar, R. W. Pyle, Jr., and R. E. Apfel

Prepared by
BOLT BERANEK AND NEWMAN, INC.
Cambridge, Mass.
for Langley Research Center

NATIONAL AERONAUTICS AND SPACE ADMINISTRATION • WASHINGTON, D. C. • SEPTEMBER 1966

NASA CR-589

LOW-FREQUENCY NOISE REDUCTION OF SPACECRAFT STRUCTURES

By R. H. Lyon, C. W. Dietrich, E. E. Ungar,
R. W. Pyle, Jr., and R. E. Apfel

Prepared under Contract No. NAS 1-4687 by
BOLT BERANEK AND NEWMAN, INC.
Cambridge, Mass.

for Langley Research Center

NATIONAL AERONAUTICS AND SPACE ADMINISTRATION

For sale by the Clearinghouse for Federal Scientific and Technical Information
Springfield, Virginia 22151 – Price $3.25

TABLE OF CONTENTS

TABLE OF CONTENTS (Continued)

TABLE OF CONTENTS (Continued)

TABLE OF CONTENTS (Continued)

LIST OF ILLUSTRATIONS

LIST OF TABLES

LOW-FREQUENCY NOISE REDUCTION OF SPACECRAFT STRUCTURES

By R. H. Lyon, C. W. Dietrich, E. E. Ungar,
R. W. Pyle, Jr., and R. E. Apfel

Bolt Beranek and Newman Inc.
Cambridge, Massachusetts

INTRODUCTION AND SUMMARY

There is an increasing interest on the part of engineers in the low-frequency sound transmission of aerospace structures. The prime reason for this interest is the discovery that low-frequency noise may have physiological and psychoacoustic effects on man (Refs. 1, 2), coupled with the fact that large space vehicles are exposed to high levels of low-frequency acoustic excitation from large rockets and from aerodynamic excitation (Ref. 3). Quite aside from spacecraft applications, low-frequency noise reduction considerations are important also in the design of enclosures for the acoustic isolation of small and compact electromechanical and electronic assemblies.

The sound-isolation effectiveness of an enclosure for a given space is described by the noise reduction (NR) of the enclosure. The NR of an enclosure is defined as the difference between the sound pressure levels which occur at a position in the enclosed space with and without use of the enclosure (Ref. 4). The noise reduction (NR) should not be confused with the transmission loss (TL), which is defined as the difference between the acoustic power level incident on one side of an infinite panel and that transmitted through the panel. The NR depends on TL and acoustic properties of the receiving space.

Traditional acoustical engineering calculations of an enclosure NR are based on the TL of its walls. However, the TL concept does not apply for panels whose dimensions are smaller than half an acoustic wavelength. At low frequencies the acoustic half-wavelengths become so large that they exceed typical major spacecraft structural dimensions; this "low-frequency" range is the one considered in this report. The exact extent of this frequency range clearly depends on the size of the structure being considered. For the Apollo Command Module, with a typical dimension of the order of 10 ft, the low-frequency range encompasses all frequencies below 55 Hz. For an electronic subassembly having a dimension of the order of 1 ft, this frequency range extends from 0 to 550 Hz.

Low-frequency sound may cause discomfort or injury to personnel or may interfere with task-performance efficiency. Such

adverse effects appear to be associated with resonances of the human body between 2 and 20 Hz (Ref. 1). Some of these resonances are primarily due to body masses vibrating in combination with muscular and tendon compliances. Others involve acoustical elements, e.g. the diaphragm may resonate with air cavities within the lungs. Criteria for vibration and sound environments for trained astronauts have not been fully established at this time.

Probably the most important adverse psychoacoustic effect of the low-frequency noise is its interference with speech communication (Ref. 2). The entire acoustic spectrum contributes to speech interference, of course, but low frequencies present a particular problem since they are not attenuated effectively by ear phones or head sets. Recent psychoacoustic studies have also shown that high-level low-frequency noise can have a masking effect over a frequency range which extends several octaves above the noise range. This effect is known as "the upward spread of masking."

The purpose of this report is to present an approach for predicting the low-frequency noise transmission of spacecraft structures on the basis of a series of experimental and theoretical analyses. The approach developed here should aid the spacecraft designer in estimating the low-frequency noise reductions he may expect, and should provide him with sufficient insight into the processes of sound transmission at low frequencies to enable him to avoid spacecraft designs which will have ineffective acoustic isolation at low frequencies.

Many of the calculations and discussions in this report refer to an acoustic model based on the Apollo Command Module (CM). This module is typical of spacecraft that have been built at this time, and it is likely to be a prototype for others to come. However, this report is not just concerned with the Apollo CM; rather, it is concerned with developing a more general, widely applicable acoustical model of axisymmetric spacecraft of single- and double-shell configuration.

Data to be obtained from laboratory and flight tests of the Apollo CM should prove extremely useful for further study of many of the notions presented in this report. One may hope for some agreement between the field data and the analyses presented here. However, for any process as complex as sound and vibration transmission in complicated built-up structures, the process of model development must be a continuing one. Although many aspects of the models developed here are expected to shed light on the test data, the test data are equally expected to suggest modifications and changes in the models.

In the following pages we build up a conceptual model of low-frequency sound transmission from a series of theoretical and experimental analyses, which are intended to emphasize various aspects of the structural and acoustic behavior of a spacecraft. In the analysis of model systems, some of which differ in appearance quite markedly from the actual spacecraft, we shall indicate the limitations of each model (i.e., the deviations of the ideal model behavior from the actual), and we shall indicate the additional effects that must then be included. Such a model development procedure is fairly commonly used in architectural acoustics, where many competing effects can occur; it is of the utmost inportance for the engineer to know over what frequency range and under what conditions each of the competing effects will have dominance.

It is also an important function of this report to suggest acoustic models and experiments for testing some of the concepts developed. Choices of such models (some of which may be similar to small-scale models which we have studied) are indicated when appropriate, based on experience gained in our test program.

Some of the major conclusions of this study are summarized below:

1. Over an important portion of the low-frequency range the noise transmission of shells is controlled by their "quasi-static" acoustic compliance. The compliance of curved and dome-like shells tends to be membrane-controlled. Such shells tend to be much stiffer than flat shell segments, the compliance of which is primarily flexure-controlled.

2. Acoustic resonances of contained spaces may occur. In the Apollo Command Module the space between the two shells is narrow and long (as measured between the two poles of symmetry). It thus permits the occurrence of a low-frequency resonance which may drastically reduce the low-frequency NR.

3. When flat segments are present, and when curved shells are interrupted by relatively stiff reinforcing members, volume-displacing structural resonances will occur at low frequencies. These resonances will be deleterious to noise reduction since they produce "volume pumping" and compression of the contained volume. The space-craft design should avoid volume-pumping structural resonances below the frequency of the first acoustic mode of the contained volume.

4. Acoustical resonances between the venting system and the structural and acoustic elements of the spacecraft may occur. The importance of such a resonance in affecting NR will depend on the resonance frequency and on the efficiency with which the exterior low-frequency sound field can "drive" the resonance.

5. Well-thought-out experimental analysis is an important adjunct to any acoustical-structural problem. This study shows that this is particularly true in the case of sound transmission, where many competing effects are present. Noise reduction experiments which are regarded only as proof tests, or as verification of a theoretical analysis, will not be so effective or so illuminating as tests which attempt to sort out competing vibrational and acoustical effects and to rank-order these in importance for the particular structure under consideration.

SYMBOLS

a	radius of flat plate or circular section
A	effective cross-section area
$A(s)$	$w(s)\ r(s)$
A_c	effective cross-section area of cylindrical shell
A_p	partition area
A_s, A_ϕ	surface areas of incremental volume
$A_s^{(p)}$	projected area of volume element in plane perpendicular to $\hat{e}_s$
$A_\phi^{(p)}$	projected area of volume element in plane perpendicular to $\hat{e}_\phi$
A_t	surface area of receiving room
B_c	$\sin \beta L + \sinh \beta L$
B_s	$\cos \beta L + \cosh \beta L$
c	sound speed of acoustic medium
c_j	slope
c_ℓ	longitudinal wave speed in shell material
C	acoustic compliance of shell
$C(s)$	acoustic compliance per unit length of outer shell
C_{con}	acoustic compliance of contained volume
C_{eq}	equivalent compliance of inner shell
C_s	acoustic compliance of contained volume within shell
C_1, C_2	constants evaluated from boundary conditions
C_{11}	acoustic compliance of interspace volume 11
C_{12}	acoustic compliance of interspace volume 12

$C_{1,2}$, C_3, $C_{4,6}$, C_5, C_7, C_8, C_9	acoustic compliances of numbered sections in Figs. 13, 14 and 15
CM	command module
CSM	command service module
d_j	intercept
D	flexural rigidity
D_c	flexural rigidity of cylindrical shell
D_p	flexural rigidity of plate
$\hat{e}_s, \hat{e}_\phi$	unit vectors
E	Young's modulus
E_c	Young's modulus for cylindrical shell
f	frequency
f_a	lowest acoustical resonance frequency
f_m	modal resonance frequency
f_r	resonance frequency
f_{min}	lowest structural resonance frequency
f_{ring}	ring frequency
F	displaced volume multiplying factor

h sum of core thickness and average skin thickness

H { homogeneous panel or skin thickness $\left(\frac{\text{surface density}}{\rho_p}\right)$ / "flare" factor of slender horn

I_o height of spherical segment

I moment of inertia of cross section

$J_m(kr)$ Bessel function of order m

k acoustic wave number at frequency ω

k_n wavenumber of horn resonance

k_m individual mount stiffness

ℓ length of tube

L length of cylindrical shell

L_{p_i} pressure level in i^{th} room

n circumferential mode number

n_c constant dependent on shell properties

n_p constant dependent on plate properties

M { edge moment, Eq. (38) / acoustic mass, Eq. (93)

M_s structural mass

M_{spar} mass of spar

M_v acoustic mass of vent

N number of shell sections

N_θ membrane forces in direction perpendicular to plane of Fig. 9

N_ϕ	membrane forces in v direction of Fig. 9
NR	noise reduction
NR_i	noise reduction of inner shell
NR_o	noise reduction of outer shell
NR_{tot}	total noise reduction of inner and outer shells
n_R	modal density of exterior acoustic space
n_s	shell modal density
p	applied pressure
p(s)	pressure at s
p(x)	solution of Webster's horn equation
$\langle p^2 \rangle$	mean-square pressure in frequency band $\Delta\omega$
p_i	internal pressure increase with applied pressure p_o
p_i^2	mean-square reverberant acoustic pressure in i^{th} room
$\langle p_i^2 \rangle$	mean-square pressure of internal sound field in frequency band $\Delta\omega$
p_{ref}	2×10^{-4} microbar
p_o	externally applied pressure, Eq. (8) peak pressure produced at s=o, Eq. (150)
$\langle p_o^2 \rangle$	mean-square pressure of external sound field in frequency band $\Delta\omega$
p_1	pressure at point just external to CM
p_2	pressure produced at test point
p_{11}	pressure in interspace volume 11
p_{12}	pressure in interior volume 12

P	panel perimeter
$\overline{P}$	mean pressure
P_{con}	gas pressure in shell before application of external pressure
P_o	average (static) pressure
P_R	amplitude of reflected pressure wave
q_c	constant dependent on shell properties
q_p	constant dependent on plate properties
Q	shell tension load
r	radial distance from center of flat plate
$r(s)$	distance from polar axis to any point on Γ
$r(x)$	circular cross section of slender horn
r_o	initial radius of slender horn
r_1	radius of curvature of surface at A
R	room constant = $A_t\ \alpha(1-\alpha)^{-1}$, Eq. (6) radius of sphere, Eq. (25)
s	lineal dimension along line of constant ϕ
S	surface area of spherical segment linear coordinate of upper pole of median surface
S_1	inner shell
S_2	outer shell
$S(x)$	horn cross sectional area
SPL	sound pressure level, also L_p

t	average skin thickness
t_c	core thickness
t_{fA}	thickness of inner skin
t_{fB}	thickness of outer skin
T	shape factor for slender horn
$\overline{T}$	mean kinetic energy
TL	transmission loss
u	radial shell deformation
$\vec{u}$	flow velocity
u_s, u_ϕ	components of flow velocity
U	{ratio defined by Eq. (38) volume velocity of shell mode
U_o	volume velocity of source
U_1	volume velocity emitted through outer shell due to source U_o
v	tangential displacement of shell
$\langle v^2 \rangle$	square of kinetic energy of resonator
v_{ic}	point motion of attachment to inner cylinder
v_s	source velocity
V	{volume decrease of shell with applied pressure p_o volume of air space, Eq. (94)
$\overline{V}$	mean potential energy
ΔV	incremental potential energy
V_{con}	volume contained in closed shell
V_e	volume of exterior acoustic space

V_m volume displaced by circular plate due only to edge moment M

V_s volume contained within shell

V_{11} {volume displacement of end-capped shell due to membrane action, Eq. (16)
interspace volume, Fig. 20

V_{12} {volume displacement of end-capped shell due to axial loads, Eq. (17)
volume contained within inner shell, Fig. 20

w radial displacement of shell

w(s) distance between A and B on line perpendicular to Γ

x_c station locations on command module

x_1, x_2 circumferential and axial coordinates on supported shell

y displacement of circular flat plate

y_a, y_b coordinates of cone frustra

Z impedance

Z_{ic} point impedance of inner cylinder

Z_{oc} point impedance of shell

Z_{spar} translational impedance of spar

α — absorption coefficient, Eq. (4)
α — $\beta L/2$, Eq. (43)
α — parameter to be optimized, Eq. (145)

β — relative stiffness parameter defined by Eq. (20)
β — $\sqrt{\frac{\kappa}{a}}$, Eq. (88)

β_c relative stiffness parameter defined by Eq. (20) for cylindrical shell

γ ratio of specific heats of enclosed gas

Γ median surface

δ radial expansion including reduction by Poisson effect

δ_f asymptotic frequency separation between structural modes

δ_o radial expansion neglecting reduction by Poisson effect

Δ increment

ϵ_θ polar strain

ϵ_ϕ circumferential strain

η loss factor

η_{rad} radiation loss factor

η_s structural loss factor

θ_c, θ_p plate edge rotations (Fig. 12)

θ_m structural modal energy

θ_R modal energy of sound field

κ radius of gyration of shell cross section

λ_c acoustic wavelength at critical frequency

ν	Poisson's ratio
ν_c	Poisson's ratio for cylindrical shell
ν_p	Poisson's ratio for plate
ν_s	ratio of modal density of shell segment to that of flat plate of equal area
π	3.1416
Π_{inc}	acoustic power incident on partition
Π_{rad}	radiated power from simple source
Π_{trans}	acoustic power transmitted by partition
ρ	density of acoustic medium
ρ_o	ambient density
ρ_p	density of panel material
σ	axial wavenumber
$\Delta\tau$	incremental volume
ϕ	azimuthal angle
ψ	flexural mode shape
$\psi(s)$	pressure mode-shape function
ψ_s	cone flexure parameter
ψ_o, ψ_1	test functions for interspace mode shape
ω	frequency
ω_c	panel acoustic critical frequency
$\Delta\omega$	frequency band including resonance frequency of structural mode

CHAPTER I

A REVIEW OF THE "CLASSICAL" NOISE REDUCTION

INTRODUCTION

Classical noise reduction (NR) calculations and concepts are reviewed in the present chapter in order to summarize the important principles involved, to point out their ranges of applicability, and to indicate why and to what extent these classical methods are generally inappropriate for dealing with the low-frequency noise reduction of spacecraft.

The problems of predicting and designing for noise reduction in buildings are treated routinely by architectural acousticians, and much related information is available. However, virtually all of the available and commonly employed data and concepts pertain only to frequencies which are "high" in the present context. The engineer concerned with spacecraft NR must be aware of the limitations of the classical approach. (As a by-product, understanding the classical approach should give him a better insight into parallel approaches taken in this report.)

"CLASSICAL ANALYSIS"

Noise reduction is usually defined (in architectural acoustics) in terms of an arrangement like that sketched in Fig. 1, in which two acoustic spaces, a "source room" and a

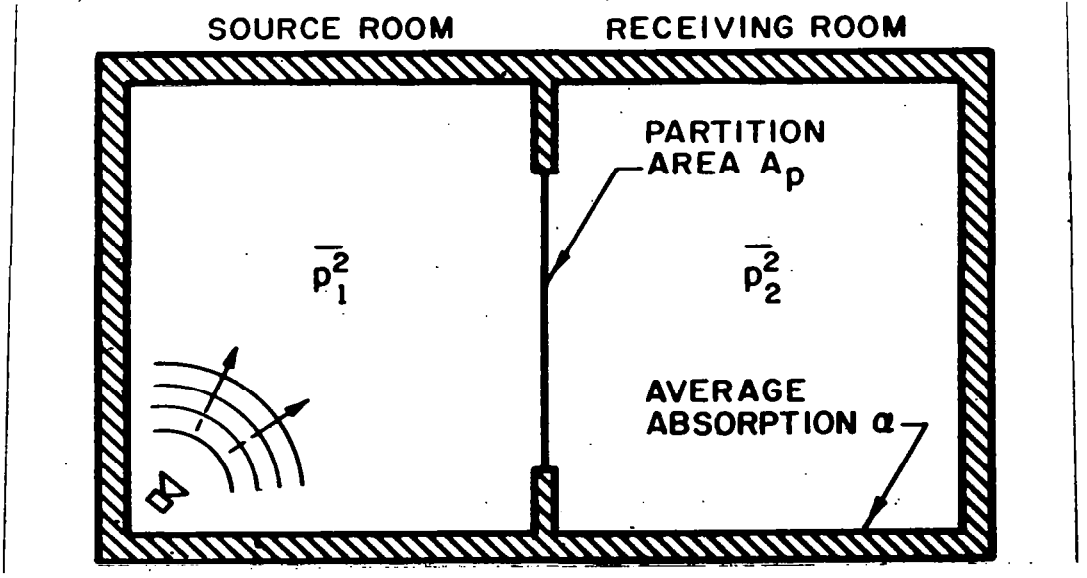

FIG. 1 TYPICAL SET-UP FOR MEASURING NR OF PARTITION

"receiving room," are separated by a partition. If a sound generator in the source room produces a (space and time average) mean-square reverberant acoustic pressure p_1^2, corresponding to which there results a mean-square pressure p_2^2 in the receiving room, then the noise reduction of the partition is defined as

$$NR = 10 \log p_1^2/p_2^2 = L_{p_1} - L_{p_2} \tag{1}$$

where $L_{p_i} \equiv 10 \log p_i^2/p_{ref}^2$, with $p_{ref} \equiv 2 \times 10^{-4}$ microbar denoting the pressure level in the i^{th} room. Clearly, the "NR afforded by the partition" depends not only on the partition, but also on the acoustic absorption properties of the receiving room.

An alternate common definition of NR equates the noise reduction to the "insertion loss" of the partition, i.e., to the reduction in the pressure level in the receiving room resulting from inserting the partition between the previously unseparated rooms. One may note that Eq. (1) defines NR as the pressure level difference between a source and a receiving space, with the partition in place, whereas the insertion loss is the difference in the pressure levels observed in the receiving space before and after insertion of the partition. The insertion loss of a partition depends on the test conditions imposed on the source, in addition to partition and receiving room parameters. (For example, holding p_1^2 constant generally results in different source and receiver pressures than holding power radiated by the source constant.)

One generally attempts to separate the contributions to NR made by the partitions from those made by the test rooms. To this purpose one defines the transmission loss (TL) of a partition as

$$TL \equiv 10 \log (\Pi_{inc}/\Pi_{trans}) \tag{2}$$

where Π_{inc} denotes the acoustic power incident on the partition from the source room side and Π_{trans} that radiated by the partition into the receiving room.

If the acoustic field in the source room is reverberant,

then Π_{inc} is related to the space-time mean-square pressure p_1^2 as (Ref. 5)

$$\Pi_{inc} = A_p \, p_1^2/4\rho c \tag{3}$$

where A_p denotes the partition area and ρc the characteristic impedance of the medium.

If one assumes that a fraction α of the power Π_{trans} transmitted through the partition into the receiving room is absorbed at the walls of this room, then the power supplied to the reverberant acoustic field in this room is $(1 - \alpha)\Pi_{trans}$ In the steady state, this power input must be equal to the power loss, which is equal to α times the power incident on the receiving room walls. The power balance equation for the receiving room is therefore

$$\Pi_{trans} \, (1 - \alpha) = \alpha A_t \, p_2^2/4\rho c \tag{4}$$

where A_t denotes the surface area of the receiving room. By combining Eqs. (1) through (4) one may obtain

$$NR = TL + 10 \log R/A_p \tag{5}$$

where

$$R = A_t \, \alpha \, (1 - \alpha)^{-1} \tag{6}$$

is called the "room constant" of the receiving room and accounts for the acoustic properties of that space.

The absorption coefficient α is usually a fairly slowly varying function of frequency, tending to be rather low at low frequencies and increasing with frequency. In designing experimental test chambers one usually tries to keep α below 10 to 20%; for spaces where good wall absorption is desired (such as broadcast studios) α values between 50 and 90% may be attained over the frequency range from 500 Hz to 2 kHz.

The transmission loss of a partition structure is often presumed to depend only on such "intrinsic" structural

properties of the partition as mass per unit area, flexural rigidity, and loss factor. (Thus, it is often presumed that by doubling the partition area one doubles the transmitted power.) This assumption is obviously invalid under conditions where the measured TL is affected by panel geometry or area, e.g., at low frequencies (for panel wavelengths of the order of a partition edge dimension) where room and partition modes, as well as acoustic diffraction effects, affect the transmitted power.

The characteristic behavior of the transmission loss of panels, as indicated in Fig. 2, may be explained in terms of the flexural motions of the panel and of how these act in the radiation of sound. Because of the spatial distribution of exciting pressures over the panel, virtually all flexural modes are excited by the incident sound, even if this sound has energy in only a narrow band of frequencies. But all of the modes will not respond the same; modes whose resonance frequencies fall within the excitation band will, of course, tend to respond more strongly than others. In addition, all modes do not radiate sound with the same efficiency. Modes whose spatial scales (wavelengths) are greater than an acoustic wavelength radiate sound relatively efficiently, whereas modes with shorter wavelengths radiate poorly (only about 1 to 10% as well as long-wavelength modes).

In studying the transmission loss of a given panel in a given frequency range, one thus looks first for modes which are both highly excited (i.e., resonant) and good radiators (i.e., which have spatial scales that exceed the acoustic wavelength). Such modes dominate sound transmission, if they occur. Such modes must have their resonances above the "critical frequency" (discussed below), and obviously can be excited resonantly only by excitation frequencies above this critical frequency.

The critical frequency of a panel is that frequency at which the acoustic wavelength in the surrounding medium is equal to the wavelength of flexural waves on the panel. Recalling that the ratio of the acoustic to the flexural wavelength decreases with increasing frequency (since the acoustic wavelength is inversely proportional to frequency, whereas the panel flexural wavelength varies inversely as the square-root of frequency), one notes that modes which resonate above the critical frequency have wavelengths shorter than acoustic waves at the modal resonance frequency, and hence radiate well when vibrating resonantly. On the other hand, modes whose resonances fall below the critical frequency radiate poorly when vibrating at resonance.

For an excitation frequency band which lies well above the panel fundamental resonances, but below the panel critical frequency, it often occurs that the sound transmission is

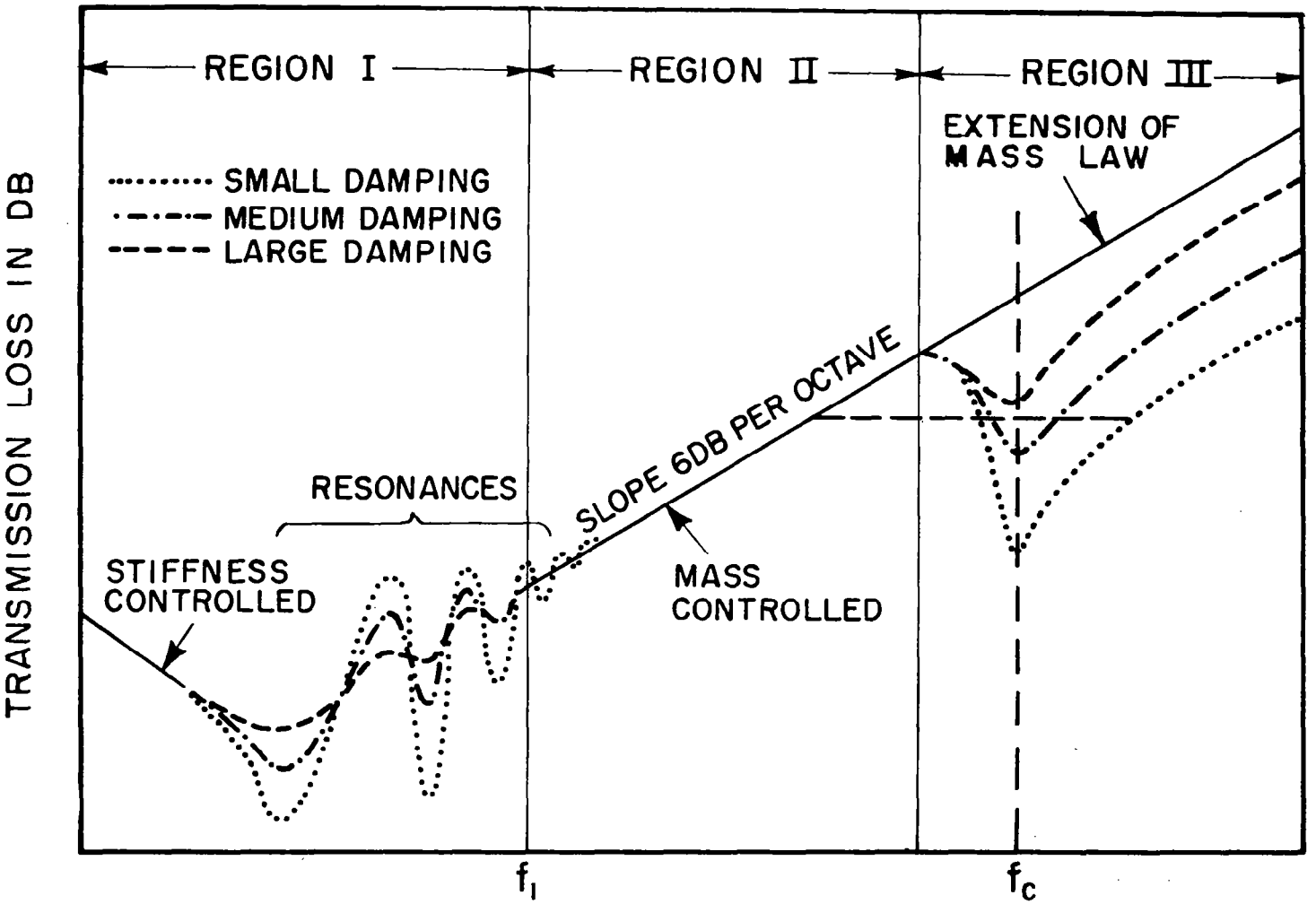

FIG. 2 TYPICAL FORM OF TL CURVE FOR A PARTITION (FROM BERANEK)

dominated by the many low-frequency, long-wavelength modes. Although these modes are excited at frequencies which are much higher than their resonances, their wavelengths may be longer than the acoustic, so that they may radiate much better than the few resonantly excited modes (which may have wavelengths shorter than the acoustic). The responses of modes excited above their resonances are "mass-controlled," that is, like the high-frequency response of a spring-mass system, the modal responses here are inversely proportional to the square of frequency and to modal mass. In building partitions it often turns out that such mass-controlled modes dominate the transmission loss behavior in the frequency regions of interest; this fact is the basis for the famous "mass law" (Ref. 6) of TL (which corresponds to that portion of Fig. 2 which rises at 20 dB/decade). Also, the dominance of the sound radiated by nonresonantly excited modes explains why the addition of structural damping (which essentially reduces only the responses of the resonantly excited modes) has no appreciable effect on the TL of building panels even though such damping may result in marked reductions of the panel vibration levels.

Now it is useful to return once more to Fig. 2, and to interpret the characteristics of a typical transmission loss curve in terms of the previously discussed phenomena. Below the lowest panel resonance, the panel response (and thus the NR) are controlled only by the panel stiffness. The portion of the TL curve below the lowest panel resonance is fictious, since the TL concept does not apply for such frequencies. At and near the few lowest panel resonances the TL is small, because of the large responses of the resonant modes. At somewhat higher frequencies, up to about an octave below the coincidence frequency, one encounters the "mass-law" region, in which sound radiated from nonresonantly vibrating but well-radiating modes dominates transmission.

Above the critical frequency the transmission loss decreases once more (from mass-law conditions) because of the presence of resonantly responding modes with good radiation efficiencies. Because of the effect of damping on resonant response, increased damping generally results in increased TL in this region. The "plateau," shown dashed in the figure, may serve as an engineering approximation to the average behavior in this frequency range. An increase at a rate somewhat greater than 20 dB/decade is usually observed at frequencies about an octave above the critical, as modal resonances are increasingly damped out and the curve tends back to the mass-law line.

CONCLUSIONS

It has been pointed out that classical NR and TL calculations apply only under certain conditions, most of which generally do not apply to spacecraft exposed to low-frequency sound. For example, calculation of the NR by Eq. (5) involves the assumption of diffuse reverberant acoustic fields in the source and receiving spaces, and such fields can be achieved only if very many acoustic modes of these spaces participate in the energy exchange process. Hence, this assumption cannot be met at or below the lowest-order acoustic resonances of a spacecraft "receiving space."

Similarly, classical (particularly mass-law) TL calculations apply only for panels whose dimensions encompass more than a few acoustic wavelengths. Hence these calculations are inappropriate for low frequencies, at which the acoustic wavelengths are longer than, or of the order of, typical spacecraft or spacecraft panel dimensions.

CHAPTER II

A SURVEY OF LOW-FREQUENCY PRESSURE TRANSMISSION

INTRODUCTION

In the previous chapter the "classical" procedures for calculating noise reduction in architectural acoustics were reviewed, and the conclusion was reached that these methods are inappropriate for the calculation of spacecraft noise reduction at low frequencies. The purpose of this chapter is to suggest the major mechanical and acoustical mechanisms that control the transmission of sound pressure in spacecraft at low frequencies, and to outline the calculations necessary for the prediction of low-frequency NR.

We consider first some previous experiments and theoretical calculations of pressure transmission in a small rectangular box with flexible walls. It is found that particular types of acoustical-mechanical behavior occur in specific frequency ranges and that similar kinds of behavior will also occur in spacecraft. However, the geometry and structure of spacecraft in general, and of the Apollo CM in particular, differ in important ways from those of the box, and therefore the analysis of spacecraft must be done differently. This review of previous studies and consideration of spacecraft configurations suggests a series of specific technical analyses required for the prediction of low-frequency pressure transmission; these analyses will be described in the subsequent chapters.

THEORETICAL ANALYSIS

A theoretical analysis of a rectangular box consisting of five rigid walls and a single flexible wall has been carried out previously (Ref. 7). The box is considered to be exposed to a reverberant sound field, and its noise reduction is defined as the difference in sound pressure levels at a given position within the box, with and without the presence of the box. The acoustical critical frequency of the flexible panel is assumed to be an octave or so above the lowest acoustic resonance frequency of the enclosed space, and the lowest panel resonance frequency is taken to be lower than this resonance frequency.

At frequencies above the first acoustic resonance both the panel and the contained acoustic space are resonant, and the panel transmission can be described as outlined in Chapter I. The calculated noise reduction of a particular box for these frequencies is shown in the "high-frequency" range of Fig. 3. Results of calculations for forced (mass-law) transmission

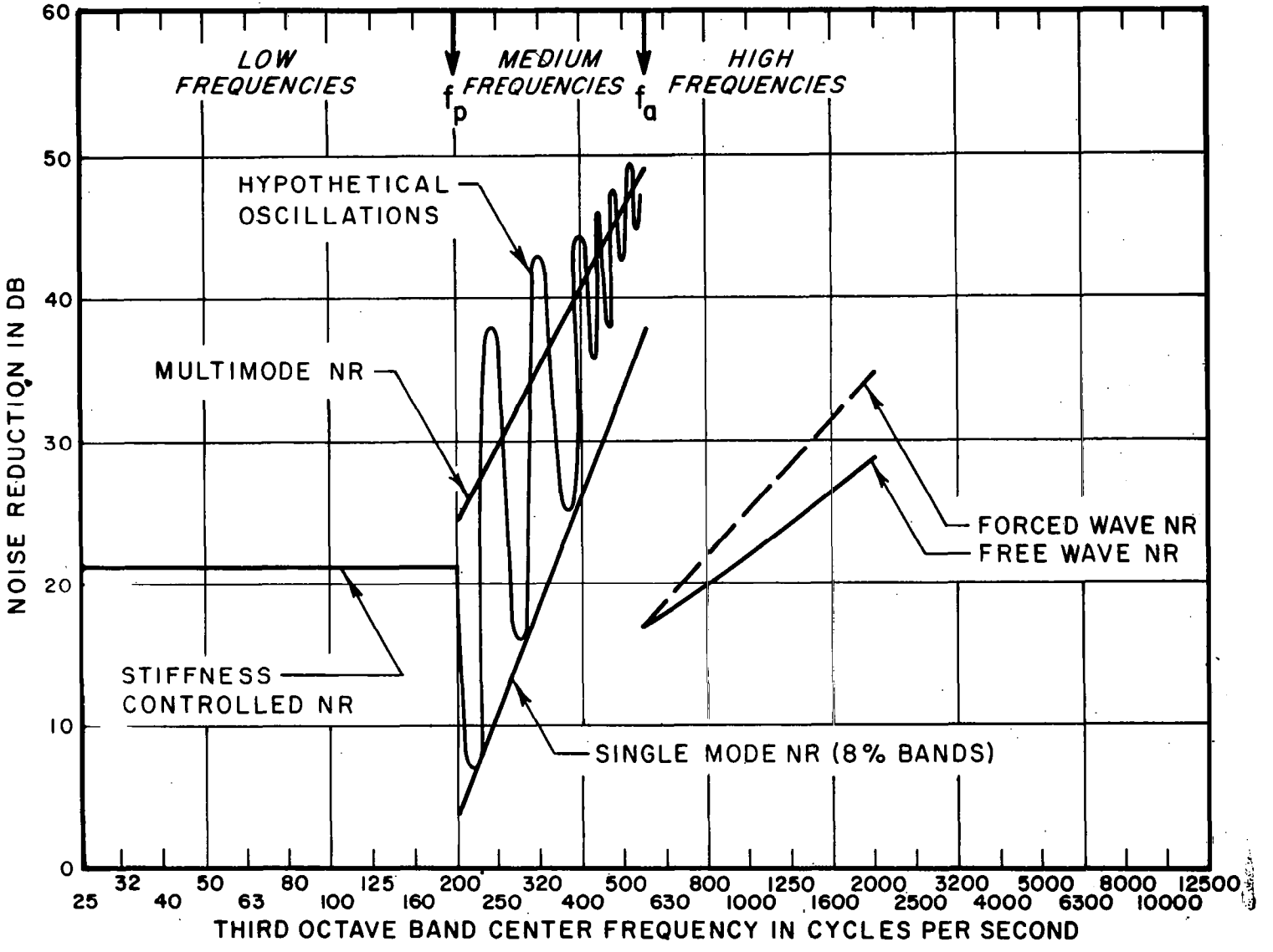

FIG. 3 THEORETICAL NOISE REDUCTION OF BOX WITH SINGLE FLEXIBLE WALL (FROM REF. 7)

and resonant-panel transmission are also given. For this panel, it occurred that the resonant transmission dominated. In this "high-frequency" range, therefore, both the structural loss factor of the panel and the acoustical absorption coefficient of the contained volume affect the level of noise reduction that is obtained.

Below the first acoustic resonance the enclosed volume behaves like an acoustic compliance, and pressure is generated within the volume principally due to net volume displacement produced by the flexible panel. If there are structural resonances in this frequency range (and there were for the box considered in the reference), then some of these resonances may cause volume displacement, and therefore increased pressure, over limited frequency intervals. The frequency interval over which volume-pumping resonances will occur is termed the "mid-frequency" range in Fig. 3. This interval usually lies between the first mechanical resonance of the panel and the lowest acoustic resonance frequency. In the "mid-frequency" range the noise reduction is dependent upon the structural damping of the panel, but is independent of the acoustic absorption within the enclosed cavity. The only parameters of an acoustic cavity which are important in this range are those which affect the cavity's acoustic compliance, namely, cavity volume and gas pressure.

If relatively wide bandwidths of acoustic noise are used, then several volume-displacing modes of the panel may contribute simultaneously to the noise reduction. With this assumption, the NR is bandwidth-independent, and behaves as the "average" NR shown in Fig. 3. If the bandwidth is narrower, then only one volume-displacing mode at a time may be excited, and the NR may be bandwidth-dependent. The result of the calculation for a particular box for an 8% band (one-tenth octave) is shown in Fig. 3 labelled "single-mode NR, 8% bands."

Finally, at frequencies below the lowest mechanical and acoustical resonances, both the flexible panel and the contained volume behave as mechanical compliances. The mechanical compliance of the panel depends on its size, flexural rigidity and mounting. The acoustic compliance depends on the contained volume and pressure. It is essentially the ratio of these compliances that controls the low-frequency pressure transmission. The panel compliance in the reference was computed for both simply supported and clamped-edge mountings. These two arrangements result in panel compliances differing by a factor of 3 for this configuration. The noise reduction in this "low-frequency" regime is independent of frequency, structural damping, and acoustic absorption. The results of the calculation of NR for this regime are also shown in Fig. 3.

We define as the "low-frequency" region of NR for spacecraft essentially the combination of the "low-frequency" and the "mid-frequency" regimes (i.e., the frequency range below the first acoustic resonance of the contained volume).

A theoretical and experimental analysis of the NR of boxes with six flexible sides has been presented by Eichler (Ref. 8). The general form of Eichler's calculations is similar to that above, but the treatment is refined by accounting for the energy reradiated by the enclosed cavity back into the surrounding room. Some experimental results for an aluminum box of 1/16 in. wall thickness, having dimensions roughly 12 x 18 x 16 in., are shown in Fig. 4. The lowest mechanical resonance occurs at approximately 60 Hz and the first acoustic resonance of the interior volume at about 400 Hz. Displayed, along with the experimental data, are the theoretical results for noise reduction in the compliance-controlled "low-frequency" region, and "average" and "lower bound" calculations for the noise reduction in the "mid-frequency" region.

CONCLUSIONS

Although the rectangular box is geometrically and dynamically different from the axisymmetric spacecraft shapes to which we are accustomed, the analyses described above shed considerable light on the procedures one should follow in developing a theory of NR. Clearly, the acoustic compliance for slow pressure changes on the shell is an important parameter in predicting its very-low-frequency noise reduction. Accordingly, in Chapter III general procedures will be outlined for determining the quasi-static acoustic compliance of axisymmetric shells.

The axial symmetry of spacecraft has another important kinematic result. It requires that mode shape functions be of the form of $\sin m\phi$, $\cos m\phi$, where ϕ is the azimuthal angle and m is an integer. For $m \neq 0$ the net volume displacement of such modes vanishes. For $m = 0$ the membrane stresses in the shell cause these modes to resonate at comparatively high frequencies, well above the range of "low frequencies" which are of concern in this report.

In the discussion of box NR the important effect of volume-pumping structural modes on the noise reduction was clearly established. The absence of low-frequency volume-pumping modes for homogeneous axisymmetric shells can cause the quasi-static compliance-controlled NR behavior to extend up to the first acoustical resonance. However, volume-pumping structural resonances may be introduced by major structural discontinuities or shell elements that allow $m = 0$ resonances to occur in the low-frequency region. We shall see the effect of this behavior in subsequent discussions.

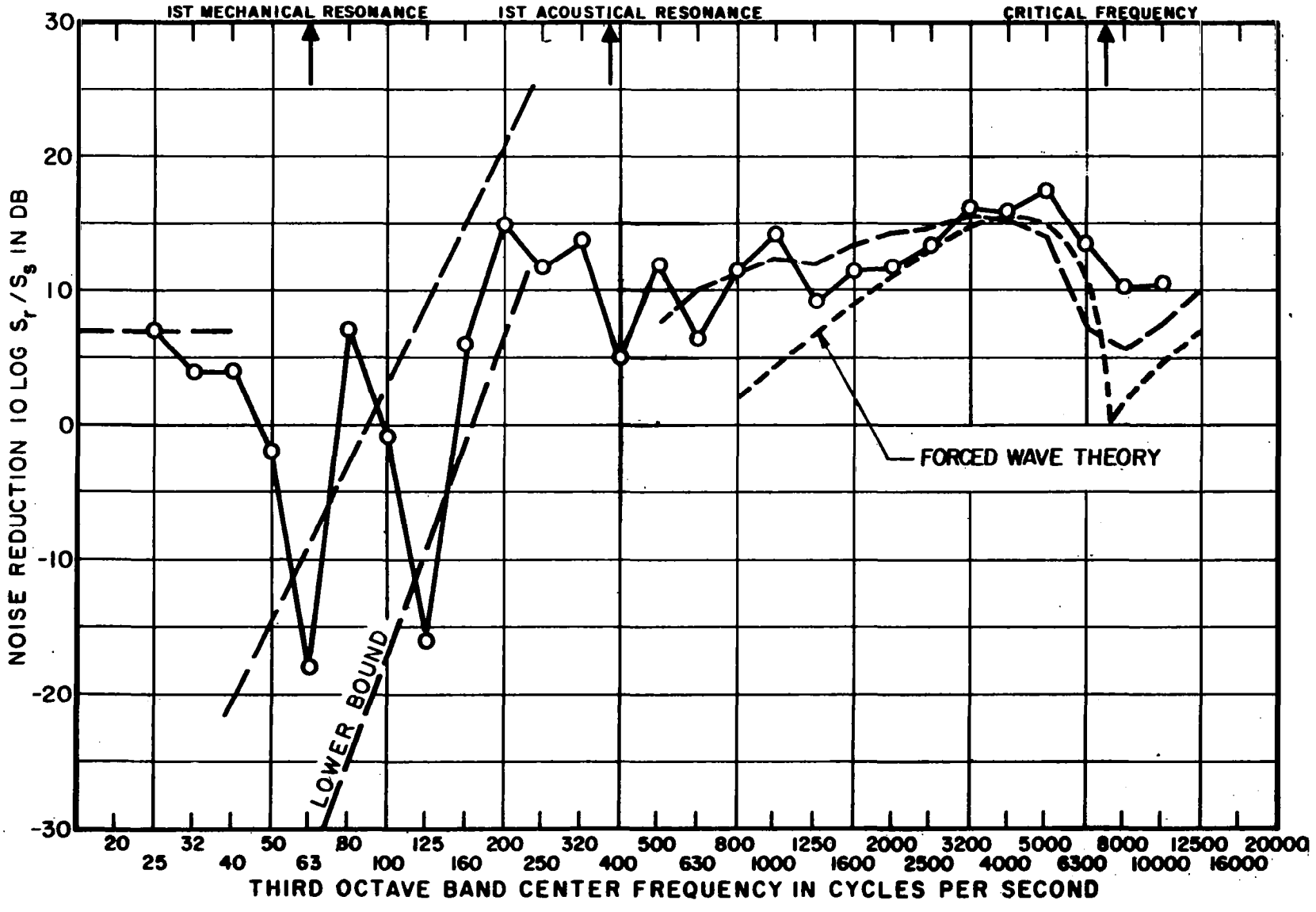

FIG. 4 EXPERIMENTAL AND CALCULATED NR OF 12 X 16 X 18 IN. BOX, 1/16 IN. ALUMINUM WALLS (FROM REF 8)

The studies of rectangular boxes do not anticipate some important acoustical and mechanical effects in spacecraft like the Apollo CM. While some of these effects are related to the double-shell construction of the Apollo CM, others are due to the venting system, the use of segmented sandwich construction, and the effects of materials and equipment that are placed within the acoustic cavities. In subsequent chapters we deal with many of these effects in some detail and try to recommend remedial actions that can be taken when such effects cause abnormally low noise reduction in important frequency ranges.

CHAPTER III

QUASI-STATIC PRESSURE TRANSMISSION OF SHELLS

INTRODUCTION

In this chapter we develop the theory of pressure transmission in single- and double-walled elastic shells. The noise reduction (NR) can be expressed in terms of shell and volume compliances.

A major portion of this chapter is devoted to finding the acoustic compliance of elastic shells, and the proper combination of these compliance elements to represent a spacecraft structure. We discuss the principal forms of elastic deformations of the shell — membrane and flexural — and the conditions under which one or the other of these will dominate.

With this background, it is then possible to predict the low-frequency NR of spacecraft. The chapter is concluded with a calculation of the NR of the Apollo Command Module (CM).

PRELIMINARY REMARKS

Noise Reduction

If a pressure p_o is applied quasi-statically on the exterior of a closed gas-filled elastic shell structure which is initially at equilibrium, then this structure will deflect, the volume V_{con} contained in it will decrease by an amount V, and the pressure in the interior will increase by an amount p_i. According to the well-known ideal gas laws, this pressure increase is related to the volume change according to (Ref. 9)

$$\frac{p_i}{P_{con}} = \gamma \frac{V}{V_{con}} \; ; \; V = p_i \frac{V_{con}}{\gamma P_{con}} \equiv p_i \, C_{con} \tag{7}$$

where P_{con} denotes the pressure of the gas contained within the structure before the external pressure is applied and γ denotes the ratio of specific heats of the enclosed gas (Ref. 10). C_{con} is defined as the acoustic compliance of the contained volume.

The volume decrease V of an elastic shell is proportional to the applied pressure difference. Thus one may write

$$V = C(p_o - p_i) \tag{8}$$

where C is defined as the acoustic compliance of the shell and may be computed from its elastic deformations.

By combining Eqs. (7) and (8) one finds that the ratio of p_o to p_i can be expressed as

$$\frac{p_o}{p_i} = 1 + \frac{C_{con}}{C} \tag{9}$$

If p_o denotes the amplitude of the (slowly) oscillating external acoustic pressure, and p_i a similar interior quantity, then the NR (in decibels) will be $20 \log_{10}(p_o/p_i)$. For low-frequency acoustic excitation (i.e., below any volume-displacing structural resonance), one may calculate the NR of a given elastic shell from

$$NR(dB) = 20 \log \left[1 + \frac{C_{con}}{C} \right] \tag{10}$$

These results can also be obtained from the equivalent circuit representation in Fig. 5. In this diagram, volume velocity is the "flow" quantity, and pressure fluctuation (relative to ambient) is the "drop" or "potential" quantity.

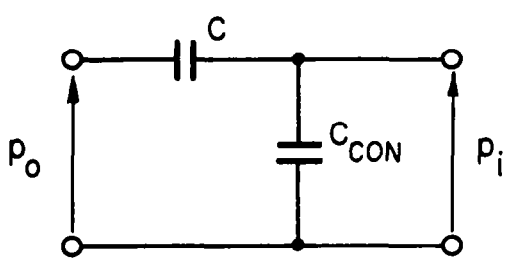

FIG. 5 EQUIVALENT ACOUSTICAL CIRCUIT FOR SHELL-ENCLOSED VOLUME

The subsequent sections deal in some detail with the analytical determination of the volume/pressure proportionality factor C for some often-encountered shells and for some composites typical of the Apollo Command Module.

Plate and Shell Rigidities

The subsequent analyses are carried out in relatively general terms, involving only the dimensions of the shells and their extensional and flexural rigidities (per unit length). The results are thus equally applicable to homogeneous and to sandwich shells.

The extensional stiffness of a shell per unit edge length may be expressed as EA, where E denotes Young's modulus and A the cross-section area (per unit edge length) that is effective in extension. Thus, with the dimensions defined in Fig. 6,

$$A \approx \begin{cases} H & \text{for homogeneous shells} \\ 2t & \text{for sandwich shells} \end{cases} \qquad (11)$$

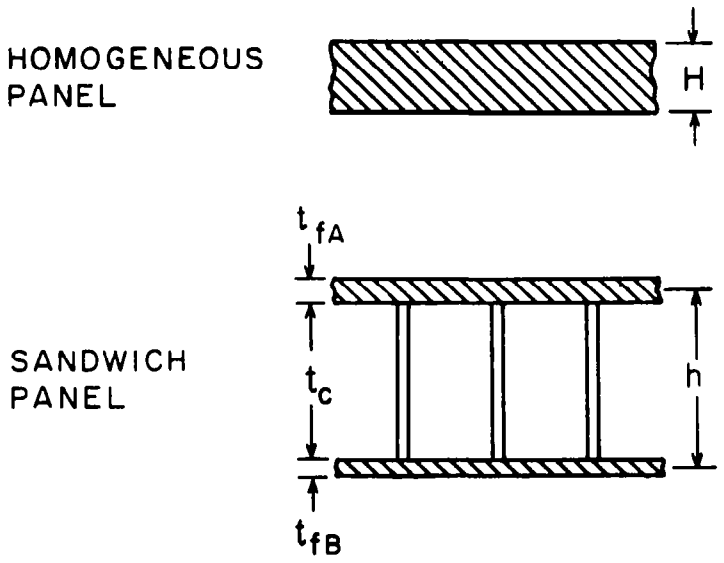

FIG. 6 SHELL SECTION DIMENSIONS

Here, and subsequently, the core of a sandwich structure is assumed to have no extensional stiffness and to be extremely rigid in shear.

The flexural rigidity D = EI of a plate or shell is found from computing the moment of inertia of the cross section, I,

$$D \approx \begin{cases} EH^3/12 & \text{for homogeneous shells} \\ Eh^2/2 & \text{for sandwich shells}^* \end{cases} \qquad (12)$$

where the cross-section dimensions H, h, t again are those defined in Fig. 6.

CIRCULAR PLATES

The displacement y of an elastic circular flat plate simply supported at its circumference and subject to a uniform pressure p (Fig. 7) is given by the expression (Ref. 11)

$$y = \frac{a^4 p}{64D}\left[\frac{5+\nu}{1+\nu} - 2\left(\frac{3+\nu}{1+\nu}\right)\left(\frac{r}{a}\right)^2 + \left(\frac{r}{a}\right)^4\right] \qquad (13)$$

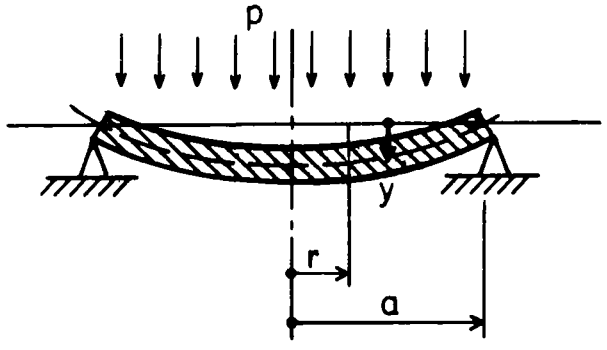

FIG. 7 FLAT CIRCULAR PLATE WITH SIMPLY SUPPORTED CIRCUMFERENCE SUBJECT TO UNIFORM PRESSURE

*This expression is valid only for shells with nearly equal skins. A much more complex (but easily derived) relation holds for shells with grossly unequal skins.

The displacement of a similar plate, but with clamped circumference, is given by (Ref. 12)

$$y = \frac{a^4 p}{64D}\left[1 - \left(\frac{r}{a}\right)^2\right]^2 \qquad (14)$$

From these expressions one may readily calculate the volume V displaced as the plate deforms:

$$V = 2\pi \int_0^a y(r)\, r\, dr$$

One finds

$$\frac{192\, V\, D}{\pi\, p\, a^6} = \begin{cases} \left(\frac{7+\nu}{1+\nu}\right) \approx 5.6 & \text{for simply supported edge} \\ \\ 1 & \text{for clamped edge} \end{cases} \qquad (15)$$

where the above approximate numerical value is obtained for a typical Poisson's ratio of $\nu = 0.3$.

Clearly, the support conditions at the circumference play an important role in establishing the volume displacement due to flexural motion, and they should be taken into account as realistically as possible in any practical calculation.

CYLINDRICAL SHELLS

A cylindrical shell (Fig. 8) subject to a uniform internal pressure p increases in radius by an amount $\delta_o = pa^2/EA$ if no axial stresses are applied to it at its edges and if the edges are also unrestrained otherwise (Ref. 13). If the internal pressure acts also on end-caps and thus causes axial tension in

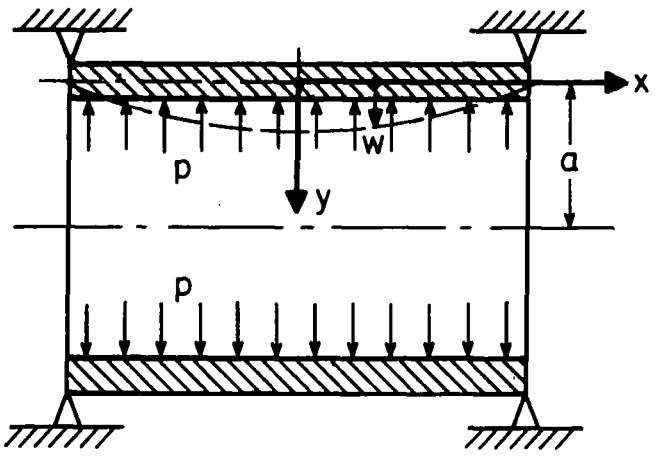

FIG. 8 CYLINDRICAL SHELL SUBJECT TO INTERNAL PRESSURE

the shell, then the radial expansion is reduced due to the Poisson effect and is given by $\delta = \delta_o(1 - \nu/2)$.

The volume displacement due to "membrane action" of the shell for the end-capped case thus is given by

$$V_1 = 2\pi aL\, \delta_o(1 - \nu/2) = 2\pi(1 - \nu/2)\, p\, a^3 L/EA \qquad (16)$$

However, the axial loads also cause the shell to increase in length by an amount $\Delta L = p(1 - \nu)aL/2EA$, which results in an additional volume displacement,

$$V_2 = \pi a^2 \Delta L = \pi a^3 L(1 - \nu)p/EA \qquad (17)$$

Thus, the total volume displacement of an end-capped cylindrical shell due to membrane action is given by

$$V = V_1 + V_2 = \frac{\pi a^3 L\, p}{EA}\left(\frac{5}{2} - 2\nu\right) \qquad (18)$$

Radial constraints imposed on the edges of the cylindrical shell reduce the deflections, and thus the volume displacement. In a later section of this chapter, pp. 44-46, it is shown that simple supports and rigid clamps at the edges have the effect of multiplying the above V_1 volume contribution by a factor F, where

$$F = \begin{cases} 1 - \dfrac{\sinh \beta L + \sin \beta L}{\beta L(\cosh \beta L + \cos \beta L)} & \text{for simply supported edges} \\ \\ 1 - \dfrac{2(\cosh \beta L - \cos \beta L)}{\beta L(\sinh \beta L + \sin \beta L)} & \text{for clamped edges} \end{cases} \tag{19}$$

The parameter β is defined by

$$\beta^4 = EA/4a^2D \tag{20}$$

and βL is a measure of the membrane rigidity relative to the flexural rigidity. From Eqs. (11) and (12),

$$\beta \approx \begin{cases} 1.285/\sqrt{aH} & \text{for homogeneous shells} \\ \\ 1/\sqrt{ah} & \text{for sandwich shells} \end{cases} \tag{21}$$

The approximate numerical coefficient above corresponds to the typical Poisson's ratio value of 0.3.

It is of interest to note that, for $\beta L > 3$, Eq. (19) reduces to

$$F \approx \begin{cases} 1 - (\beta L)^{-1} & \text{for simply supported edges} \\ \\ 1 - 2(\beta L)^{-1} & \text{for clamped edges} \end{cases} \tag{22}$$

Thus, for $\beta L > 20$, F differs from unity by less than 10% for all boundary conditions; i.e., then flexure has no appreciable effect on the shell displacement volume.

MEMBRANE DEFORMATIONS OF SHELLS OF REVOLUTION

General Relations

As evident from this analysis of cylindrical shells, the deformations due to edge constraints often have relatively little effect on the total volume displacement produced by an applied pressure. Except for very "short" shells, the volume displacement is almost entirely associated with membrane deformations of the shell; the flexural deformations associated with the edge conditions may then be neglected.

It is known that for conical- or spherical-segment shells the effects of edge loads are attenuated more rapidly (with distance along the shell) than for similar cylindrical shells (Refs. 14, 15). Thus, one may hope to obtain reasonable approximations to the "volume displacement" of non-cylindrical shells by neglecting flexure effects, consideration of which would lead generally to lengthy and complicated calculations.

Consider a general shell of revolution subject to axially symmetrical loading. Let r_o denote the radial distance measured from the shell axis to a generic point A on the shell mid-surface, and let r_1 denote the radius of curvature of this surface measured at A in a plane containing the shell axis (Fig. 9). One finds from Timoshenko (Ref. 16) that one may write the following

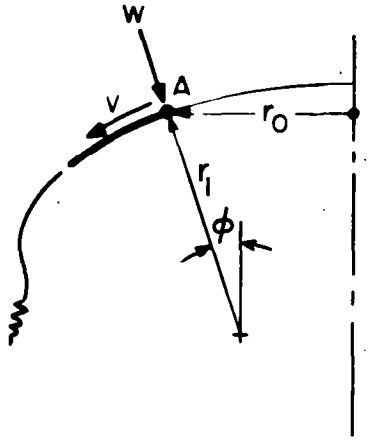

FIG. 9 GENERAL SHELL OF REVOLUTION

expressions for the normal displacement w and the tangential displacement v of the shell:

$$\left.\begin{aligned} w &= v \cot \phi + \frac{r_o}{EA \sin \phi} (N_\theta - \nu N_\phi) \\ v &= \sin \phi \left[C + \int \frac{f(\phi)\, d\phi}{\sin \phi} \right] \\ EA \cdot f(\phi) &= N_\phi \left(r_1 + \frac{\nu r_o}{\sin \phi} \right) - N_\theta \left(\frac{r_o}{\sin \phi} + \nu r_1 \right) \end{aligned}\right\} \quad (23)$$

Here C is a constant of integration, which must be evaluated from boundary conditions, and N_ϕ and N_θ denote the membrane (tension) forces (per unit length along the surface) acting respectively in the "v" direction of Fig. 9 and perpendicular to the plane of this figure.

The membrane forces can be evaluated directly from equilibrium conditions. For a loading consisting of a pressure p (here taken as positive in the positive w direction of Fig. 9), one obtains (Ref. 17)

$$\left.\begin{aligned} N_\theta &= - \frac{r_o}{\sin \phi} \left(p + \frac{N_\phi}{r_1} \right) \\ N_\phi &= - \frac{1}{r_o \sin \phi} \int_o^\phi p\, r_o\, r_1 \cos \phi \, d\phi \end{aligned}\right\} \quad (24)$$

Thus, one may determine the volume displaced by the membrane deformation of the shell (produced by an applied pressure p) by calculating N_ϕ, N_θ from Eq. (24), then substituting the results into Eq. (23) to find w, adjusting C to satisfy the appropriate boundary condition, then integrating w over the entire shell surface.

Spherical Segment

For the special case of a spherical shell (or a portion thereof), $r_1 = R$ and $r_o = R \sin \phi$, where R denotes the radius of the sphere. Then

$$\left.\begin{aligned} N_\phi &= - p\, R/2 \;, \quad N_\theta = p\, R/2 \\ f(\phi) &= 0 \\ v &= C \sin \phi \\ w &= \frac{p\, R^2}{2EA} (1 - \nu) + C \cos \phi \end{aligned}\right\} \qquad (25)$$

If the tangential displacement is prescribed to vanish at some location other than at $\phi = 0$, then $C = 0$, $v = 0$ and the above relation for w is also correspondingly reduced.

Thus, the volume displaced by membrane deflection of a spherical segment of height H_o is given by

$$V = \frac{p\, R^2\, S}{2EA} (1 - \nu) \qquad (26)$$

if $v = 0$, where

$$S = 2\pi\, R\, H_o \qquad (27)$$

denotes the surface area of the spherical segment.

The relations presented here may also be readily applied to shells which are toroidal segments, or to the numerical analysis of any given shell of revolution. However, they are not directly suited for dealing with conical shells, since for such shells the radius of curvature r_1 is infinite.

Conical Shell

For a shell whose middle surface is a full or frustrated right circular cone (Fig. 10) one finds that

$$N_\phi = - p\, r_o/2 \sin \phi \qquad (28)$$

if the top of the frustum is closed off in any manner. This relation may be obtained directly from equilibrium considerations.

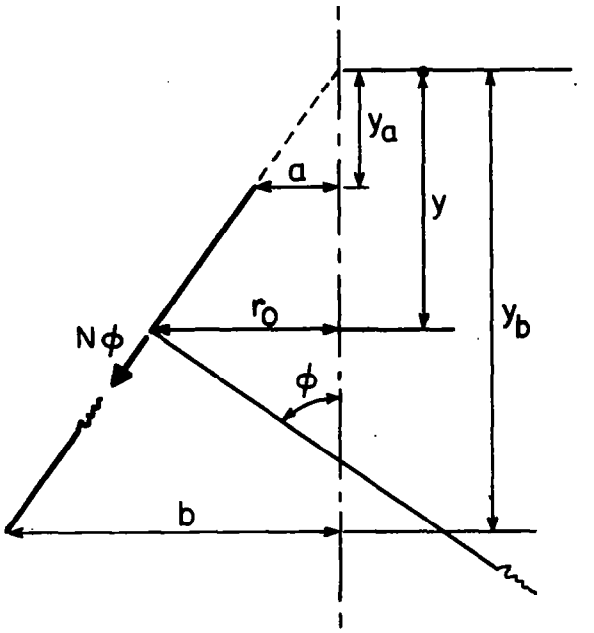

FIG. 10 FRUSTRATED CONICAL SHELL

From Eq. (24) one also obtains

$$N_\theta = - p\, r_o/\sin \phi \qquad (29)$$

since here r_1 is infinite.

The stress-strain relations (Ref. 18) are

$$\left.\begin{aligned} \epsilon_\phi \cdot EA &= N_\phi - \nu\, N_\theta \\ \epsilon_\theta \cdot EA &= N_\theta - \nu\, N_\phi \end{aligned}\right\} \qquad (30)$$

The volume displacement of a conical shell can be found from consideration of the volume element shown in Fig. 11.

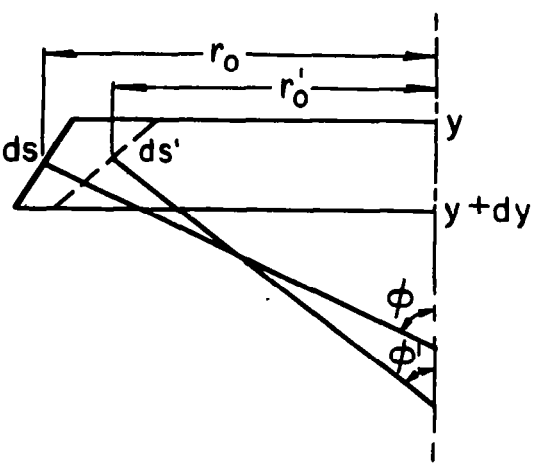

FIG. 11 VOLUME ELEMENTS OF AXISYMMETRIC SHELL

When a pressure differential is applied to the conical shell, the volume enclosed by the shell element of height dy decreases from $\pi r_o^2 dy$ to $\pi r_o'^2 dy$, or by an amount

$$dV = \pi(r_o'^2 - r_o^2)\, dy \qquad (31)$$

If the circumferential strain is ϵ_θ, then the new radius r_o' is $(1 + \epsilon_\theta)$ times the initial radius r_o, and $r_o'^2 - r_o^2 = r_o^2 \epsilon_\theta$ if higher-order terms in ϵ_θ are neglected.

The total volume displacement between the two coordinates $y = y_a$, y_b is given by

$$V = \int_{y_a}^{y_b} dV = 2\pi \int_{y_a}^{y_b} r_o^2 \, \epsilon_\theta \, dy \tag{32}$$

From Eqs. (28) through (30),

$$\epsilon_\theta = - \frac{p \, r_o}{EA \sin \phi} (1 - \nu/2) \tag{33}$$

Thus, substituting $r_o = y \cot \phi$,

$$C \equiv - \frac{V}{p} = \frac{\pi(b^4 - a^4)}{2EA \cos \phi} (1 - \nu/2) \tag{34}$$

This result applies to cases where the ends y_a, y_b do not move. In cases where the ends do move, the volume displacements due to the end motions must also be taken into account.

PLATE TERMINATING LONG CYLINDRICAL SHELL

In view of the important effect that edge support conditions have on the deformations of circular plates and on the associated volume displacement, it is of interest to consider in some more detail a plate whose circumference is connected to a cylindrical shell.

Such a plate-plus-shell composite structure may be analyzed by calculating the deformations of the individual component structures produced by the applied pressures and the interaction loads shown in Fig. 12. With the conventions indicated in that figure one may write the plate and shell edge rotations θ_p and θ_c as

$$\left.\begin{aligned} \theta_r &= m_p \cdot M + q_p\, p \\ \theta_c &= m_c \cdot M + q_c\, p \end{aligned}\right\} \qquad (35)$$

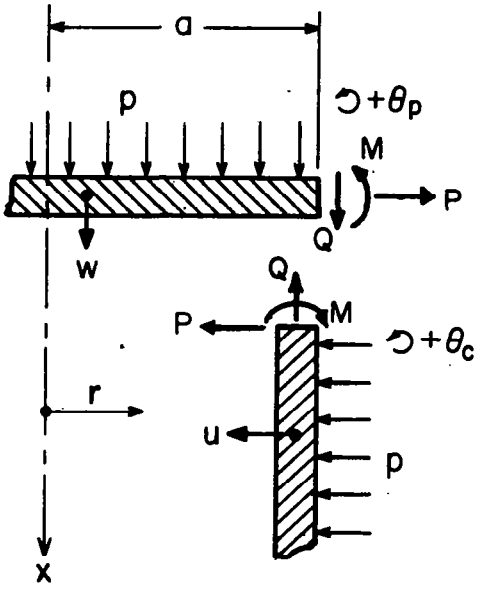

FIG. 12 DISCONTINUITY ANALYSIS OF PLATE TERMINATING LONG CYLINDRICAL SHELL

The first of these relations represents the plate edge rotation produced by the edge moment M and an external pressure p; the second represents a similarly produced cylindrical shell edge rotation. The coefficients m_p and q_p are constants that depend on the plate properties; m_c and q_c similarly depend only on the shell properties. (The plate deformation is assumed to be unaffected by the in-plane load P. The radial shell deformation u is assumed to be unaffected by the shell tension load Q, and u = 0 is assumed at the junction, corresponding to zero radial deformation of the plate.)

From expressions given by (Ref. 19) one may determine

$$q_p = \frac{a^3}{8\, D_p(1 + \nu_p)}, \quad m_p = \frac{a}{D_p(1 + \nu_p)} \tag{36}$$

and from Timoshenko's discussion of cylindrical shells (Ref. 20) one may obtain

$$q_c = -\frac{\beta_c\, a^2}{E_c\, A_c}\left(1 - \frac{\nu_c}{2}\right), \quad m_c = \frac{-1}{2\beta_c D_c} \tag{37}$$

where subscripts p and c have been appended to the previously introduced symbols in order to distinguish between those pertaining to the plate and those referring to the cylindrical shell.

For the case where the plate and shell edges are rigidly joined to each other one may set $\theta_p = \theta_c$ and obtain

$$\frac{-M}{a^2 p} = \frac{q_p - q_c}{a^2(m_p - m_c)} = \frac{\frac{1}{8} + \frac{\beta_c D_p(1 - \nu_p)\left(1 - \frac{\nu_c}{2}\right)}{E_c A_c\, a}}{1 + \frac{D_p(1 + \nu_p)}{2D_c\, \beta_c\, a}} \equiv U \tag{38}$$

The volume V_m displaced by the circular plate due only to application of an edge moment M may be calculated from the appropriate deflection equation (Ref. 19) to be given by

$$V_m = \frac{\pi\, a^4\, M}{4\, D_p(1 + \nu_p)} \tag{39}$$

whereas the volume displaced due only to an applied pressure is given by the first of Eqs. (15). The net volume displaced by the plate due to both the applied pressure and the edge moment supplied by the cylindrical shell is found to be given by

$$V = \frac{\pi a^6 p}{192 D_p} \left(\frac{7 + \nu_p}{1 + \nu_p}\right) \left[1 - \frac{8U}{7 + \nu_p}\right] \tag{40}$$

in view of Eqs. (38), (39) and (18). Here U denotes the ratio given by Eq. (38), and the coefficient of the bracketed term may be recognized as the volume displacement of a simply supported plate.

EFFECT OF EDGE CONSTRAINTS ON VOLUME DISPLACEMENT OF CYLINDRICAL SHELLS

The radial displacement w of a cylindrical shell (Fig. 8) is given by an expression of the form (Ref. 13)

$$w = -\delta + C_1 \sin \beta x \sinh \beta x + C_2 \cos \beta x \cosh \beta x \tag{41}$$

if terms that are anti-symmetric with respect to the middle of the cylinder are discarded (in view of the symmetry of the solutions required here). Here δ denotes the radial membrane expansion, as discussed in the paragraph preceding Eq. (16), and β is the relative stiffness parameter defined in Eq. (20). The constants C_1 and C_2 may be evaluated from the conditions prescribed at the boundaries.

For simply supported edges the boundary conditions are $w(L/2) = w'(L/2) = 0$, for which one finds (Ref. 13):

$$\left.\begin{aligned} C_1 B_s &= 2\delta \sinh \alpha \sin \alpha \\ C_2 B_s &= 2\delta \cosh \alpha \cos \alpha \\ B_s &\equiv \cos \beta L + \cosh \beta L \end{aligned}\right\} \tag{42}$$

:here

$$\alpha \equiv \beta L/2 \tag{43}$$

as been introduced for the sake of convenience. For clamped dges, for which the boundary conditions are $w(L/2) = w'(L/2) = 0$, ne similarly obtains:

$$\left.\begin{aligned} C_1 \cdot B_c &= 2\delta\ (\cosh\alpha \sin\alpha - \sinh\alpha \cos\alpha) \\ C_2 \cdot B_c &= 2\delta\ (\cosh\alpha \sin\alpha + \sinh\alpha \cos\alpha) \\ B_c &\equiv \sin\beta L + \sinh\beta L \end{aligned}\right\} \tag{44}$$

The volume V displaced may be obtained from Eq. (41) as

$$\left.\begin{aligned} V &= -2\pi a \int_{-L/2}^{L/2} w(x)\, dx \\ &= 2\pi a \delta L \left[1 - \frac{C_1}{\delta\beta L} (\cosh\alpha \sin\alpha - \sinh\alpha \cos\alpha) \right. \\ &\quad \left. - \frac{C_2}{\delta\beta L} (\cosh\alpha \sin\alpha + \sinh\alpha \cos\alpha) \right] \end{aligned}\right\} \tag{45}$$

Substitution of Eqs. (42) and (44) into (45) permits one to write

$$V = (2\pi a \delta L) \cdot F$$

where

$$F = \begin{cases} 1 - \dfrac{(\sinh \beta L + \sin \beta L)}{\beta L(\cosh \beta L + \cos \beta L)} & \text{for simply supported edges} \\ \\ 1 - \dfrac{2(\cosh \beta L - \cos \beta L)}{\beta L(\sinh \beta L + \sin \beta L)} & \text{for clamped edges} \end{cases} \tag{46}$$

This result has been quoted previously, as Eq. (19).

APPLICATION TO APOLLO CM

This section presents results of our efforts to estimate the low-frequency NR of the Apollo CM. Our model of the exterior sound-pressure field at low frequencies is one of simple spatially uniform compression. A simplified diagram of the CM shell system is shown in Fig. 13. It consists of separate outer and inner shells, mounted on a cylindrical fairing to the service module (SM). Our analysis procedure consists of dividing the shells into simple geometrical shapes (frustrated cones, cylinders, spherical segments, planes), using the previously presented results to calculate the acoustical compliances (ratio of volume displacement to pressure differential) due to each structural segment, and then to add all effects in order to obtain the compliance of the complete shell.

After we have computed the acoustic compliances, we combine them appropriately to determine the net NR of the total structure, i.e., the ratio of the external acoustic pressure to that in the space within the inner shell. By this process we are able to single out those structural elements which result in the least NR. Once these "weak links" have been identified, one should be able to suggest ways to increase the system NR if this seems desirable.

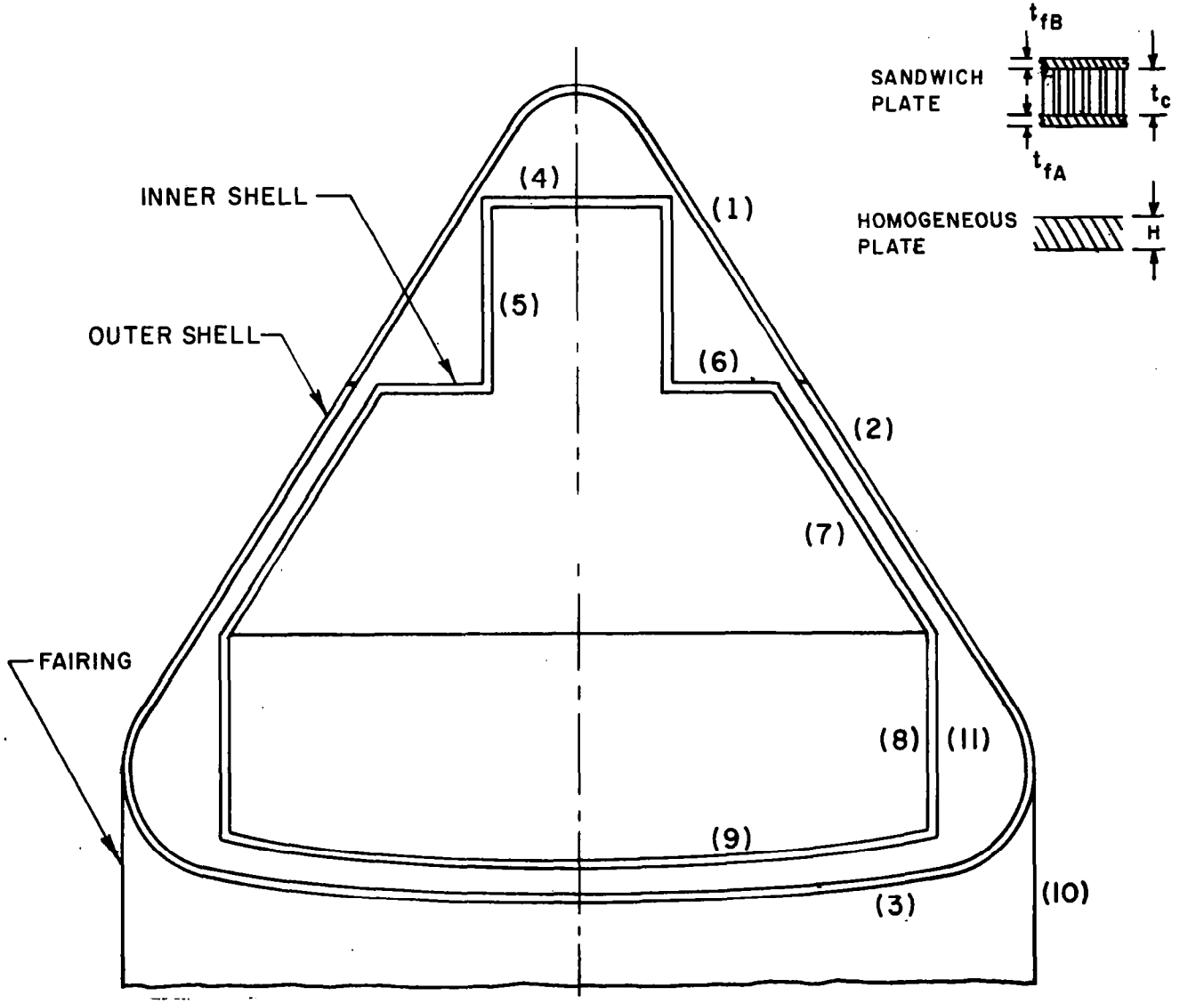

FIG. 13 SIMPLIFIED SKETCH OF MAJOR STRUCTURAL ELEMENTS OF COMMAND MODULE (CM) STRUCTURE

Description of the Structure

General Features.—The two axisymmetric shells that make up the basic structure of the CM are formed from metal sandwich panels. Stainless steel is used for the outer shell, and aluminum for the inner one. The thickness and density of the sandwich core and the facing sheets for the sandwich vary along the axis of the module. There are structural irregularities on the surface of the shells due to strengthening members, hatches, compartments, etc.

The volume between the two shells has added thermal insulation in the form of blankets of "Q-felt," a glass-fiber blanket covered with aluminum foil. The outer surface of the CM is covered with an ablative coating of varying thickness. (The acoustical and mechanical effects of the Q-felt and the ablative coating will not be considered here.) The volume within the inner shell is partially filled with equipment and personnel.

Description of Outer Shell.—For the purposes of our analysis, the outer shell, shown in Fig. 14, will be treated as a right circular cone with a generating angle of 30° and a base radius of 72 in., connected to a base which is a spherical segment having a radius of curvature of 180 in. The dimensions of the sandwich panels are given in Table I, in terms of the notation defined in Fig. 6.

The upper part of the conical section 1 (see Fig. 14) consists of a stainless steel sandwich made of 8-mil facing plates on an 0.592-in. thick core having a density of 5.7 lb/cu ft. The lower part 2 has the same facing skins but a core 0.51 in. thick with a density of 5.4 lb/cu ft. The spherical base is made from a stainless steel sandwich with 61-mil skins and a 2-in. core with a density of 5.4 lb/cu ft.

Description of Inner Shell.—We have divided the inner shell of the CM into six structural elements: upper hatch cover 4, upper hatch cylinder 5, ledge 6, cone 7, lower cylinder 8 (actually a frustrated cone) and spherical base 9. These surfaces are not structurally homogeneous since they all, and particularly the cone 7, have hatches, windows, structural reinforcements, conduits, etc.

The dimensions of the inner shell structural elements are shown in Fig. 15. Except for the hatch cover 4, all dimensions and sandwich specifications have been taken from NASA drawings. On the base 9 there is a gradation in core density; the core sandwich material is lighter in the center and becomes progressively more dense toward the periphery.

TABLE I

DIMENSIONS AND MATERIALS OF SANDWICH PANELS SHOWN IN FIG. 13

Section	Material	Core Thickness t_c(in.)	Thickness of Inner and Outer Skins t_{fA}, t_{fB} (10^{-3} in.)	$t=\frac{1}{2}(t_{fA}+t_{fB})$	$h=t_c+t$
1	steel	0.592	8,8	8	0.600
2	"	0.50	8,8	8	0.508
3	"	2.0	68,68	68	2.068
4	aluminum	1.18	20,20	20	1.20
5	"	0.25	10,10	10	0.26
6	"	0.72	16,22	19	0.739
7	"	0.92	20,20	20	0.94
8	"	0.75	16,16	16	0.766
9	"	1.50	33,33	33	1.533

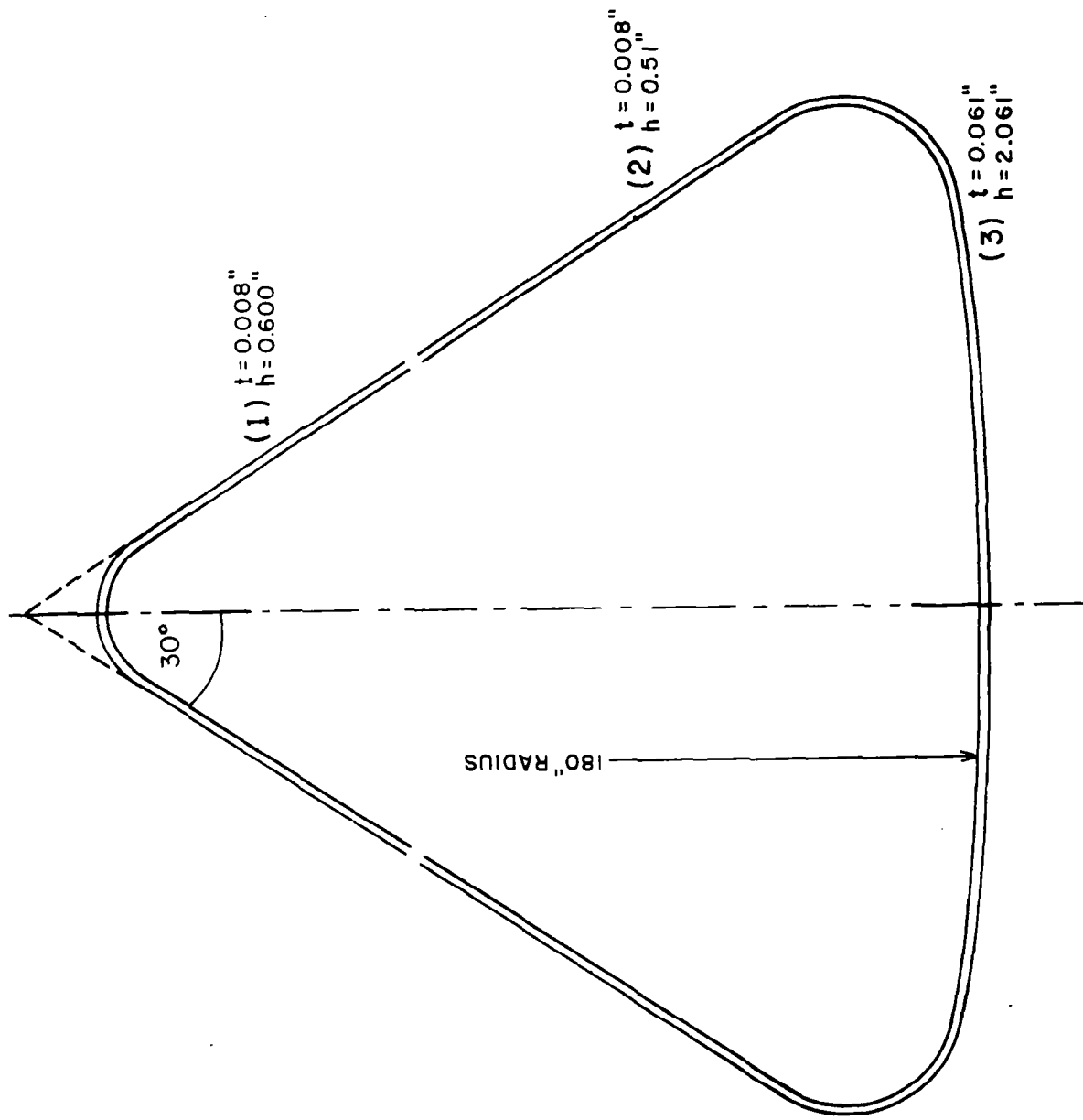

FIG. 14 MAJOR STRUCTURAL SECTIONS OF OUTER SHEL (STAINLESS STEEL SANDWICH)

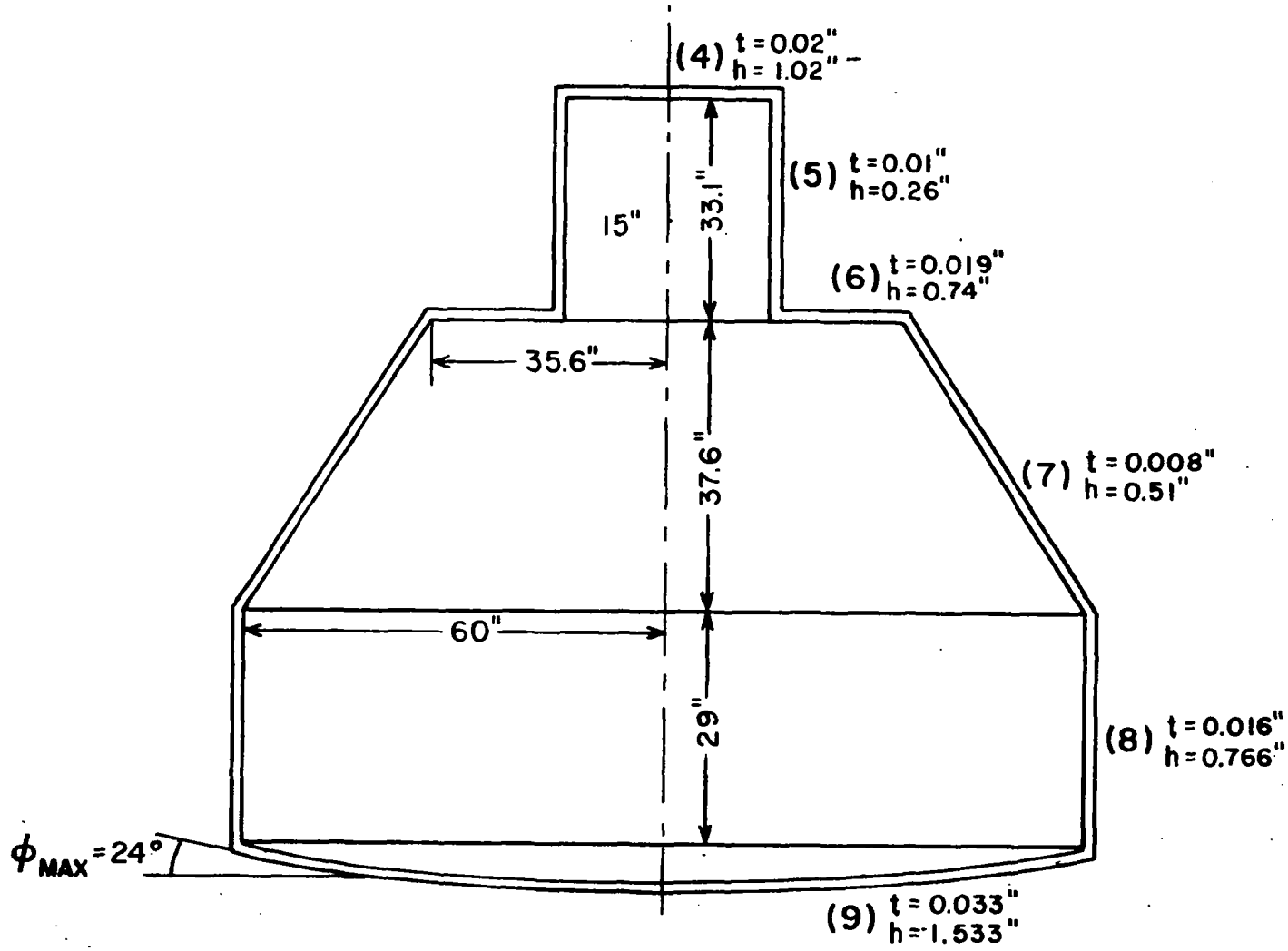

FIG. 15 MAJOR STRUCTURAL SECTIONS OF INNER SHELL (ALUMINUM SANDWICH)

Properties of Contained Volumes.—The inner shell contains a volume of approximately 4.75×10^5 cu in., or about 275 cu ft. If we assume that roughly one-third of this is occupied by equipment and personnel, we estimate the free volume to be 3×10^5 cu in.

The acoustic compliance of a contained free volume V is given in Eq. (7). For the volume contained by the inner shell, the acoustic compliance is

$$C_{12} = 3 \times 10^5/20 = 1.5 \times 10^4 \text{ (in)}^3/\text{psi} \qquad (47)$$

The total volume enclosed by the outer shell is approximately 8×10^5 cu in. If we deduct from this the inner volume, we have left 3.25×10^5 cu in. Further, subtracting 0.25×10^5 cu in., the estimated volume of the inner shell wall structure plus the rest of the volume-occupying elements in the space contained between the shells, leaves 3×10^5 cu in. for the contained volume. If the pressure variations in this space are adiabatic its compliance is given by (7). However, because of the presence of the Q-felt, the pressure variations are likely to be more nearly isothermal. The compliance then is (Ref. 10)

$$C_{11} = \frac{V}{P_o} = 2 \times 10^4 \frac{\text{cu in.}}{\text{psi}} \text{ (isothermal)} \qquad (48)$$

P_o denotes the average (static) pressure in the space.

The temperature and density assumed for the air in the interior volumes are those at launch. If the average pressure P_o is reduced, the acoustic compliance of the volume is increased, but the mechanical compliances are not changed, since the structural mechanics are not significantly affected by ambient pressure. The effect of reduced pressure P_o thus is to increase the NR of the structure.

Other Noise-Transmitting Elements.—In addition to the previously discussed major elements which affect the acoustic transmission, elements which form a "mechanical bridge" between the two shells, i.e., which facilitate the transmission of vibrations and sound in localized regions, can influence the NR significantly. The assessment of the effect on NR of electrica and service connections between the shells will be aided by a better understanding of the structural dynamics. We shall defer discussion of bridging elements to chapter VI.

Dynamics of Structure

In this section we review those aspects of the dynamical behavior of the structure shown in Fig. 13 which are pertinent to the pressure transmission characteristics of that structure. We concentrate on the quasi-static "forced" motion of the mechanical structure and the acoustic spaces. The resonant vibrations of the structure and/or the acoustic spaces will be discussed later.

Quasi-Static or "Forced" Motion of Shells.—Our investigations in Chapter II indicated that a substantial portion of low-frequency noise within the CM will be due to forced, nonresonant response of the inner and outer shells and the connecting air space. The nature of the motion will be different from that of the flat wall discussed in Chapter I. Since the volume-displacing modes of cylinders, for example, occur at or near the "ring resonance" frequency, these modes which couple well to the sound field generally will resonate above the frequency range of interest. In contrast to the wall transmission, which has a mass-controlled response, the forced-wave transmission for axisymmetric shells is stiffness-controlled. We evaluate the volume displacement of the shells, therefore, by quasi-static calculations of deflection due to a constant pressure differential. Resonance effects will be considered in Chapter IV.

The quasi-static volume displacements of several elementary shell structures have been analyzed previously. In order to obtain the total volume deflection of the inner shell of the CM, we must know the pressure differential between the interspace volume 11 and the contained volume 12. In order to obtain the pressure in 11, we must know the difference in the volume deflections of the inner and outer shells. In this section we shall derive these parameters.

Acoustic Compliance of Inner Shell.—The structural elements of the inner shell, as illustrated in Fig. 15, will now be considered separately as acoustic compliance elements. The cylindrical hatch 5 was described above under Description of Inner Shell. From Eq. (21)

$$\beta L = \frac{L}{\sqrt{ah}} = \frac{33}{\sqrt{(15)(.26)}} = 16.7 \qquad (49)$$

Since, as previously discussed, a large value of βL indicates that flexural effects are relatively unimportant, one may here estimate the volume displacement of the shell on the basis of only its membrane deflection. From Eq. (18), the ratio of volume displacement to pressure differential for this cylindrical shell then is

$$\left.\begin{aligned} c_5 &= \frac{V}{p} = \frac{\pi a^3 L}{2Et}(5/2 - 2\nu) \\ &= \frac{\pi(15)^3(33)}{2(10^{-2})\ 10^7}(1.9) = 3.33 \text{ cu in./psi} \end{aligned}\right\} \quad (50)$$

The hatch cover 4 and the ledge 6 may be treated together as a single flat circular plate with a radius of 35.6 in. An error in volume displacement may be expected in this treatment, because the boundary conditions on the inner edge of ledge 6 and on the outer edge of the cover 4 are not properly represented. However, the error is thought to be relatively unimportant and not to warrant the additional complications involved in more exact calculations. From Eqs. (15) and (12), the compliance for the cover and ledge combination is found to be

$$c_{4,6} = \frac{\pi a^6}{192D}(5.6) = (5.6)\frac{\pi a^6}{96Eh^2t} \quad (51)$$

$$= \frac{\pi(35.6)^6}{96\ 10^7(0.74)^2(1.9)10^{-2}}(5.6) = (5.6)(6.3)\cdot 10^2 \text{ cu in./psi}$$

In the foregoing relation the factor of 5.6 should be included if the plate edges are supported; it should be omitted if they are clamped. In either event, the plate compliance $c_{4,6}$ is substantially larger than the shell compliance c_5, and the inner volume compliance c_{12}, Eq. (47), is greater than the plate compliance.

The conical section 7 will be membrane-controlled if $\psi_s a \gg 1$, where (Refs. 14, 15)

$$\psi_s^4 \equiv \frac{EA \sin^2\phi}{4a^2 D} \tag{52}$$

and a is the radius of the base of the conical section. For section 7

$$\psi_s a = \left(\frac{a}{h} \sin \phi \right)^{1/2} \approx \left[\frac{(50)(3)}{(0.5)(4)} \right]^{1/2} \approx 8.5 \tag{53}$$

We conclude that this section will act as a membrane. The acoustical compliance of the conical section is found from Eq. (34),

$$C_7 = \frac{\pi a^4 (1 - \nu/2)}{2EA \cos \phi} \left[\left(\frac{b}{a} \right)^4 - 1 \right] \tag{54}$$

with $b/a = 1.69$, $a = 35.6$ in., $\phi = 60^\circ$, $A = 16 \times 10^{-3}$ in., $E = 10^7$ psi, and $\nu = 0.3$, to be

$$C_7 = 190 \text{ cu in./psi} \tag{55}$$

If we treat section 8 as a cylinder, we find its compliance from Eq. (50) to be

$$C_8 = \frac{\pi(60)^3(29)(1.9)}{2(10^7)(1.6 \times 10^{-2})} = 1.17 \times 10^2 \text{ cu in./psi} \tag{56}$$

a value which is fairly close to C_7.

The spherical base has a membrane compliance given by

$$C_9 = \frac{\pi R^3 H_o}{2Et} (1 - \nu) \tag{57}$$

where R is the radius of curvature and H_o is the height of the spherical segment. If R = 180 in., t = 0.033 in., and H_o = 9.7 in.,

$$C_9 = \frac{\pi(1.8)^3(9.7)10^6(0.7)}{2\,(3.3)\,10^{-2}\,10^{-7}} = 1.89 \times 10^2 \text{ cu in./psi} \qquad (58)$$

We can get an estimate of the validity of this membrane result by applying the criterion for a cone, as stated just before Eq. (52). We could use an average value of $a^2\sin^2\phi$. But instead, we merely note that

$$(\psi_s a)^4 \leq \left(\frac{a_{max}}{h}\right)^2 \sin^2 \phi_{max} = \left(\frac{60}{1.5}\right)^2 (0.16) = 256 \qquad (59)$$

where a_{max} = 60 in. and $\phi_{max} = 24^o$. If we correct this upper bound value by factors of $(1/3)^2$ for averages over $\sin^2\phi$ and a^2, we find $\psi_s a \approx 2.5$, which indicates that membrane stiffness will indeed dominate.

It appears that the ledge structure 6 is the most compliant part of the internal shell structure.

Acoustic Compliance of Outer Shell.—Referring to Fig. 14, we note that there is a break in the structure and different sandwich constructions are used for sections 1 and 2. However, the volume-displacing membrane deformation is governed by the facing thickness "t," and this is continuous. We therefore calculate the shell compliance for sections 1 and 2 as a single element. The volume displacement of a complete cone is given by Eq. (34) with a = 0. For the cone in Fig. 14, b = 76 in., $\phi = 60^o$, and t = 0.008 in. This gives

$$C_{1,2} = \frac{\pi b^4 (1 - \nu/2)}{4Et \cos\phi} = \frac{\pi(76)^4 (.85)2}{4(3 \times 10^7)(8 \times 10^{-3})}$$

$$= 190 \text{ cu in./psi} \qquad (60)$$

The base 3 of the outer shell is a spherical segment concentric with section 9 of the inner shell. (Although it is shielded from exterior pressures by the Command Service Module (CSM) fairing, it will be subject to low-frequency sound pressures that are transmitted through the fairing.) We assume that the compliance of section 3 is membrane-controlled. Its compliance is given by Eq. (26),

$$C_3 = \frac{\pi R^3 H_o}{2Et} (1 - \nu) \qquad (61)$$

with H_o = 24 in., R = 180 in., t = 61 mils. For steel the Young's modulus is E = 3 x 10^7 psi and Poisson's ratio is ν = 0.3. The result is

$$C_3 = \frac{\pi(180)^3 \cdot 24(0.7)}{2 \times 2 \times 10^7 \times 61 \times 10^{-3}} = 1.44 \times 10^2 \text{ cu in./psi} \qquad (62)$$

Since this part of the structure is shielded by the CSM fairing, it probably has no significant effect on the NR. We include it in our NR calculation, however, since it will contribute to transmission under test conditions, where the CSM fairing is not present.

Calculation of Noise Reduction

The noise reduction for a shell enclosing a volume is derived earlier in this chapter, and the result is given in Eq. (10). The governing equations were represented by the equivalent acoustical circuit shown in Fig. 5. An equivalent circuit for a double-shell enclosure like the CM is shown in Fig. 16.

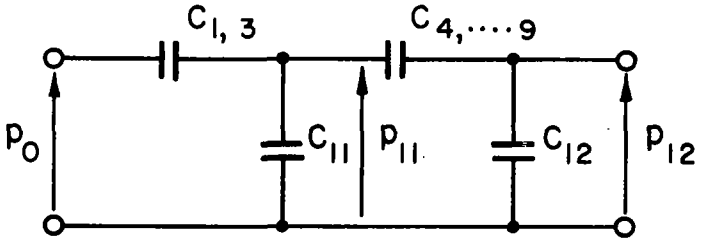

FIG. 16 EQUIVALENT ACOUSTICAL CIRCUIT FOR DOUBLE SHELL-ENCLOSED VOLUME

The relation between p_{11} (the pressure in the interspace volume 11) and p_{12} (the pressure in the interior volume 12), as obtained from Fig. 16, is

$$p_{12} = p_{11} \frac{1/C_{12}}{1/C_{4..9} + 1/C_{12}} = p_{11} \frac{C_{4..9}}{C_{12} + C_{4..9}} \tag{63}$$

By definition, the noise reduction NR_i of the inner shell is

$$NR = 20 \log p_{11}/p_{12} = 20 \log \left[1 + \frac{C_{12}}{C_{4..9}} \right] \tag{64}$$

The compliance $C_{4..9}$ is the sum of the compliances of the sections of the inner shell,

$$C_{4..9} = C_4 + C_5 + \ldots + C_9 \tag{65}$$

The previous calculations show that this sum is dominated by the compliance of the ledge-hatch cover combination $C_{4,6}$. If we assume that this combination is a simply supported plate, we obtain

$$C_{4..9} \approx 4 \times 10^3 \text{ cu in./psi} \tag{66}$$

from Eqs. (9), (12), (13) and (15). If we take a value of 3×10^5 cu in. for the free volume 12, as suggested earlier, then we find the noise reduction of the inner shell to be

$$NR_1 = 20 \log \left[1 + \frac{1.5 \times 10^4}{4 \times 10^3} \right] \approx 11.7 \text{ dB} \tag{67}$$

From the symmetry of the circuit shown in Fig. 16, it is clear that the relation between p_o and p_{11} is similar to that between p_{11} and p_{12}. Thus, the overall pressure ratio

$$20 \log p_o/p_{12} = 20 \log p_o/p_{11} + 20 \log p_{11}/p_{12} \tag{68}$$

may be evaluated with the aid of

$$20 \log p_o/p_{11} = 20 \log \left[1 + \frac{C_{eq}}{C_{1,3}} \right]$$

where

$$C_{eq} = C_{11} + \frac{C_{4..9}\, C_{12}}{C_{4..9} + C_{12}} = C_{11} + C_{12}(1 + C_{12}/C_{4..9})^{-1} \qquad (69)$$

and

$$C_{1,3} = C_1 + C_2 + C_3 = 3.34 \times 10^2 \text{ cu in./psi} \qquad (70)$$

If the interspace volume 11 is sufficiently filled with porous material so that its pressure fluctuations are isothermal, then its compliance is given by Eq. (47), and

$$C_{eq} = (2 \times 10^4) + (1.5 \times 10^4)(38.5)^{-1} \approx 2 \times 10^4 \text{ cu in./psi} \qquad (71)$$

The noise reduction NR_o of the outer shell therefore is

$$NR_o = 20 \log p_o/p_{11} = 20 \log (1 + C_{11}/C_{1,3}) = 20 \log [1 + (2 \times 10^4)/(3.34 \times 10^2)] = 40 \text{ dB} \qquad (72)$$

Adding the NR provided by the inner and outer shells gives

$$NR_{tot} = 11.7 + 40 = 51.7 \text{ dB}$$

Discussion and Conclusions

In the preceding sections, we have developed an estimate of the NR provided by the Apollo Command Module at low frequencies, in the absence of any structural or acoustical resonances. We conclude that the inner shell is relatively compliant, due to the flat ledge and flat hatch cover sections. It provides only about 10 dB of NR. The outer shell, however, is fairly effective, since its uniform conical construction is relatively non-compliant. It provides approximately 40 dB of NR. If the inner shell were of a similar shape, we might expect the CM to supply NR of the order of 80 dB at low frequencies instead of the 50 dB estimated for the present design.

The foregoing conclusions would not hold if acoustical and structural resonances should occur. Chapter VI will describe some experiments on a model of the upper portion of the inner shell hatch structure, which indicate that the forced "quasi-static" compliance model is appropriate to portions of the structure. Nevertheless, calculations of the effect of structural stiffeners on low-frequency NR indicate that volume-pumping modes of the shells may be a problem.

CHAPTER IV

EFFECT OF STRUCTURAL RESONANCE ON THE NOISE REDUCTION OF SPACECRAFT

INTRODUCTION

In the previous chapter we saw that it is possible to achieve relatively large values of low-frequency NR with axisymmetric structural shells. This occurs particularly when the shell responses are quasi-static, and when the corresponding acoustic compliances are membrane-controlled.

Uninterrupted, axisymmetric shells may have low-frequency resonances that are non-volume-displacing. Such resonances do not affect NR. However, if there is a structural discontinuity, such as a reinforcing longeron or a cutout for a hatch, then the low-frequency resonating modes may become volume-displacing and reduce NR. In this chapter we develop estimates of the sound transmission of the shell when such volume-displacing resonances exist. We shall illustrate the general results by applying them to the case of a simply supported cylindrical shell that has a single rigid longeron.

GENERAL THEORY

We are interested in the sound transmission into the volume contained by a closed shell at frequencies below acoustic resonances of the contained volume. The situation is that described in earlier work for the "intermediate-frequency region." If the resonant structural modes are volume-displacing, then they will have an appreciable coupling to the external sound field, resulting in a structural modal energy (Ref. 21)

$$\theta_m = \frac{M_s \langle v^2 \rangle}{n_s \Delta\omega} = \frac{\theta_R \eta_{rad}}{\eta_s + \eta_{rad}} \qquad (73)$$

Here, $\langle v^2 \rangle$ is the square of the "kinetic velocity" of the resonator, n_s is the shell modal density, and θ_R is the modal energy of the sound field, given by

$$\theta_R = \frac{\langle p_o^2 \rangle V}{\rho c^2 n_R \Delta\omega} \tag{74}$$

Also, $\langle p_o^2 \rangle$ is the mean-square pressure of the external sound field in a frequency band $\Delta\omega$ which includes the resonance frequency of the structural modes, ρ and c are the density and sound speed of the acoustic medium, and

$$n_R = \frac{\omega^2 V_e}{2\pi^2 c^3} \tag{75}$$

is the modal density of the exterior acoustic space, whose volume is V_e.

The radiation loss factor η_{rad} will depend on the volume velocity U of the shell mode. The structural loss factor η_s is usually assumed large compared with η_{rad}. No reliable prediction methods exist for this parameter.

The radiated power from a simple source of volume velocity U can be readily computed (Ref. 22). It is given by

$$\Pi_{rad} = \frac{k^2 \rho c}{4\pi} U^2 = \langle v^2 \rangle \omega M_s \eta_{rad} \tag{76}$$

where k denotes the acoustic wavenumber at frequency ω, and M_s represents the structural mass. The pressure fluctuation in the air volume within the shell is also related to U, as

$$\langle p_i^2 \rangle = U^2/\omega^2 C_s^2 \tag{77}$$

where $C_s \equiv V_s/\rho c^2$ is the acoustic compliance of the contained volume V_s within the shell. Combining Eqs. (73) through (77), we get

$$\frac{\langle p_i^2 \rangle}{\langle p_o^2 \rangle} = \frac{2\pi^2 c^5 A_p}{\omega^5 V_s^2 \kappa} \frac{c}{c_\ell} \frac{\eta_{rad}^2}{\eta_s + \eta_{rad}} \nu_s \tag{78}$$

where ν_s is the ratio of the modal density of the vibrating shell segment to that of a flat plate of the same area, and where we have introduced the expression for flat plate modal density given in Ref. 23. The radius of gyration of the shell cross section is κ and the longitudinal wave speed in its material is c_ℓ.

If the shell is divided into N sections, then

$$\langle p_i^2 \rangle = \sum_{j=1}^{N} \langle p_i^2 \rangle_j \quad \text{(incoherent sections)} \tag{79}$$

where the structural parameters in (78) must be evaluated for each section, and we have assumed that the volume-pumping from each section is incoherent with that of others. At low frequencies, however, it is likely that the shell segments will be excited in phase. If this is the case, the total volume velocity will be

$$U = \sum_{j=1}^{N} U_j \tag{80}$$

and the mean-square internal pressure will be

$$\langle p_i^2 \rangle = \left\langle \left(\sum_{j=1}^{N} p_i^{(j)} \right)^2 \right\rangle \tag{81}$$

where $p_i^{(j)} = U_j / \omega C_s$.

APPLICATION TO A CYLINDRICAL SHELL

Let us imagine that the shell in question is the right circular cylinder with rigid end caps shown in Fig. 17. It has a single longeron, which we model as a simply supported line. The flexural mode shapes for such a shell are of the form

$$\psi \approx \sin \frac{n x_1}{2a} \sin \frac{m \pi x_2}{\ell} ; \qquad n,m \text{ integers} \tag{82}$$

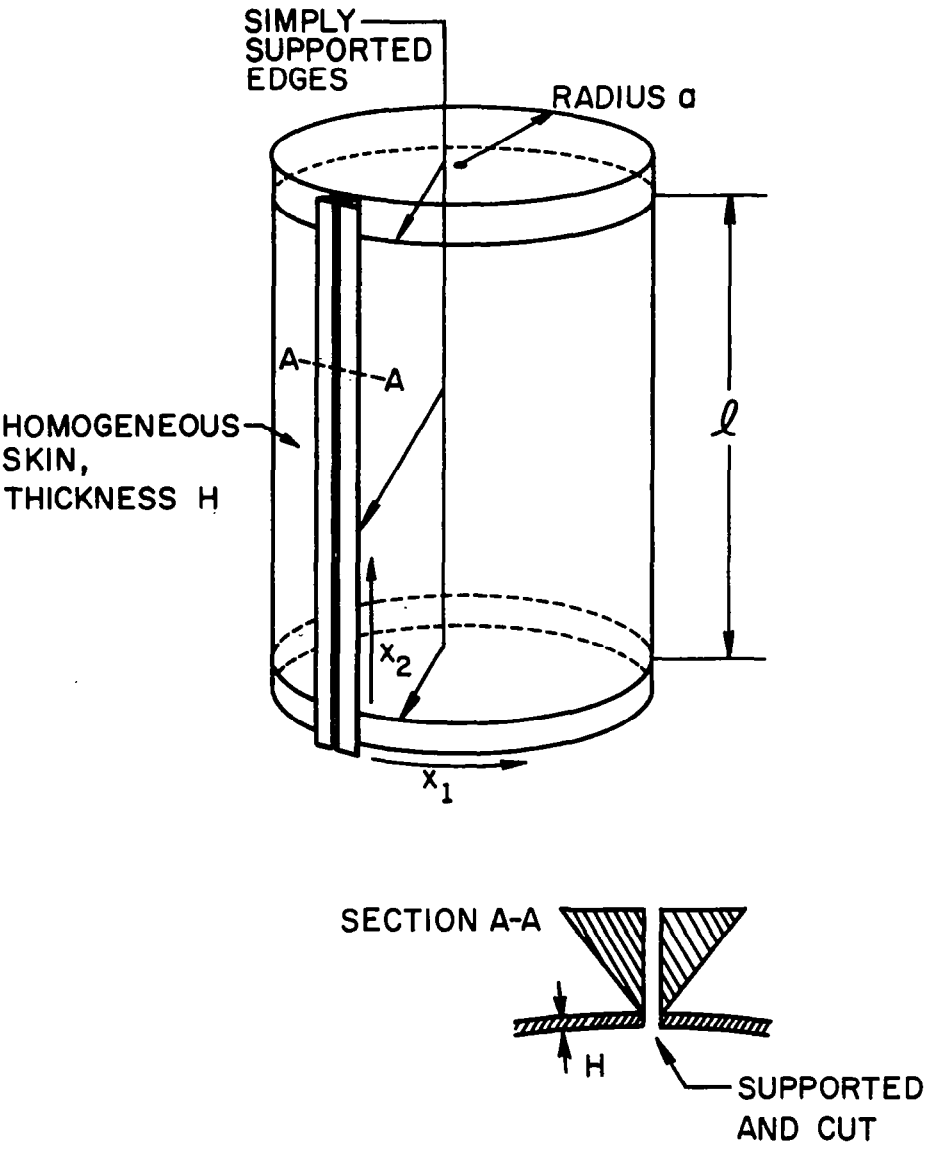

FIG. 17 TEST CYLINDER WITH SIMPLY SUPPORTED EDGES

The ratio of the modal density of this shell to that of a flat plate of the same area has been derived by Manning (Ref. 24), and is given in Fig. 18 (for groups of modes averaged over 1/3-octave bands).

The modes for which n and m are odd will cause volume-pumping. They make up one-fourth of all the modes of the cylinder. The average radiation loss factor for this set of modes for a panel has been found by Maidanik to be (Ref. 25):

$$\eta_{rad} = \frac{2}{\pi^4} \frac{\rho c \; P \; \lambda_c}{M_s (\omega \; \omega_c)^{1/2}} \qquad (83)$$

where M_s is the panel mass, P is its perimeter, $\omega_c = c^2/\kappa c_\ell$ is the acoustic critical frequency of the panel, and $\lambda_c = 2\pi c/\omega_c$ is the acoustic wavelength at the critical frequency. From (83) then,

$$\eta_{rad}^2 = \frac{16}{\pi^6} \left(\frac{\rho}{\rho_p}\right)^2 \left(\frac{c_\ell}{c}\right)^2 \left(\frac{\kappa}{H}\right)^2 \frac{\kappa c_\ell P^2}{\omega A_p^2} \qquad (84)$$

where ρ_p is the density of the panel material and H is defined so that $\rho_p H$ is the surface density of the panel.

Our cylindrical shell is divided into a single section, with

$$\left.\begin{aligned} A_p &= 2\pi a \ell \\ V_s &= \pi a^2 \ell \\ P &= 2(\ell + 2\pi a) \\ (\kappa/H)^2 &= 1/12 \end{aligned}\right\} \qquad (85)$$

Placing (83) through (85) in (78), we get

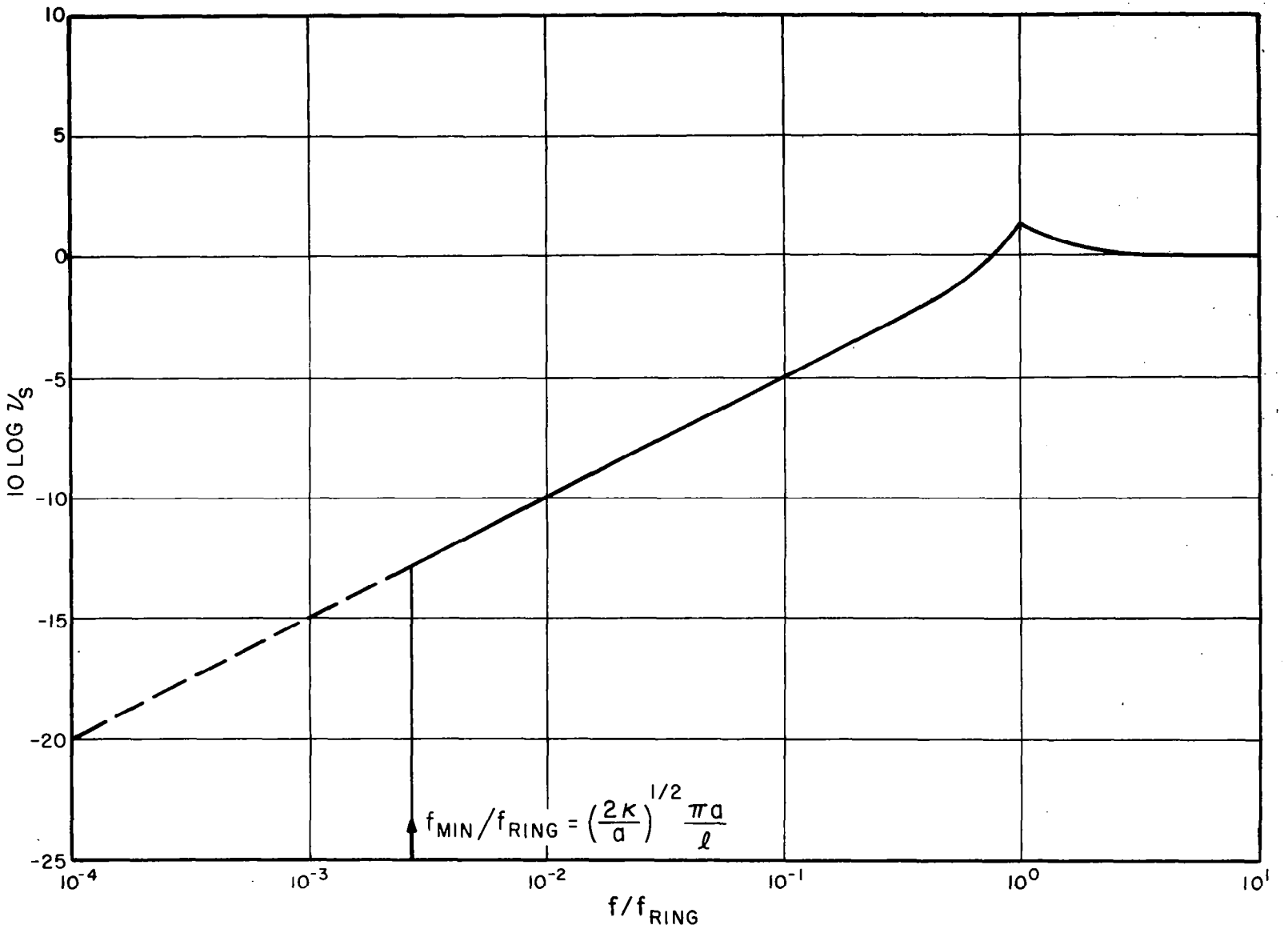

FIG. 18 RATIO OF MODAL DENSITY OF CYLINDER TO THAT OF FLAT PLATE OF EQUAL AREA, AVERAGED OVER ONE-THIRD OCTAVE BANDS

$$NR \equiv -10 \log \langle p_i^2 \rangle / \langle p^2 \rangle$$

$$= 10 \log[3\pi^{11}(f^6 a^3 \ell^3/c^6)\ (\rho_p/\rho)^2 (c/c_\ell)^2\ (1+\ell/2\pi a)^{-2}\ ]$$

$$+ 10 \log \eta_s - 10 \log \nu_s \qquad (86)$$

where we have assumed $\eta_s \gg \eta_{rad}$. If we also assume that η_s is frequency-independent, then, referring to Fig. 18 for the frequency-dependence of ν_s, we see that the NR will rise at a rate of 65 dB/decade as the frequency is increased in the frequency range for which resonant volume-pumping modes occur.

For a particular model, an experimental study of which will be described in Chapter VI, $\rho_p = 2.7$ gm/cm^3, $2a = \ell = 18$ cm, and $H = 1.25 \times 10^{-2}$ cm. For these values,

$$NR \approx 60 \log 10^{-2} f + 10 \log \eta_s - 10 \log \nu_s + 31 \qquad (87)$$

A curve showing the NR of this model cylinder is shown in Fig. 19, based on an assumed value of $\eta_s = 10^{-2}$. Also indicated on the same graph are the predicted and measured membrane NR's for this cylinder.

The result of Eq. (86) is valid for the frequency range where structural resonances occur, i.e., above the fundamental structural resonance frequency. For a flat plate, the fundamental resonance is relatively simple to estimate for a wide variety of boundary conditions (Ref. 26). For a cylinder, however, the calculation is somewhat more involved. We can use formulas developed by Heckl (Ref. 27) to derive an estimate of this frequency for supported cylinders.

Heckl's formula for the ratio of modal resonance frequency f_m to ring frequency f_{ring} (at which the fundamental "breathing mode" occurs) for short cylinders is (Ref. 28)

$$(f_m/f_{ring})^2 = (1-\nu^2)\ \frac{\sigma^2}{\sigma^2 + m^2} + \beta^2(\sigma+m^2)^2 \qquad (88)$$

where ν is Poisson's ratio, m is the circumferential mode number, σ is the axial wave number $n\pi a/\ell$, and $\beta \equiv \sqrt{\kappa/a}$. If we minimize (88) by differentiating with respect to m, the result is

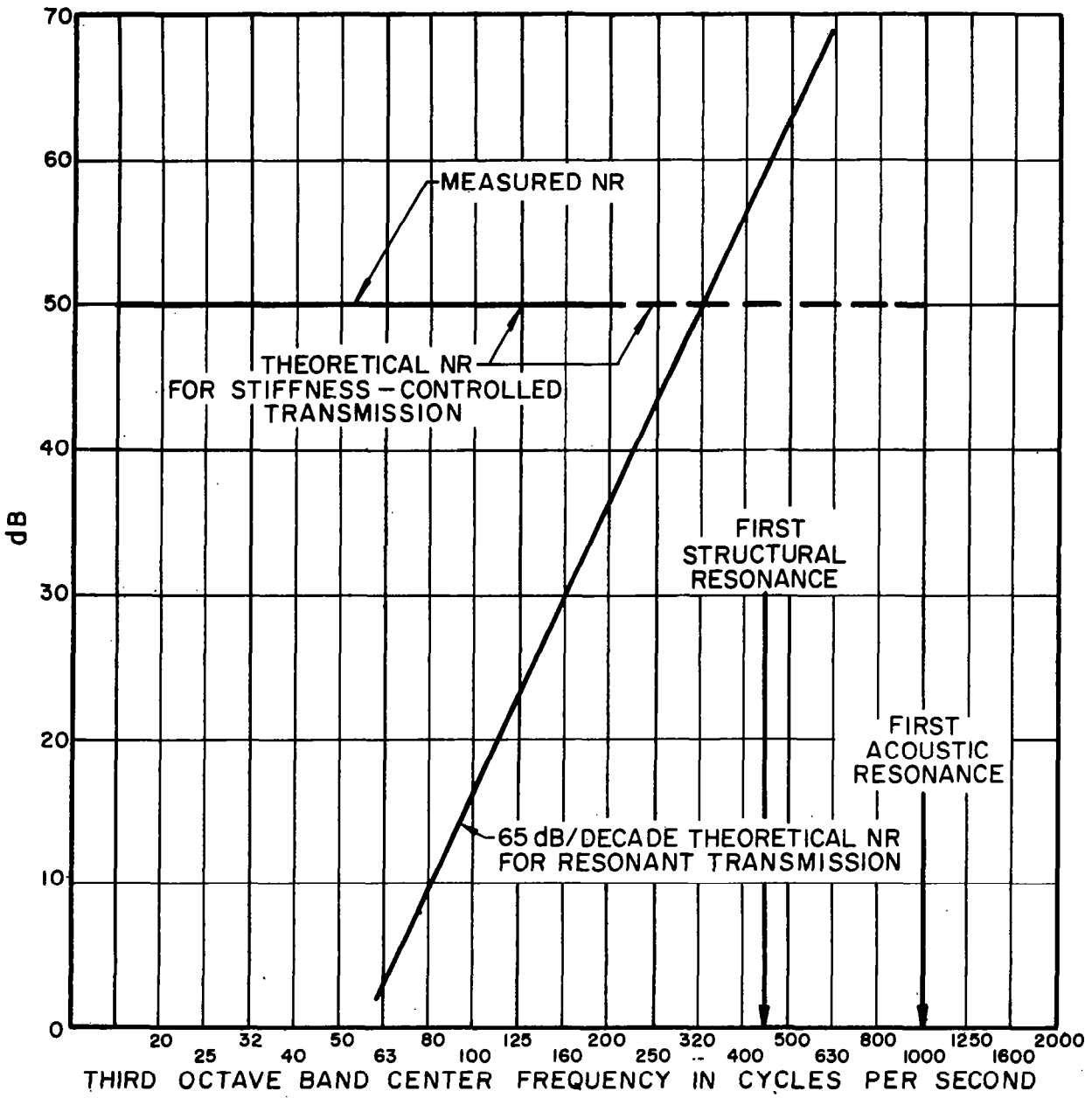

FIG. 19 NR OF CYLINDER MODEL OF FIG. 17

$$(f_m/f_{ring})_{min} = \sqrt{2\beta}\ \sigma = \sqrt{2\kappa/a}\ \frac{\pi a}{\ell} \qquad (89)$$

where the smallest value of σ has been taken, corresponding to n=1.

It is interesting to compare the lowest structural resonance frequency with the lowest acoustical resonance frequency f_a:

$$f_{min}/f_a = \sqrt{\frac{2\kappa}{a}} \cdot \frac{\pi a}{\ell} \cdot \frac{c_\ell}{2\pi a} \cdot \frac{2\ell}{c} = \sqrt{\frac{2\kappa}{a}} \cdot \frac{c_\ell}{c} \qquad (90)$$

For the cylinder in our example,

$$f_{min}/f_a = 0.47 \qquad (91)$$

Since the lowest acoustic resonance frequency is

$$f_a = \frac{c}{2\ell} = \frac{3.45 \times 10^4}{36} = 960 \text{ Hz} \qquad (92)$$

the lowest structural resonance is 450 Hz.

We note, from Fig. 19, that the resonant contribution to sound transmission is exceeded by the compliant (nonresonant) contribution at frequencies above 300 Hz. We would not expect, therefore, to see the effect of structural resonance on the NR of this cylinder. The data presented in Chapter VI indicates that this is the case.

DISCUSSION AND CONCLUSIONS

In the frequency region below the first acoustic resonance, the upper bound on the NR is the quasistatic membrane compliance prediction. For frequencies within an octave above the fundamental resonance frequency of the cylinder, however, structural discontinuities may cause large reductions in NR relative to this upper bound, if their compliance is very large.

A good design rule of thumb for reinforced shell structures might be to avoid panel resonances that occur less than an octave below the resonances of the contained air space. Use of this rule should result in the probable retention of the quasi-static NR at least up to the first acoustic resonance.

Experimental data on the effects of structural resonance on the vibration and NR of cylindrical and conical shells are presented in Chapter VI.

CHAPTER V

EFFECTS OF ACOUSTIC RESONANCE ON LOW-FREQUENCY NOISE REDUCTION

INTRODUCTION

We have defined "low frequencies" in the context of this report as frequencies below the first acoustic resonance of the receiving space. For the Apollo CM, this resonance occurs at approximately 50 Hz. Even in this low-frequency range, however, there may occur acoustic resonances which are associated with the interspace volume.

Such low-frequency resonances may occur as the result of an interaction between the interspace volume and an air vent connecting this volume to the CM exterior. A resonance may be associated with the acoustic mass of the vent acting in conjunction with the compliance of the interspace. The effect on the system NR of such resonances and of related resonances are studied in the present chapter.

Since the entire CM is axisymmetric, aside from perturbing effects of equipments, the interspace between the shells shares this symmetry. The shortest distance measured within the interspace between the two poles of symmetry of this space is long enough to permit an acoustic resonance to occur at a relatively low frequency. The acoustics of the interspace resonances and the potential effects of such resonances on the low-frequency NR are also treated explicitly in this chapter. Experimental studies of these resonances are described in Chapter VI.

EFFECTS OF AN AIR VENT ON CM MODEL NOISE REDUCTION

Air Vent Resonance

The interspace between the inner and outer shells of the Apollo command module is vented to the exterior via a tube which connects the interspace with the service module interior. At very low frequencies such venting will allow the pressure fluctuations on the exterior of the vehicle to be directly applied to the internal shell (neglecting any NR of the service module). This venting reduces the NR markedly, since it is the outer conical shell of the CM that supplies most of the noise reduction at these low frequencies. It is therefore of considerable interest to discover the range of frequencies over which the exterior shell will be effectively acoustically "short-circuited" by the vent.

If the dissipation in the tube is small enough, then there also exists the possibility of a Helmholtz resonance involving the acoustic mass of the air vent and the acoustic compliance of the interspace volume. Such a resonance will lead to pressure amplification within the interspace and an increase in the noise in the CM.

One may also expect to find an antiresonance at a higher frequency, involving the air vent acoustic mass and the acoustic compliance of the outer shell. Near the antiresonance frequency the noise reduction will be increased, since volume-pumping by the outer shell will be almost exactly balanced by the reversed-phase volume-pumping in the air vent.

In this section we shall examine the effect of the air vent on the low-frequency noise reduction. We shall here limit our discussion to a study of the probable range of resonant frequencies for such effects on Apollo-like structures. Calculations for other structures may be carried out on the basis of the methods given here.

Estimate of Resonance Frequencies for CM Model

The frequency of the resonance between an acoustic mass M and a compliance C is given by

$$f_r = \frac{1}{2\pi} (MC)^{-1/2} \tag{93}$$

In terms of the volume of the air space V, the ambient density ρ, and the sound speed, the compliance of the air space is given by

$$C = V/\rho\, c^2 \tag{94}$$

or by eq. (7), which is equivalent.

The acoustic mass of air contained in a tube of cross-sectional area A and length ℓ is (Ref. 29)

$$M = \rho \ell/A \tag{95}$$

Placing (94) and (95) into (93) results in

$$f_r = \frac{c}{2\pi} \left(\frac{A}{\ell V}\right)^{1/2} \tag{96}$$

In Chapter III we noted that a reasonable value for the interspace volume is 3×10^5 cu in. Let us assume that the vent has a cross-sectional area of 1 sq in. and a length of 20 in. Then the resonance frequency is approximately

$$f_r = 0.9 \text{ Hz} \tag{97}$$

The compliance of the interspace volume, assuming adiabatic fluctuations, is approximately 1.5×10^4 cu in./psi. The compliance of the outer shell, which was given in Eq. (60), is approximately 1.5×10^2 cu in./psi. According to Eq. (93), the ratio of resonance frequencies is inversely proportional to the square root of the compliance ratio. This means that the antiresonance between the air vent and the shell is approximately ten times higher in frequency than the resonance:

$$f_a = 9 \text{ Hz} \tag{98}$$

Effect of Resonances on Structural NR

A schematic diagram of the system discussed here is shown in Fig. 20. The air vent is shown as a small tube, the interspace volume is V_1, and the volume contained within the inner shell is V_2. The inner and outer shells are designated as S_1 and S_2, respectively.

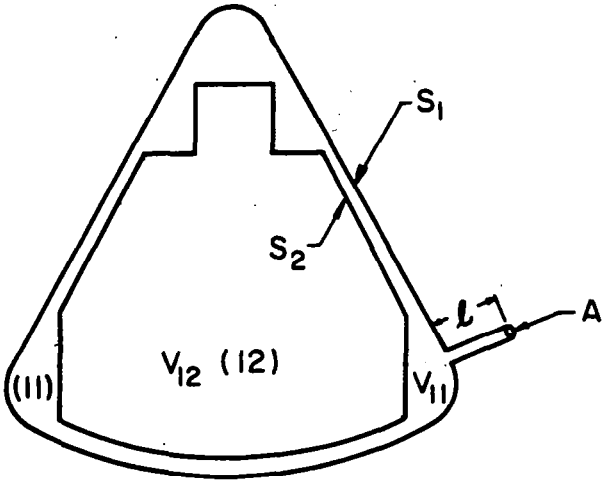

FIG. 20 "DOUBLE WALL" HELMHOLTZ RESONATOR

The electrical equivalent circuit by means of which one may study the pressure transmission of this system is shown in Fig. 21. This circuit is a modification of Fig. 16. If M_v is infinite (obtained by $A \to 0$), the system is reduced to one with no vent. The presence of the acoustic mass of the vent is found to give rise to resonances and antiresonances, and to result in a noise reduction curve like that shown in Fig. 22. The noise reduction for $f > f_a$ approaches the value computed for a system with no vent. The noise reduction in the decade between f_r and f_a changes rapidly from a very low to a very high value, and very little noise reduction is obtained for frequencies below f_r.

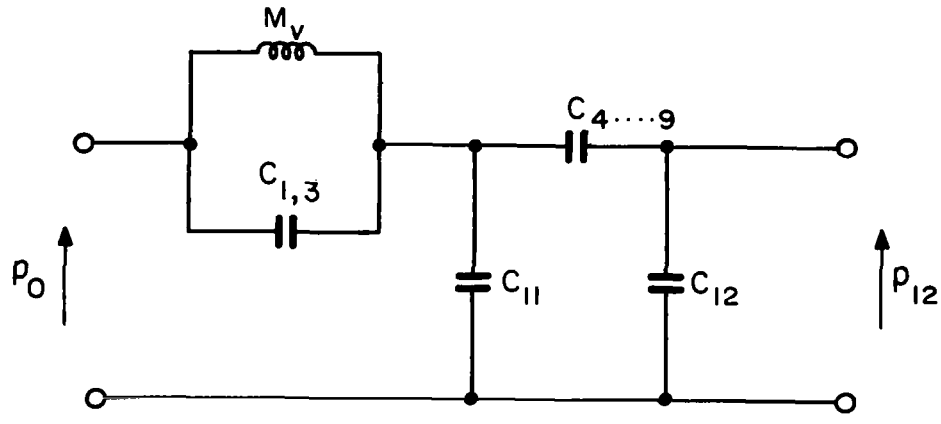

FIG. 21 ACOUSTIC ANALOG EQUIVALENT CIRCUIT

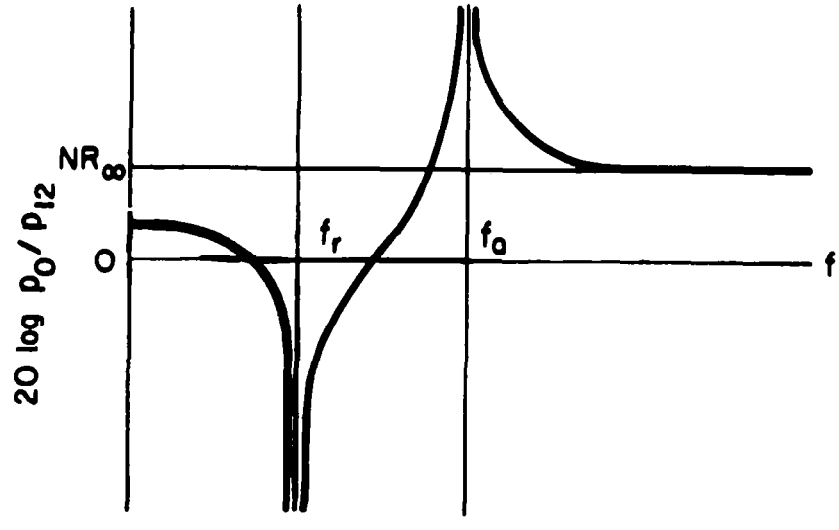

FIG. 22 NR BEHAVIOR OF SYSTEM IN FIG. 20

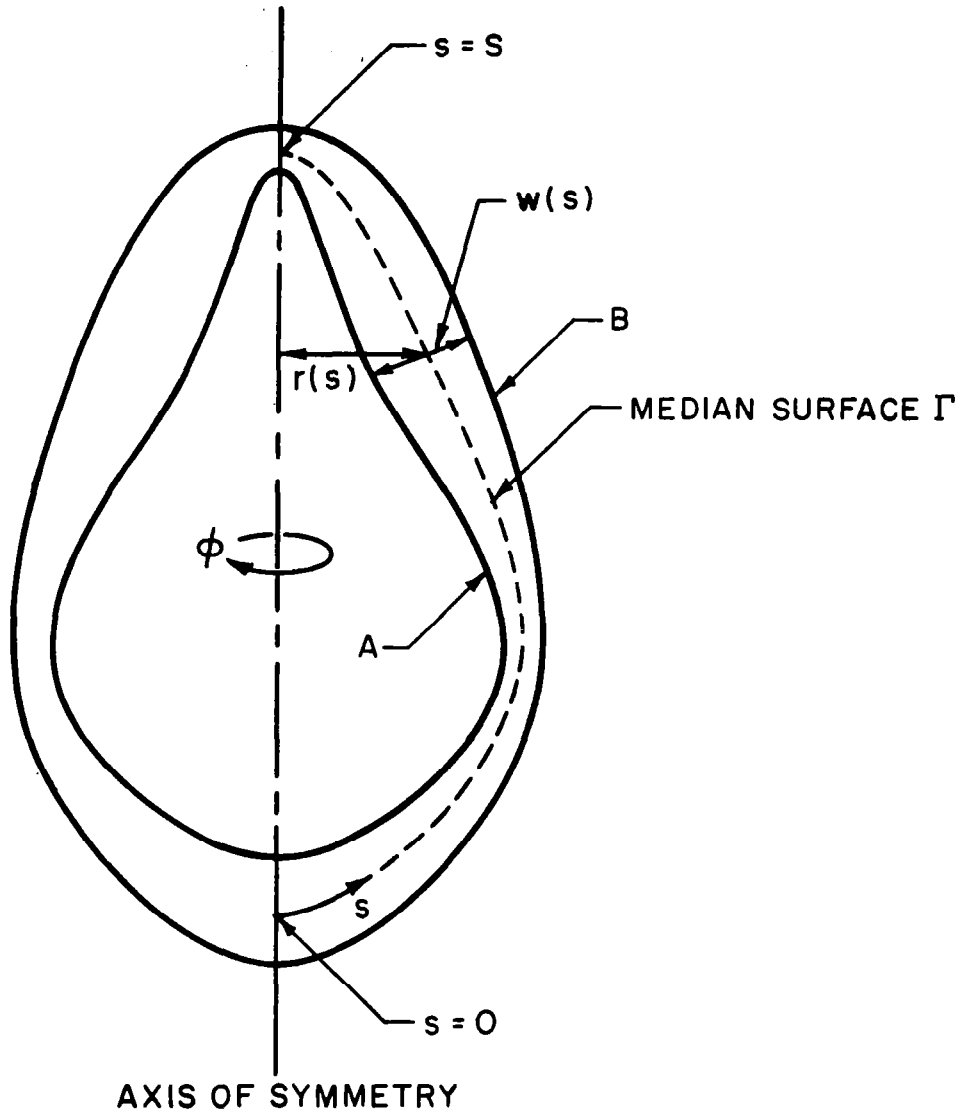

FIG. 23 DEFINING SURFACES AND DIMENSIONS FOR AXISYMMETRIC INTERSPACE VOLUME

Clearly, it is desirable to keep f_r and f_a as low as possible so that the noise-reducing qualities of the outer shell frequencies at which appreciable acoustic excitation is present. It is not practical to reduce these frequencies by increasing the compliance of the outer shell, since such an increase reduces the asymptotic (higher frequency) noise reduction. Therefore the acoustic mass of the air vent should be kept as high as possible; that is, the opening should be kept as constricted as possible.

ACOUSTICS OF SPACES BETWEEN AXISYMMETRIC SHELLS

The acoustic resonances of a fluid contained between two axisymmetric rigid shells can be derived exactly for a few simple shapes. Generally, however, the shapes will be so complicated that an exact treatment of the basic differential equations and their solutions will not be possible. In this section we describe how an acoustic equation for the space can be derived and solved by some approximate methods.

Derivation of the Wave Equation

Let us consider the fluid contained between two axisymmetric shells A and B, as shown in Fig. 23. The shape of this interspace or coupling volume is defined by the shape of the median surface Γ that is equidistant from A and B, and by the distance between A and B at any position on this surface. Positions on Γ have coordinates (ϕ,s) where ϕ is the azimuthal angle and s is a lineal dimension along a line of constant ϕ. We take $s = 0$ on the lower "pole" of Γ and $s = S$ at the upper pole. The distance from any position on Γ to the polar axis is $r(s)$ and the distance between A and B along a line perpendicular to Γ is $w(s)$.

The major simplifying assumption made, aside from linearity, is that the acoustic field variables are constant along lines perpendicular to Γ. This restricts us to that frequency range where the acoustic wavelength is long compared with the greatest value of $w(s)$.

To construct an equation of motion, we consider a section of the volume bounded by A and B and by the surfaces $s = \text{const}$,

$s + \Delta s = \text{const}$, $\phi = \text{const}$, and $\phi + \Delta\phi = \text{const}$. This volume element is sketched in Fig. 24. We next write down the mass conservation equation, the force equation, and the state-energy relation. Effects of viscosity and thermal conduction in the gas and at the boundaries will be ignored.

Continuity Equation (Conservation of Mass). - If the flow velocity is resolved into components u_s and u_ϕ parallel to the unit vectors $\hat{e}_s$ and $\hat{e}_\phi$, and the fluid density is ρ, then the rate of mass addition to V is

$$\rho\, u_\phi A_\phi \Big|_\phi + \rho u_s A_s \Big|_s$$

and the rate of mass loss is

$$\rho\, u_\phi A_\phi \Big|_{\phi + \Delta\phi} + \rho u_s A_s \Big|_{s + \Delta s}$$

The difference between rates of mass addition and loss results in a rate of change of mass contained in $\Delta\tau$:

$$\frac{\partial}{\partial t}(\rho\, \Delta V) = \rho u_\phi A_\phi \Big|_\phi - \rho u_\phi A_\phi \Big|_{\phi + \Delta} + \rho u_s A_s \Big|_s - \rho u_s A_s \Big|_{s + \Delta s}$$

Approximating the differences by partial derivatives gives

$$\Delta s\, \Delta\phi\, rw \frac{\partial \rho}{\partial t} = - \Delta s\, \Delta\phi \frac{\partial}{\partial \phi}(\rho u_\phi w) - \Delta s\, \Delta\rho \frac{\partial}{\partial s}(\rho u_s rw)$$

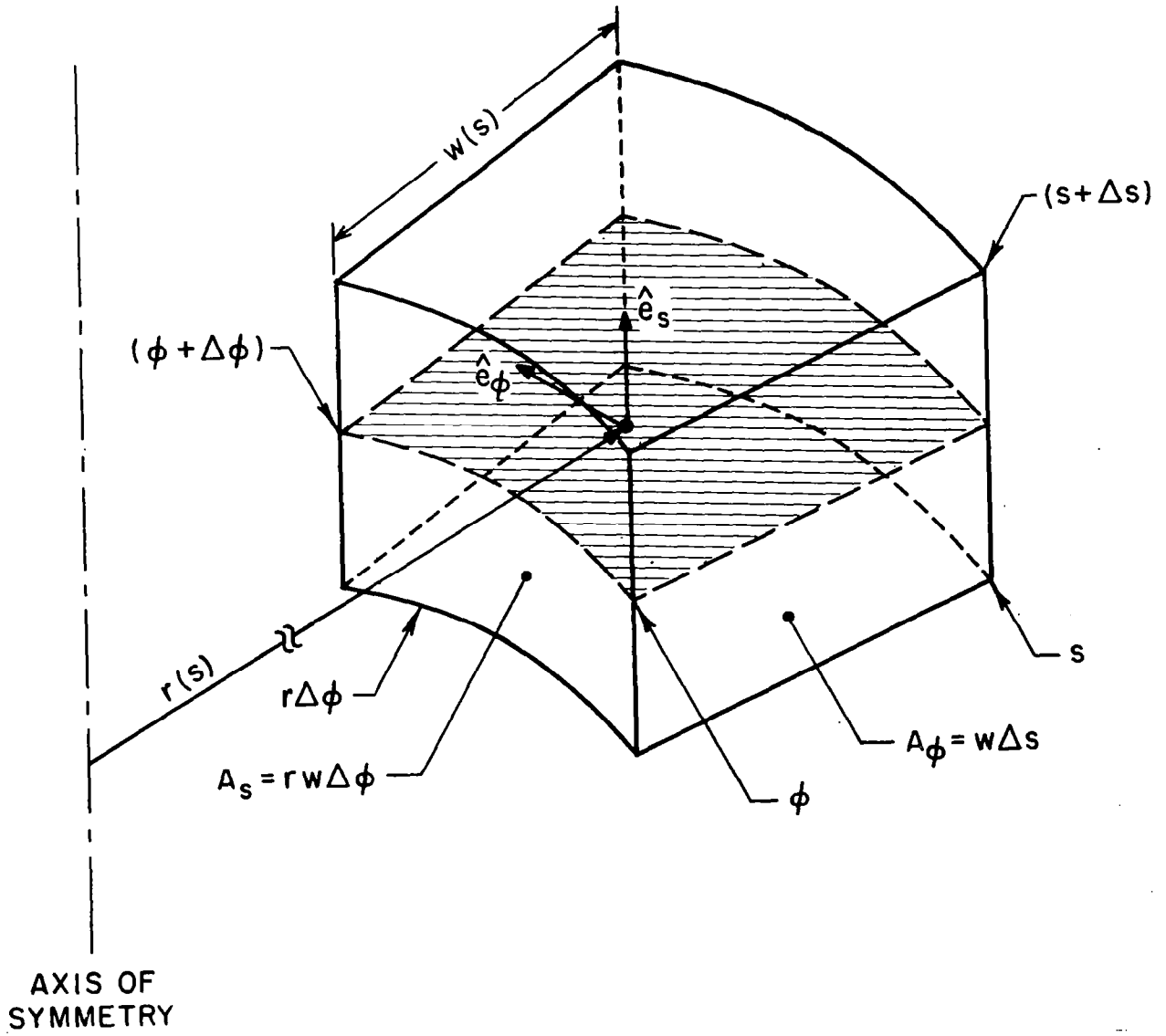

FIG. 24 VOLUME ELEMENT OF INTERSPACE
$\Delta\tau$ (INCREMENTAL VOLUME) = $w(s)\, r(s)\, \Delta s \Delta\phi$

which can be rewritten

$$\frac{\partial \rho}{\partial t} + \rho_o \nabla \cdot \vec{u} + \rho_o u_s \frac{\partial}{\partial s} \ell n\, rw = 0 \qquad (99)$$

In deriving (99) we have taken $\rho = \rho_o$, the ambient density, when it multiplies a fluctuating variable, since we consider linear terms only.

Force Equation (Conservation of Momentum).- The fluid element contained in $\Delta\tau$ is accelerated by a net force acting on it. A change in pressure along s results in a force $p(s)A_s^{(p)}$ in the +s direction where p(s) is the pressure at s and $A_s^{(p)}$ is the projected area of the volume element in a plane perpendicular to $\hat{e}_s$. Similarly, the force in the -s direction is $p(s + \Delta s)\, A_s^{(p)}$. The net force in the s direction and the resulting acceleration of the volume element obey.

$$-A_s^{(p)} \frac{\partial p}{\partial s} \Delta s = \frac{\partial}{\partial t} (\rho u_s \Delta\tau)$$

The corresponding equation for the ϕ component of acceleration is

$$-A_\phi^{(p)} \frac{\partial p}{\partial \phi} \Delta\phi = \frac{\partial}{\partial t} (\rho u_\phi \Delta\tau)$$

Combining these, and linearizing (using $A_s^{(p)} = A_s$ and $A_\phi^{(p)} = A_\phi$), gives

$$\rho_o \frac{\partial \vec{u}}{\partial t} + \nabla p = 0 \qquad (100)$$

Energy-State Equation. - When viscosity and thermal conduction effects can be ignored, then relations for the equation of state of a gas and conservation of energy result in

$$\frac{dp}{d\rho} = \frac{\gamma P_o}{\rho_o} \equiv c^2 \qquad (101)$$

where γ denotes the ratio of specific heats and c the velocity of sound.

We combine (99), (100) and (101) to obtain the desired equation.

Wave Equation.- The wave equation is found by eliminating ϕ and u. We do this by operating on (99) with $\partial/\partial t$ and on (100) with ∇, then subtracting (100) from (99) to obtain

$$\frac{\partial^2 p}{\partial t^2} + \rho_o \frac{\partial u_s}{\partial t} \frac{\partial}{\partial s} \ell n\ rw - \nabla^2 p = 0$$

We then use (101) and the s-component of (100) to get

$$\frac{1}{c^2} \frac{\partial^2 p}{\partial t^2} - \frac{\partial p}{\partial s} \frac{d}{ds} (\ell n\ rw) - \nabla^2 p = 0 \qquad (102)$$

This is the desired equation. It is very similar in form to the traditional "Webster horn equation," as we shall see.

Comparison with Horn Equation

Consider a slender horn of circular cross section specified by r(x) (see Fig. 25). With the assumption that the maximum value of r(x) is small compared with the wavelength, we can derive the traditional Webster's horn equation. Continuity, force and energy state equations are stated below.

Continuity Equation (Conservation of Mass)

$$\frac{\partial \rho}{\partial t} + \rho_o \nabla \cdot \vec{u} + \rho_o u_x \frac{\partial}{\partial x} [\ell n\ S(x)] = 0 \qquad (103)$$

Force Equation (Conservation of Momentum)

$$\rho_o \frac{\partial \vec{u}}{\partial t} + \nabla p = 0 \tag{104}$$

Energy-State Equation

$$\frac{dp}{d\rho} = \frac{\gamma P_o}{\rho_o} \equiv c^2 \tag{105}$$

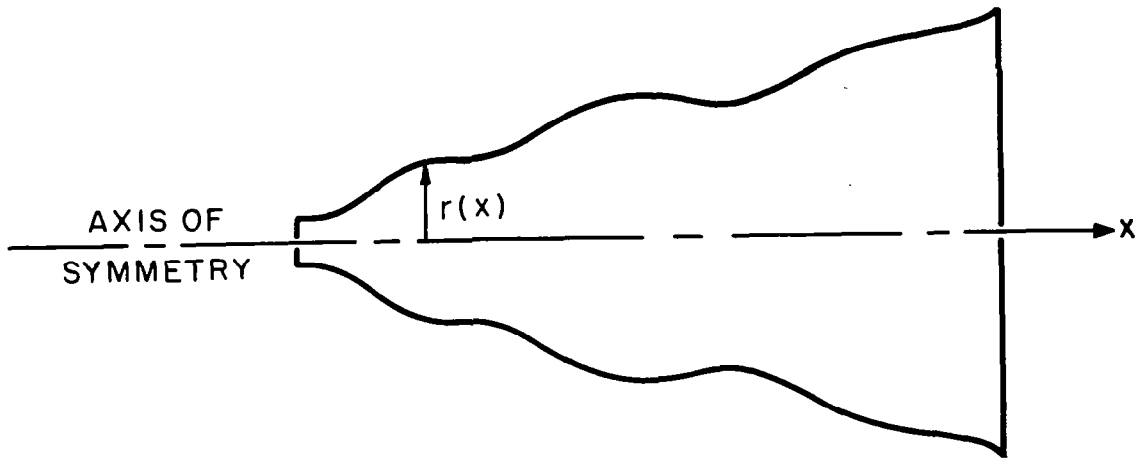

FIG. 25 SLENDER HORN OF CIRCULAR CROSS SECTION SPECIFIED BY r(x)

These results are based on the same premises as in the derivation of the generalized differential equation governing the pressure within the interspace between axisymmetric shells. Using (103), (104), and (105), we get Webster's horn equation:

$$\frac{1}{c^2} \frac{\partial^2 p}{\partial t^2} - \frac{\partial p}{\partial x} \frac{d}{dx} \ell n\, S(x) - \nabla^2 p = 0 \tag{106}$$

Assuming $e^{im\phi}$ and $e^{-i\omega t}$ dependence, this equation becomes:

$$\frac{\partial^2 p}{\partial x^2} + \frac{\partial p}{\partial x}\frac{d}{dx}\ell n\, S(x) + \left[k^2 - \frac{m^2}{r^2(x)} \right] p = 0 \qquad (107)$$

The interspace counterpart is:

$$\frac{\partial^2 p}{\partial s^2} + \frac{\partial p}{\partial s}\frac{d}{ds}\ell n[w(s)\, r(s)] + \left[\left(k^2 - \frac{m^2}{r^2(s)} \right) \right] p = 0 \qquad (108)$$

Even though these equations are identical in form, with $S(x)$ corresponding to $w(s)r(s)$, there is an essential difference which should be noticed. Whereas the assumption governing the Webster equation is that the maximum value of $r(x)$ $(= \sqrt{S(x)/\pi})$ is small compared with the wavelength, the interspace equation is only restricted in that $w(s)$ is small compared with the wavelength. The product $w(s)r(s)$ may be large. Thus, it appears that the range of validity of the interspace equation is greater than that of the Webster equation.

Extensive work on the Webster horn equation has been done by Salmon (Ref. 30). For the $m = 0$ case, Salmon found a solution for horns characterized by:

$$r(x) = r_o \left[\cosh\left(\frac{x}{H} \right) + T \sinh\left(\frac{x}{H} \right) \right] \qquad (109)$$

where r_o is the initial radius, H is a "flare" factor, and T is the shape factor which varies from zero to infinity.

$T = \infty$: Conical Horn

$T = 1$: Exponential Horn

$T = 0$: Catenoidal Horn

Salmon's solution to the Webster equation is:

$$p = \frac{1}{r(x)} \left[P_o e^{\frac{i\omega}{c}(\beta x - ct)} + P_R e^{-\frac{i\omega}{c}(\beta x - ct)} \right] \qquad (110)$$

where

$$\beta \equiv \sqrt{1 - \left(\frac{c}{\omega_H} \right)^2} \qquad (111)$$

For particular shape factors and for $m \neq 0$, Webster's horn equation can be solved. These will not be enumerated here.

A difficulty in the analysis of interspace acoustics lies in the fact that most problems considered are not analytically solvable. It is useful, therefore, to establish an approximate method for analyzing the acoustic properties, and the acoustic resonant frequencies in particular, of axisymmetric enclosures. The validity of the approximation method can be verified, in part, by comparison with results obtained from an analytical study of simple horn shapes.

The Rayleigh-Ritz Method

An approximation technique useful for finding resonant frequencies is the Rayleigh-Ritz method. This method is based on Rayleigh's principle, which states that "in the fundamental mode of vibration of an elastic system, the distribution of kinetic and potential energies is such as to make the frequency a minimum (Ref. 31). Since "the frequency of vibration varies as the square root of the ratio of stiffness to inertia, any constraint applied to a system will increase the frequency" (Ref. 30). Thus, "if we consider any constrained mode of vibration and calculate its mean potential and kinetic energies, the result of equating them will yield the frequency of this constrained mode, which is necessarily not less than the frequency of free vibrations" (Ref. 30). This energy method, therefore, yields an upper limit to the natural frequency of vibration. The accuracy of the method is based on the fact that first-order changes in energy produce only second-order changes in frequency. In the language of the calculus of variations, the first-order variation of energy with respect to frequency is zero.

Illustration of Rayleigh-Ritz Approximation Method

A simple example will prove to be both an illustration and verification of the Rayleigh principle. Consider an exponential horn for m = 0, specified as in Fig. 26. We shall first solve for the resonances analytically.

Analytical Treatment.—The solution of the Webster's differential equation can be written

$$p(x) = e^{-x/H}\left[P_o\, e^{-i\beta kx} + P_R\, e^{+i\beta kx} \right] \qquad (112)$$

where

$$\beta \equiv \left(1 - \frac{1}{H^2k^2} \right)^{1/2} \qquad (113)$$

Applying the two boundary conditions:

$$\left.\frac{dp}{dx}\right|_{x = 0} = \left.\frac{dp}{dx}\right|_{x = \ell} = 0$$

we get:

$$\cos\left[4\sqrt{\frac{H^2k^2 - 1}{H}} \right] = 1, \text{ or } \frac{4\sqrt{H^2k^2 - 1}}{H} = 2n\pi$$

Solving for k_n^2:

$$k_n^2 = \left(\frac{n\pi}{2} \right)^2 + \frac{1}{H^2} \qquad (114)$$

which specifies the resonances.

Rayleigh Approximation.- We must first pick a shape function representing a constrained mode of vibration. Our first attempt at finding this shape function might be a third-order

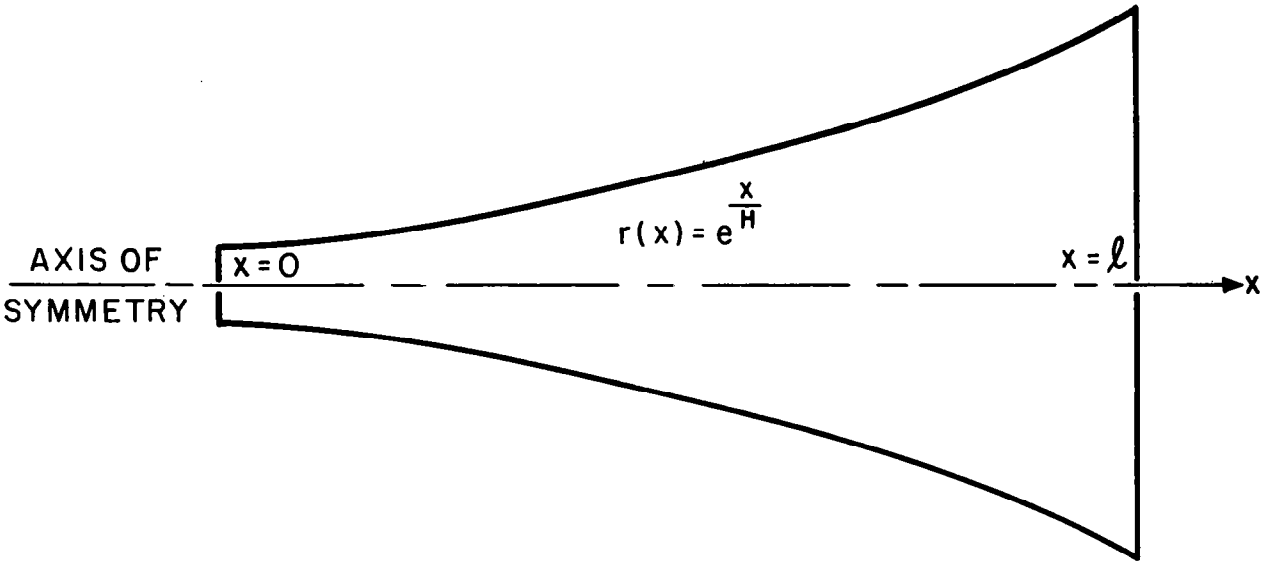

FIG. 26 SKETCH OF AN EXPONENTIAL HORN TO BE STUDIED ANALYTICALLY AND BY THE RAYLEIGH-RITZ APPROXIMATION METHOD

polynomial weighted by $e^{-x/H}$, i.e.

$$\psi = e^{-x/H} (ax^3 + bx^2 + cx + d) \tag{115}$$

where the pressure is given by $p = A\psi$. With the boundary conditions:

$$\left.\frac{dp}{dx}\right|_{x=0} = \left.\frac{dp}{dx}\right|_{x=\ell} = 0, \text{ and } p(x)\Big|_0 = 1, \; p(x)\Big|_\ell = (-1)\, e^{-\ell/H}$$

the shape function becomes

$$\psi = e^{-x/H} \left(\frac{x^3}{2} - \frac{3}{2} x^2 + 1 \right) \tag{116}$$

We must now find the mean kinetic and potential energies. The incremental energies can be written:

$$\begin{aligned} \Delta T &= \text{incremental kinetic energy} = \tfrac{1}{2} \rho \left|u\right|^2 \Delta\tau \\ \Delta V &= \text{incremental potential energy} = \frac{p^2}{2\rho c^2} \Delta\tau \end{aligned} \tag{117}$$

where

$$\Delta\tau \text{ (incremental volume)} = S(x)\, \Delta x = \pi r^2(x)\, \Delta x = \pi e^{2x/H}\, \Delta x \tag{118}$$

From the force equation:

$$\rho_o \frac{\partial u}{\partial t} = - \frac{\partial p}{\partial x}$$

Assuming $e^{-i\omega t}$ harmonic dependence, we have:

$$u = -\frac{1}{\omega\rho_o}\frac{\partial p}{\partial x}$$

or

$$|u|^2 = \left|\frac{\partial p}{\partial x}\right|^2 \Big/ \omega^2\rho_o^2 \tag{119}$$

Therefore, the mean energies can be written:

$$\overline{T} = \frac{1}{2}T = \frac{1}{2}\int_0^{\ell} dT = \frac{1}{2}\int_0^{\ell}\frac{1}{2}\rho|u|^2 S(x)dx = \frac{\pi}{4\rho\omega^2}\int_0^{\ell}\left(\frac{\partial p}{\partial x}\right)^2 e^{2x/H}dx \tag{120}$$

$$\overline{V} = \frac{1}{2}V = \frac{1}{2}\int_0^{\ell} dV = \frac{1}{2}\int_0^{\ell}\frac{1}{2}\frac{p^2}{\rho_o c^2} S(x)dx = \frac{\pi}{4\rho_o c^2}\int_0^{\ell} p^2\, e^{2x/H}dx \tag{121}$$

We must now find $\left(\frac{\partial p}{\partial x}\right)^2$ and p^2. After some simple steps we have:

$$\left(\frac{\partial p}{\partial x}\right)^2 = \left[\frac{x^6}{4H^2} - \frac{3}{2H}\left(1+\frac{1}{H}\right)x^5 + \left[\frac{3}{H} + \frac{9}{4}\left(1+\frac{1}{H}\right)^2\right]x^4 + \left[\frac{1}{H^2} - 9\left(1+\frac{1}{H}\right)\right]x^3 + \left[-\frac{3}{H}\left(1+\frac{1}{H}\right)+9\right]x^2 + \frac{6}{H}x + \frac{1}{H^2}\right]e^{-2x/H} \tag{122}$$

and

$$p^2 = \left(\frac{x^6}{4} - \frac{3}{2}x^5 + \frac{9}{4}x^4 = x^3 - 3x^2 + 1\right)e^{-2x/H} \tag{123}$$

According to Rayleigh's principle, we can equate the average potential and kinetic energies and solve for the frequency. This yields:

$$k^2 = \frac{\omega^2}{c^2} = \frac{\int_0^{\ell}\left(\frac{\partial p}{\partial x}\right)^2 e^{2x/H}\,dx}{\int_0^{\ell} p^2\, e^{2x/H}\,dx} \tag{124}$$

If we take $\ell = 2$, as an example, then

$$0.97\ k^2 = \left[\frac{32}{7H^2} - \frac{16}{H}\left(1 + \frac{1}{H}\right) + \left[\frac{3}{H} + \frac{9}{4}\left(1 + \frac{1}{H}\right)^2\right]\frac{32}{5} + 4\left[\frac{1}{H^2} - 9\left(1 + \frac{1}{H}\right)\right]\right.$$

$$\left. + 8\left(-\frac{1}{H}\left(1 + \frac{1}{H}\right) + 3\right) + \frac{12}{H} + \frac{2}{H^2}\right] \qquad (125)$$

We can now compare both methods:

	Approx. Rayleigh $k^2 = \omega^2/c^2$	Exact Analytical $k^2 = \omega^2/c^2$
$H \to \infty$	2.474	2.467
$H = 10$	2.484	2.477

Note that, if we had guessed a shape function, $\psi = \cos\frac{\pi x}{2}\, e^{-x/H}$, we would have obtained the exact analytic results, as expected, since we would have picked the exact mode shape of free vibrations. Note also that the exact results are lower than the approximate results. Theory suggests that this is a general result.

We are led to believe, therefore, that the Rayleigh approximation method applies with sufficient accuracy to horns as well as spaces between two axisymmetric shells, if mode shape functions are carefully chosen.

Ritz's Contribution

Now let us indicate Ritz's contribution to the Rayleigh-Ritz method. To improve the accuracy of the estimation, a second term is often added to the shape function as a way of better approximating the mode shape of free vibrations. That is, we use

$$\psi = \psi_o + \alpha\psi_1 \tag{126}$$

where ψ_1 also satisfies the boundary conditions. We then proceed as before, now solving for $k = \frac{\omega}{c} = \frac{\omega(\alpha)}{c}$. We desire that value of the parameter α for which the variation of ω with respect to α is a minimum, that is, the value α_o, that satisfies

$$\frac{d\omega}{d\alpha} = 0 \tag{127}$$

Having optimized our solution, we then obtain $\omega = \omega(\alpha_o)$. With this method, the exact solution is presumed to be approximated more exactly.

Application to Apollo CM Acoustic Model

The acoustic model of the Apollo CM is shown again in Fig. 27 The first task in analyzing the natural resonances of the interspac is to establish the boundary conditions on the pressure. The boundary conditions are applied at the poles of symmetry: s = 0 and s = S. At these positions the geometry is similar to that of a disc or pill box, Fig. 28. The pressure field for a space having this shape is proportional to $J_m(kr)\cos m\phi$.

The functional behavior of the field will be:

$m = 0$; $\frac{\partial J}{\partial r}(kr)\Big|_{r=0} = 0$; $J(0) = 1$; behaves as a (cosine) for long wavelength. (128a)

$m = 1$; $\frac{\partial J}{\partial r}(kr)\Big|_{r=0} \neq 0$; $J(0) = 0$; behaves as a (sin) for long wavelength. (128b)

$m > 1$; $\frac{\partial J}{\partial r}(kr)\Big|_{r=0} = 0$; $J(0) = 0$; behaves as (1-cos) for long wavelength. (128c)

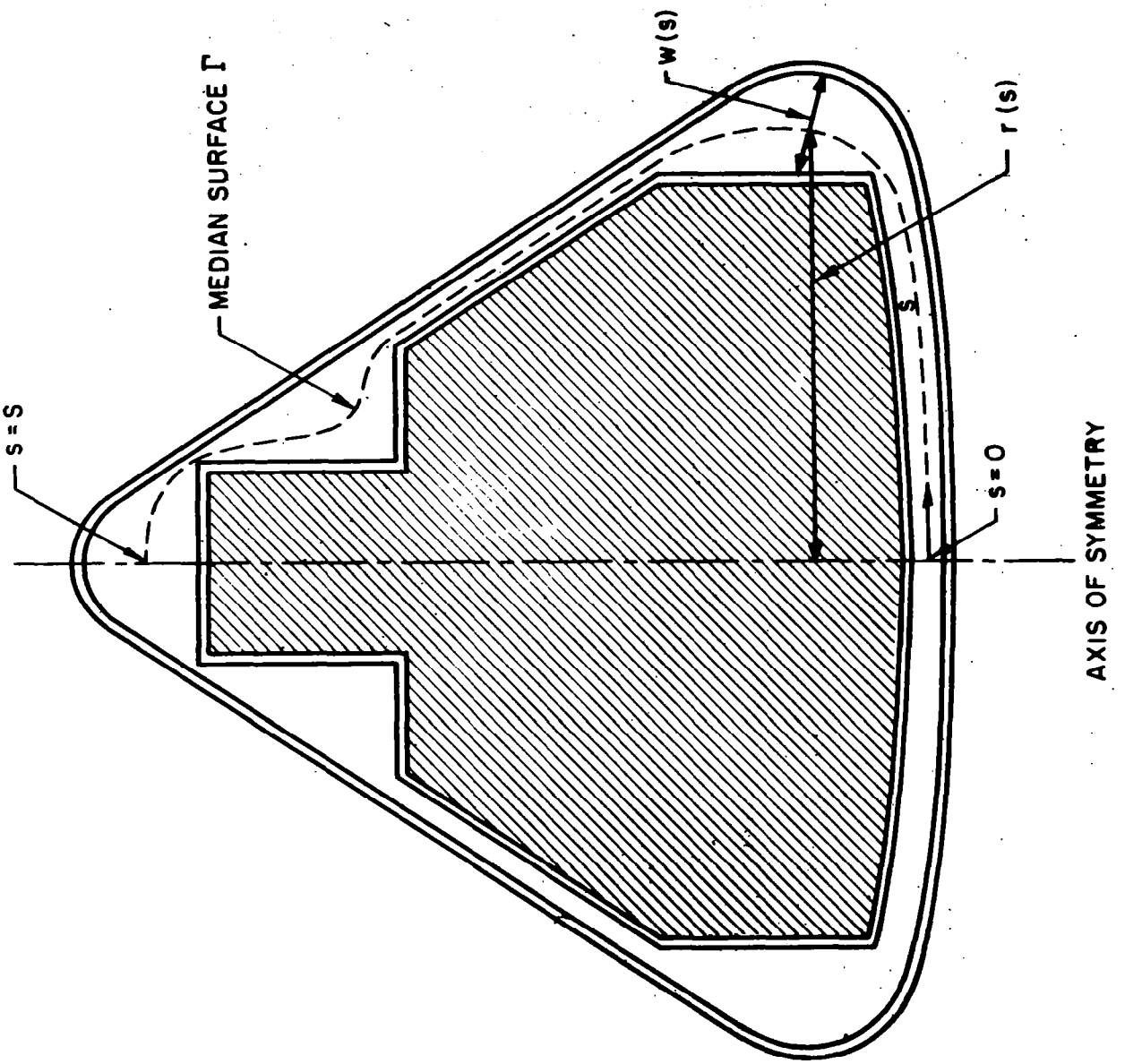

FIG. 27 ACOUSTIC MODEL OF APOLLO COMMAND MODULE SHELL. MEDIAN COORDINATE s. w(s) EVERYWHERE PERPENDICULAR TO s. r(s), POLAR COORDINATE, DRAWN TO CENTER OF w(s)

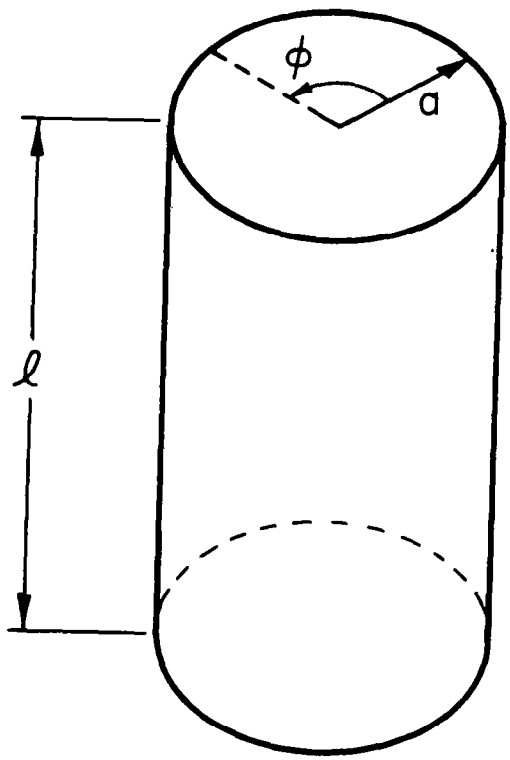

FIG. 28 DISC OR " PILL BOX ". $a \ll \ell$. THE PRESSURE DISTRIBUTION IS PROPORTIONAL TO $J_m(kr)$ COS $m\Phi$

These conditions are to be met both at $s = 0$ and at $s = S$. This suggests the following shape functions:

$$m = 0;\ \psi = \cos \frac{n\pi s}{S} \tag{129a}$$

$$m = 1;\ \psi = \sin\left(\frac{n\pi s}{S}\right) \cos m\phi \tag{129b}$$

$$m > 1;\ \psi = \left[\, 1-\cos \frac{2n\pi s}{S} \,\right] \cos m\phi \tag{129c}$$

Considering ϕ dependence also, we have for the particle velocity:

$$\left|u_s\right| = \frac{1}{\omega\rho_o}\left|\frac{\partial p}{\partial s}\right| \tag{130}$$

$$\left|u_\phi\right| = \frac{1}{\omega\rho_o r(s)}\left|\frac{\partial p}{\partial \phi}\right| \tag{131}$$

The incremental kinetic energy can now be written:

$$\Delta T = \frac{1}{2}\rho|u|^2\,\Delta\tau = \frac{1}{2}\rho\left(|u_s|^2 + |u_\phi|^2\right)\Delta\tau = \frac{1}{2\rho\omega^2}\left[\left(\frac{\partial p}{\partial s}\right)^2 + \frac{1}{r^2(s)}\left(\frac{\partial p}{\partial \phi}\right)\right]^2 \Delta\tau \tag{132}$$

where (see Fig. 24)

$$\begin{aligned}\Delta\tau &= w(s)\ r(s)\ \Delta s\ \Delta\phi \\ &= A(s)\ \Delta s\ \Delta\phi\end{aligned} \tag{133}$$

and (see Fig. 29)

$$A(s) \equiv w(s)\ r(s)$$

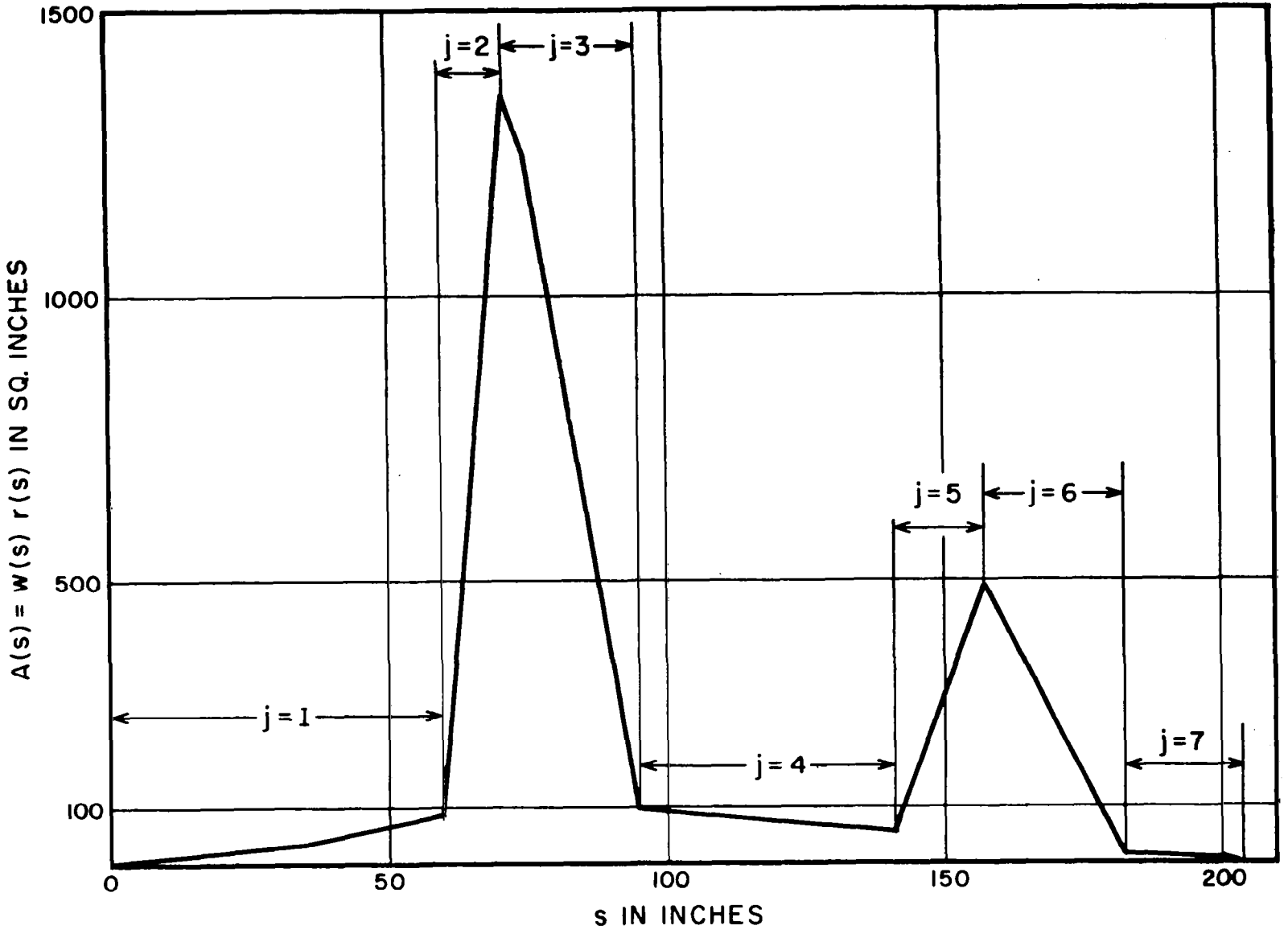

FIG. 29 PLOT OF A(s) VERSUS s

$\Delta\tau$ is the same as in previous discussion. Therefore, equating mean potential and kinetic energies, we get:

$$k^2 = \left(\frac{\omega}{c}\right)^2 = \frac{\int_0^{2\pi}\int_0^{S}\left[\left(\frac{\partial p}{\partial s}\right)^2\right]A(s)\,ds\,d\phi + \int_0^{2\pi}\int_0^{S}\frac{1}{r^2(s)}\left(\frac{\partial p}{\partial \phi}\right)^2 A(s)\,ds\,d\phi}{\int_0^{2\pi}\int_0^{S} p^2\,A(s)\,ds\,d\phi} \tag{134}$$

Let us now investigate the product $w(s)\,r(s) = A(s)$. In Fig. 29 we have plotted $A(s)$ vs s. We can see that, to a very good approximation, $A(s)$ can be represented as seven linear segments, $c_j\,s + d_j$. (The values of the variables s, $r(s)$, $w(s)$, $A(s)$, c_j, and d_j are tabulated in Table II.) This linear property suggests that integrals that we encounter such as

$$\int_0^{S}\left\{\begin{array}{c}\sin^w\left(\frac{n\pi s}{S}\right)\\ \\ \cos^w\left(\frac{n\pi s}{S}\right)\end{array}\right\}A(s)\,ds \tag{135}$$

be written as:

TABLE II

VALUES OF VARIABLES USED IN CALCULATIONS

s	r(s)	w(s)	$A(s) = w(s)r(s)$	c_j	d_j	$\left[\overline{r^2}(s_j)\right]^{1/2}$
inches	inches	inches	sq.inches	slope	intercept	sq.inches
0	0	1	0	1.46	0	not used
60.0	58.2	1.5	87.3	112.8	-6681.3	62.1
71.2	65.9	20.5	1350.95	-53.3	5147	64
94.8	61.6	1.5	92.40	-.8	168.5	49
141.6	36.8	1.5	55.20	27.5	-3839	29.4
157.6	22.0	22.5	495.00	-18.7	3440.8	19.2
183.2	16.4	1.0	16.40	-.80	164.7	9
203.6	0	24.5	0			

$$\sum_{j=1}^{7} \left[\int_{s_j}^{s_{j+1}} \left\{ \begin{matrix} \sin^w \frac{n\pi s}{S} \\ \cos^w \frac{n\pi s}{S} \end{matrix} \right\} (c_j s + d_j) \right] ds \qquad (136)$$

where w can be 1, 2, 3, 4, ---. Such integrals may be handled analytically and summed as indicated.

m=0. - For the m = 0 case

$$\psi = \cos \frac{n\pi s}{S} \qquad (137)$$

$$p = A\psi = A \cos \frac{n\pi s}{S} \qquad (138a)$$

$$\frac{\partial p}{\partial s} = - A \frac{n\pi}{S} \sin \frac{n\pi s}{S} \qquad (138b)$$

$$\frac{\partial p}{\partial \phi} = 0 \qquad (138c)$$

This yields:

$$\kappa^2 = \frac{\left(\frac{n\pi}{S}\right)^2 \int_0^S \sin^2 \left(\frac{n\pi s}{S}\right) A(s) ds}{\int_0^S \cos^2 \left(\frac{n\pi s}{S}\right) A(s) ds} = \frac{\left(\frac{n\pi}{S}\right)^2 \sum_{j=1}^{7} \int_{s_j}^{s_{j+1}} \sin^2 \left(\frac{n\pi s}{S}\right) (c_j s + d_j) ds}{\sum_{j=1}^{7} \int_{s_j}^{s_{j+1}} \cos^2 \left(\frac{n\pi s}{S}\right) (c_j s + d_j) ds} \qquad (139)$$

The values of c_j and d_j are taken from Table II.

m = 1. - For the m = 1 case

$$\psi = \sin \frac{n\pi s}{S} \cos m\phi \tag{140a}$$

$$p = A\psi = A \sin \frac{n\pi s}{S} \cos m\phi \tag{140b}$$

$$\frac{\partial p}{\partial s} = A \frac{n\pi}{S} \cos \frac{n\pi s}{S} \cos m\phi \tag{140c}$$

$$\frac{\partial p}{\partial \phi} = - mA \sin \left(\frac{n\pi s}{S}\right) \sin m\phi \tag{140d}$$

This yields:

$$k^2 = \frac{\left(\frac{n\pi}{S}\right)^2 \int_0^{2\pi}\int_0^S \cos^2 \left(\frac{n\pi s}{S}\right) \cos^2 m\phi \, A(s) ds d\phi}{\int_0^{2\pi}\int_0^S \sin^2 \left(\frac{n\pi s}{S}\right) \sin^2 m\phi \, A(s) ds d\phi}$$

$$+ \frac{m^2 \int_0^{2\pi}\int_0^S \sin^2 \left(\frac{n\pi s}{S}\right) \sin^2 m\phi \, \frac{A(s)}{r^2(s)} \, ds d\phi}{\int_0^{2\pi}\int_0^S \sin^2 \left(\frac{n\pi s}{S}\right) \sin^2 m\phi \, A(s) \, ds d\phi} \tag{141}$$

These integrals can be handled as before except for the one containing the $r^2(s)$ in the denominator. Since $A(s) = r(s)w(s)$ and $r(s) \approx s$ for $s = 0 \rightarrow 60$ in. and $w(s) \approx 1$ in. for $s = 0 \rightarrow 60$ in., we can write this integral as:

$$m^2 \int_0^{2\pi} \sin^2 m\phi \, d\phi \left[\int_0^{60} \frac{\sin^2\left(\frac{n\pi s}{S}\right)}{s} ds \right.$$

$$\left. + \sum_{j=2}^{7} \frac{1}{\overline{r^2}(s_j)} \int_{s_j}^{s_{j+1}} \sin^2 \left(\frac{n\pi s}{S}\right)(c_j s + d_j) ds \right] \qquad (142)$$

We replace r(s) in Eq. (141) by its rms value $[\overline{r^2}(s_j)]^{1/2}$ It is then removed from the second integral since its variation is relatively slow. This rms radius is also tabulated in Table II. The solution of the first integral is an infinite sum, the first several terms of which yield the required accuracy.

<u>m > 1</u>.- For the m > 1 case

$$\psi = \left(1 - \cos \frac{2n\pi s}{S}\right) \cos m\phi = 2 \sin^2 \left(\frac{n\pi s}{S}\right) \cos m\phi \qquad (143a)$$

$$p = A\psi = 2A \sin^2 \left(\frac{n\pi s}{S}\right) \cos m\phi \qquad (143b)$$

$$\frac{\partial p}{\partial s} = \frac{2n\pi}{S} A \sin \frac{2n\pi s}{S} \cos m\phi \qquad (143c)$$

$$\frac{\partial p}{\partial \phi} = - mA \left[1 - \cos \left(\frac{2n\pi s}{S}\right)\right] \sin m\phi \qquad (143d)$$

This yields:

$$k^2 = \frac{\left(\frac{n\pi}{S}\right)^2 \int_0^{2\pi}\int_0^{S} \sin^2\left(\frac{n\pi s}{S}\right) \cos^2 m\phi \, A(s) ds d\phi}{4 \int_0^{2\pi}\int_0^{S} \sin^4\left(\frac{n\pi s}{S}\right) \cos^2 m\phi \, A(s) ds d\phi}$$

$$+ \frac{4m^2 \int_0^{2\pi}\int_0^{S} \frac{\sin^4\left(\frac{n\pi s}{S}\right) \cos^2 m\phi \, A(s)}{r^2(s)} ds d\phi}{4 \int_0^{2\pi}\int_0^{S} \sin^4\left(\frac{n\pi s}{S}\right) \cos^2 m\phi \, A(s) ds d\phi} \qquad (144)$$

These integrals are handled in a similar manner to those previously discussed.

Ritz Modification

The Ritz modification, as discussed above, is straightforward. Reviewing, the mode-shape function is represented by a linear sum:

$$\psi(s,\phi) = \left[\psi_o(s) + \alpha \psi_1(s) \right] \cos m\phi \qquad (145)$$

where α is a parameter to be optimized. A procedure for picking $\psi_1(s)$ that satisfies the boundary conditions is to write

$$\psi_1(s) = \psi_o(2s) \qquad (146)$$

This constitutes, in effect, the addition of a second spatial harmonic term. The shape functions become:

$$m = 0 \quad \psi = \left[\cos\left(\frac{n\pi s}{S}\right) + \alpha \cos\left(\frac{2n\pi s}{S}\right)\right] \tag{147a}$$

$$m = 1 \quad \psi = \left[\sin\left(\frac{n\pi s}{S}\right) + \alpha \sin\left(\frac{2n\pi s}{S}\right)\right] \cos\phi \tag{147b}$$

$$m > 1 \quad \psi = \left[\left(1 - \cos\frac{2n\pi s}{S}\right) + \alpha\left(1 - \cos\frac{4n\pi s}{S}\right)\right] \cos m\phi \tag{147c}$$

After integration, the result is in the form

$$k^2 = \frac{A + B\alpha + C\alpha^2}{D + E\alpha + F\alpha^2} \tag{148}$$

We take the derivative, $d(k^2)/d\alpha$, and set it equal to zero. This allows us to solve for <u>two</u> values of α. The value of α that reduces the frequency from the $\alpha = 0$ case is chosen as the proper coefficient of the second harmonic term. Preliminary results for $\alpha = 0$ (Rayleigh) and $\alpha \neq 0$ (Rayleigh-Ritz) are recorded in Tables III, IV, and V.

Conclusions

According to the results in Tables III, IV, and V, it is evident that, for the $n = 1$; $m = 0,1$ modes, the resonant frequencies are below 50 Hz. The possibility of sound transmission into the inner shell of the Apollo CM model is dependent upon whether this resonance condition is accompanied by a significant volume displacement. A measure of this volume displacement is obtained from mean pressure calculations which were carried out for $m = 0$; $n = 1,2,3$. The assumed mode shape is, as before:

$$p = A\psi = A\left(\cos\frac{n\pi s}{S} + \alpha \cos\frac{2n\pi s}{S}\right)$$

TABLE III

RESONANT FREQUENCIES FOR m=0

ASSUMED MODE SHAPE: $\psi = \cos \frac{n\pi s}{S} + \alpha \cos 2\frac{n\pi s}{S}$

n = 1		n = 2		n = 3	
α	f Hz	α	f Hz	α	f Hz
0	50.4	0	83.4	0	85.5
-0.361	40.5	0.234	75.8	-0.059	80.9

TABLE IV

RESONANT FREQUENCIES FOR m=1

ASSUMED MODE SHAPE: $\psi = \left(\sin \frac{n\pi s}{S} + \alpha \sin 2\frac{n\pi s}{S}\right)\cos m\phi$

n = 1		n = 2		n = 3	
α	f Hz	α	f Hz	α	f Hz
0	54.8	0	87.6	0	146.1
0.476	43.2	-0.422	78.9	0.350	131.4

TABLE V

RESONANT FREQUENCIES FOR m > 1

ASSUMED MODE SHAPE:

$$\psi = \left[\left(1-\cos\ 2\frac{n\pi s}{S}\right) + \alpha\left(1-\cos\ 4\frac{n\pi s}{S}\right)\right] \cos\ m\phi$$

	n = 1	
	α	f Hz
m = 2	0	87.0
	-0.302	80.5
m = 3	0	124.3
	-0.388	106.1
m = 4	0	162.7
	-0.418	132.9
m = 5	0	201.6
	-0.432	160.7

Normalizing at the boundaries (setting A = 1) we get:

	(n=1)	(n=2)	(n=3)
$\bar{P}$ (Mean Pressure) $= \dfrac{\int_0^S PA(s)ds}{\int_0^S A(s)ds} =$	.195	-.435	-.413
Resonant Frequency (Hz)	40.5	75.8	80.9

When m = 0, the pressure has a maximum value of -1.361 at s = S. We see,therefore, that the mean pressure is about 15% of the maximum pressure. For n = 2 and 3 the mean pressure is over 30% of the maximum value. It should be realized that the mean pressure is calculated for an approximate mode shape. The percentage error in mean pressure calculations may be significantly higher than in resonant frequency calculations. Nevertheless, these calculations indicate the possibility of potentially undesirable acoustic resonances of the interspace.

EFFECT OF INTERSPACE RESONANCE ON NOISE REDUCTION OF THE COMMAND MODULE

In this section we shall calculate the degree to which the lowest axisymmetric resonant mode (m = 0, n = 1) of the CM interspace can be excited by a uniform acoustic pressure applied to the CM exterior. We shall use the principle of reciprocity in deriving an expression for the NR.

General Formulation of NR

The principle of reciprocity in acoustics states: if a source of volume velocity is placed at one position in a passive acoustical system at rest and the resulting sound pressure is measured by a receiver at some other position, then the same pressure will be measured if the positions of source and receiver are interchanged. Suppose we inject a known volume velocity at a point in the interspace of the CM,

at the resonance frequency of the m = 0, n = 1 mode of the interspace. We then calculate the amplitude to which the mode is excited, and from it the deflection of the outer shell it produces, and then the pressure which results at a test point far from the CM. Reciprocity tells us that this same pressure will be produced at the original source point in the interspace if the volume velocity source is placed at the test point far from the CM. If we can then calculate the pressure produced just outside the CM, we shall know the noise reduction of the system.

At s = 0, we inject a volume velocity $U_o e^{-i\omega t}$. (Hereafter, we assume $e^{-i\omega t}$ time dependence for all acoustic field variables. As a phase reference, we take U_o to be real.) The frequency ω is the resonance frequency of the lowest mode of the interspace. The volume velocity U_o produces a pressure in the interspace $p_o\psi(s)$, where ψ is the dimensionless pressure mode shape normalized so that $\psi(0) = 1$. The quantity p_o is the peak pressure produced at s = 0.

We assume that we know the loss factor of the resonant mode. The loss factor η is defined as

$$\eta = \frac{\text{average power dissipated}}{\omega \cdot \text{maximum potential energy}} \tag{149}$$

Since we are operating at resonance, the input impedance seen by U_o is purely resistive, and therefore p_o is real. The average power dissipated, which is equal to the power supplied by U_o, is thus $p_o U_o/2$. We can now calculate the pressure magnitude p_o in terms of η and U_o.

The time-wise maximum potential energy of the system is

$$(P.E.)_{max} = \frac{\pi}{\rho c^2} \int_0^S [p_o\psi(s)]^2 A(s)ds \tag{150}$$

where $2\pi A(s)$ is the cross-sectional area of the interspace.

We can therefore write p_o as

$$p_o = \frac{\rho c^2 U_o}{2\pi\omega\eta \int_0^S \psi^2(s)A(s)ds} \tag{151}$$

We now wish to find the volume velocity emitted by the CM through the outer shell due to the source U_o. Let us call this volume velocity U_1. We can write

$$U_1 = - i\omega \int_0^S p_o \psi(s) C(s) ds \tag{152}$$

where C(s) is the acoustic compliance per unit length of the outer shell. The integral in Eq. (152) is the volume displacement; multiplication by $-i\omega$ is equivalent to taking the time derivative and changes this displacement to the corresponding velocity. The quantity C(s) is to be calculated from the membrane theory for rotationally symmetric shells developed in Chapter III. Here it is assumed that the motion of the shell is stiffness-controlled; i.e., that the resonance frequency of the interspace mode being studied is well below any resonances of the outer shell. It is also assumed in Eq. (152) that the pressure on the outside of the outer shell due to radiation loading is negligible compared with the modal pressure in the interspace.

Let us now consider a test point relatively far from the CM, and assume that the frequency is low enough so that the CM behaves like a simple source. The volume velocity U_o, injected at s = 0 in the interspace, produces a pressure p_2 at the test point. We can also consider p_2 to be produced by the emission of volume velocity U_1 by the CM. According to the principle of reciprocity, if we now inject U_o at the test point, a pressure p_2 will result at s = 0. Furthermore, the pressure just outside the CM will be related to U_o in the same way that p_2 was related to U_1 when the CM was radiating. Let us call this pressure just external to the CM p_1. We have then

$$p_1 = \frac{U_o p_2}{U_1} \tag{153}$$

But the quantity we seek is the pressure in the CM in response to a uniform external pressure, or

$$\frac{p_2}{p_1} = \frac{U_1}{U_o} \tag{154}$$

If we substitute in Eq. (152) the value of p_o given by Eq. (151) we obtain

$$\frac{U_1}{U_o} = -i \frac{\rho c^2 \int_0^S \psi(s)C(s)ds}{2\pi\eta \int_0^S \psi^2(s)A(s)ds} = \frac{p_2}{p_1} \qquad (155)$$

The pressure distribution in the interspace, in response to an externally applied pressure p_1, is then $\psi(s)p_2$.

To achieve the best noise reduction we must minimize p_2/p_1. From Eq. (152) it is obvious that, all other factors remaining constant, we must maximize η. One could increase η somewhat by introducing damping material into the interspace. (The lowest η is obtained if the only source of damping is radiation from the CM.)

Numerical Calculation of NR at Interspace Resonance Frequency

In the preceding section we derived Eq. (155) for the NR of the outer shell at the frequency of the fundamental resonance of the interspace. In this section we shall evaluate this NR numerically.

In order to evaluate the integrals in (155), we must know three functions: $2\pi A(s)$, the cross-sectional area of the interspace; $\psi(s)$, the dimensionless pressure mode-shape function; and $C(s)$, the distributed compliance per unit length of the outer shell. The coordinate s is defined and functions $A(s)$ and $\psi(s)$ are given earlier in this chapter. As in the preceding section, we take $\psi(s)$ to be normalized so that $\psi(0) = 1$.

The small end and the base of the outer shell are essentially spherical caps and can reasonably be expected to be substantially stiffer than the conical section. We shall therefore assume that C(s) is zero, except for the conical section. This assumption should not have an appreciable effect on the value of the integral in the denominator of (155), since by using this assumption we are neglecting only a small contribution to the integral.

The distributed compliance, C(s), is just the ratio of the change in area of the cross section of the shell (a circle of radius r_o; see Fig. 10) to the pressure producing the change. To deduce its functional form we shall assume that the applied pressure varies slowly enough in space so that we may safely take the membrane forces at a point on the shell to be the same as those produced by a spatially uniform pressure equal in magnitude to the pressure applied at that point. The applied pressure will produce a fractional change in the radius of the cross section, r_o, equal to the circumferential strain, ϵ_θ. We then have

$$C(s) = \frac{\pi r_o^2 - \pi[r_o(1 + \epsilon_\theta)]^2}{p} = -\frac{2\pi r_o^2 \epsilon_\theta}{p} \qquad (156)$$

where p is the applied pressure and we have neglected the quadratic term in the strain. From Eqs. (28), (29), and (30) of Chapter III we find ϵ_θ for a cone under a uniform applied pressure. Using these relations, the equation for C(s) becomes

$$C(s) = -\frac{2\pi r_o^2 (N_\theta - \nu N_\phi)}{EAp} = \frac{(2 - \nu)\pi}{EA \sin\phi} r_o^3(s) \qquad (157)$$

With dimensions (in inches) taken from the Apollo CM, we have

$$C(s) = \frac{2\pi(2 - \nu)}{\sqrt{3}\ EA}(110 - 0.5\ s)^3 \qquad (158)$$

Using this expression for C(s), and the seven-segment linear approximation to A(s) and the Ritz-modified mode-shape function $\psi(s)$ taken from earlier sections of this chapter, Eq. (155) is found to give

$$\left|\frac{p_2}{p_1}\right| = 1.9 \times 10^3 \times \frac{\rho c^2 (2 - \nu)}{\eta E A} \qquad (159)$$

If we take $\rho c^2 = 20$ psi, $\nu = 0.3$, $E = 3 \times 10^7$ psi, $A = 0.016$ in. and $\eta = 0.02$, this beomes

$$\left|\frac{p_2}{p_1}\right| = 6.8 \qquad (160)$$

In other words, at the frequency of the fundamental interspace resonance, the pressure in the interspace at s = 0 exceeds the external acoustic pressure field by $20 \log_{10} 6.8 = 17$dB.

The NR of the inner shell is primarily determined by the compliance of the "top hat" structure at the upper end, the most compliant portion of the shell. Due to the form of the mode-shape function, $\psi(s)$, the average modal pressure in this region is some 3 dB higher than the pressure at s = 0. In Chapter III we calculated the NR of the inner shell to be about 12 dB. Thus, we anticipate that at the interspace resonance frequency the NR within the inner shell will drop to 12-17-3 = -8dB. This result is perhaps unduly pessimistic. It should not be too difficult to make η greater than 0.02. Also, it is clear, from the cubic dependence of C(s) upon r_o, that most of the volume-pumping excitation of the resonant mode occurs near the large end of the conical part of the outer shell. Since the most compliant part of the inner shell is near the small end, the belt of Q-felt which fills the interspace between the two ends would appear to be in a good location to help improve the NR at this resonance frequency.

CHAPTER VI

EXPERIMENTAL ANALYSIS AND TESTING

INTRODUCTION

The purpose of this chapter is threefold. First, we discuss the uses of experiments in vibration and acoustic analysis. This discussion is intended as a general guide to the purposes and methods of experimental analysis in sound transmission. Second, these methods are implemented in a series of (incomplete) experimental studies of various features of sound transmission in axisymmetric shells and spaces. These experiments are intended to clarify certain features of the acoustic and vibrational behavior of segments of the system. Finally, experimental models are described that can be used by NASA for comparison with the analyses presented here.

PURPOSES AND METHODS OF EXPERIMENTAL ANALYSIS

Structural configurations, such as the Apollo CM, that are exposed to acoustic environments, are subjected to experiments for a wide variety of purposes. Included in the field of environmental testing are experiments designed to "proof test" a structure. In such tests, the structure is subjected to an anticipated environment in order to determine whether or not its structural integrity and/or its operational behavior are affected by the environment. Tests may also be carried out at lower levels of excitation to determine anticipated response at locations where sensitive equipment may be mounted. Such tests make it possible for vibration and acoustic specifications to be generated for particular equipments.

A second class of experiments is designed to gather data on structural and acoustic parameters. These parameters are usually obtained experimentally, either because they cannot be directly or conveniently calculated or because it is desirable to correlate a calculation with an experimental study. Some experiments are designed to gather only a few bits of structural information, while others are designed to define almost all of the major parameters on the system. In either case the result of the experiment is a list of data to be used in theoretical analyses for the prediction of some other more complex bit of information about structural

behavior or sound transmission. The experiments on cylinders and cones described in this chapter fall within this category. In fact, we propose some measurements of structural parameters that can be calculated from theoretical concepts, thus enabling predictions of sound transmission to be based upon as much experimentally derived information as possible.

Finally, of course, there are experiments that could be called "research tests". Such experiments are used to test directly theoretical calculations of modal density, response ratios, damping, or other parameters. They may also be used to test theoretical assumptions about the way the structure is behaving in various segments, frequency ranges, or modes of motion. The experiments that we describe on interspace resonance fall in this category.

It is this use of experiment to determine the basic physical processes governing system behavior that we define as "experimental analysis". The structures or configurations used in the analysis of the Apollo CM, for example, might involve panels having the same membrane rigidity as the CM but having greatly differing flexural rigidity. If the NR shown by the model agrees with the theoretical analysis, and with tests on the CM itself, then the presumption that membrane stiffness controls the dominant behavior is valid.

The example above serves to exemplify the methods of experimental analysis. Frequently, the "model" will be quite different from the system being studied. The actual structure may consist of segmented sandwich structures with reinforcing frames and longerons. The model may be a homogeneous cylinder having one skin thickness when membrane stiffness is studied, a second thickness when flexural stiffness is studied, and a third thickness when structural resonances are studied.

Once the dominant mechanical behavior has been analyzed, changes in the model can be introduced to affect the response (or sound transmission) in a desired manner. If, for example, we find that resonant effects dominate, we might want to add structural damping. If stiffness effects dominate, a change in panel thickness could be introduced. Such changes can be tested in the model and then, if desirable, incorporated into the actual system for evaluation.

It has not been possible, during the course of this study, to carry out a complete experimental analysis of the Apollo CM acoustic model. We have been able to test some particular theoretical concepts, and such testing has enabled us to modify and improve our analyses. Three parts of the CM have been studied in some detail: the inner shell hatch cylinder (item 5), the exterior cone (items 1,2), and the shell interspace volume (item 11). These studies will now be described.

EXPERIMENTAL INVESTIGATIONS OF HATCH CYLINDER

Scaling of Hatch Section of Inner Shell

It is possible to investigate the NR of the CM in scale model. However, difficulties in the scaling process itself make this task complicated for such a complex structure. The approach we use is to scale the properties (membrane and/or flexural rigidity) of the various geometrical shapes appropriate to a given frequency range, and keep careful watch on the non-scaled properties (such as resonance frequencies and the non-scaled rigidity) to insure a valid experiment.

For the present investigation, a 1:4 scale of dimension was selected. The first model constructed was the inner shell hatch including the cylindrical section and the hatch cover, shown in Fig. 30. A linear dimension scale of 1:4 will give a frequency scale of 4:1 if the stiffness ratios are preserved. The NR will be invariant if all significant stiffnesses are scaled the same.

The hatch cover and hatch require both cylindrical and flat plate geometry in the first model. This requirement illustrates the dependence on the model described above, with a different scaling technique used for each kind of behavior. The cylindrical section responds to very slow pressure changes by changing radius uniformly as described in Chapter III. The appropriate property to scale is the in-plane stress, and, since this is borne by the faces of the sandwich structure, the scale cylinder section has a wall thickness of 1/4 the total of the inner and outer face thicknesses.

Such a scale model will be valid for static pressure changes and for very slowly varying pressure. It is logical to inquire: "What is the highest frequency for which such a scale model can be considered valid?" The answer to this question lies in the disposition of both the original and the scale-model resonant modes. For the hatch, the first resonance will be higher in the original than in the scale model, since we have scaled stiffness by 1:64 and mass by 1:4, increasing the mass-to-stiffness ratio. Concentrating our attention on the scale model, we find the first dishing mode to be at 600 Hz. Interpreting this for the original hatch, we can say that the first dishing mode is much higher than 150 Hz.

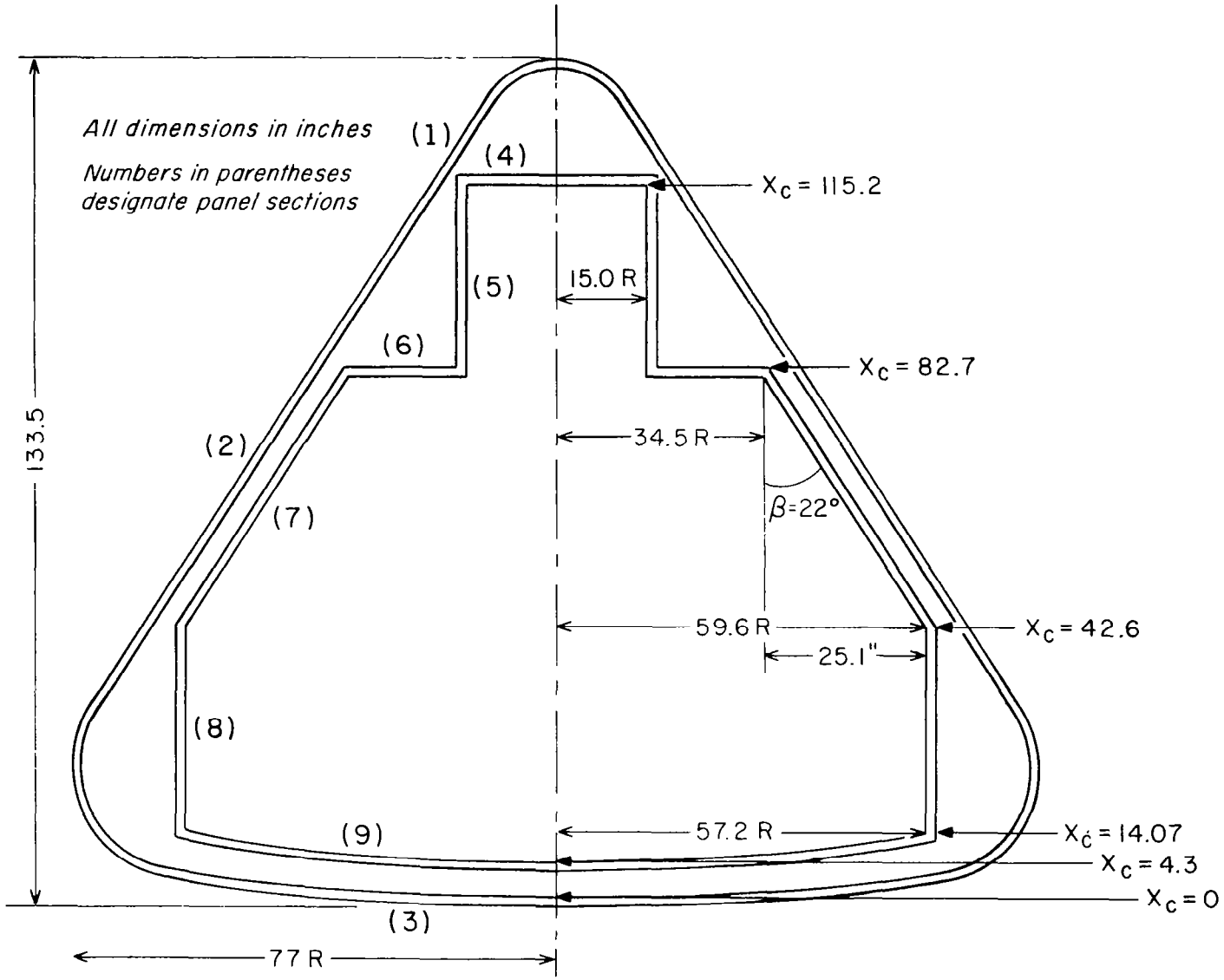

FIG. 30 OUTLINE OF APOLLO COMMAND MODULE SHELL

One set of resonant modes of the cylindrical shell involves bending waves in the shell along both the circumference and the height. Since only integral wavelengths are permitted along the circumference, no net volume displacement results from such modes. An observer located on the axis of the cylinder would see no pressure disturbance from such modes. The first radius expansion mode (ring mode, m = 0) will occur at f_{ring} = 4600 Hz in the 1:4 scale model, and 1150 Hz in the original structure. In summary. we could use such a model in experiments up to at least 300 Hz.

Quasi-Static Pressure Response Experiments

The low-frequency model tests are conducted by immersing the model into a spatially uniform pressure field. This field is generated in a sealed test chamber. Figure 31 shows the test

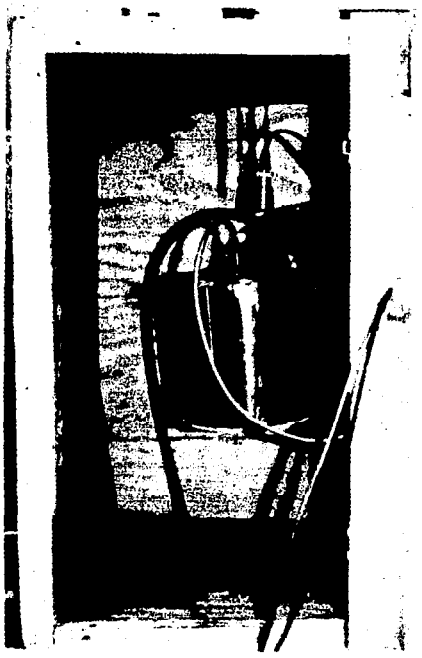

FIG. 31 SCALE MODEL IN TEST CHAMBER

chamber, a plywood box of inside dimensions 1.9 x 2.3 x 2.3 ft. An Altec-Lansing #20802 air-cooled high-intensity 15" loudspeaker mounted on one wall excites the air space. Quick-release catches allow access through the gasketed rear panel. Uniformity of the pressure field inside is assured by operation below the first acoustical resonance of the air space; the lowest mode occurs at 20 Hz to 200 Hz. This range would correspond to 5 Hz to 50 Hz in a full-scale experiment. The loudspeaker will produce sound pressure levels over 120 dB inside the box. Levels of 105 and 110 dB were used to provide adequate signal levels inside the scale model.

The electrical apparatus was arranged as shown in Fig. 32. The reference microphone is part of a feedback loop which amplitude-modulates the oscillator output and holds the sound pressure constant inside the test chamber. The motorized drive linking the oscillator and the pen recorder slowly sweeps the frequency range, and the recorder traces the amplitude of the sound pressure inside the model, as measured by the receiving microphone.

Vibration sensitivity of the microphones could be a significant source of error, since the reference microphone and the scale model hang from hooks in the top panel of the test enclosure. Panel resonances of the enclosure do occur in the experimental frequency range. Two approaches were combined to combat this problem. Stiffeners were used to increase the panel resonance frequencies. Applied damping to the panels is combined with spring-mass isolation for the receiving and reference microphones to provide considerable vibration reduction at the higher panel resonance frequency.

The measuring apparatus was first calibrated by selecting two microphones of nearly identical pressure-vs-frequency response, and adjusting the voltage gain of the sound level meters to give the same absolute response with excitation from a B and K pistonphone source standard. Since the experiment measures the difference between two levels, a final check is made by placing the receiver microphone in position without the model, and plotting the difference between it and the reference. With this difference set at zero, small values of NR can be measured quite accurately. This calibration procedure was repeated for each experiment.

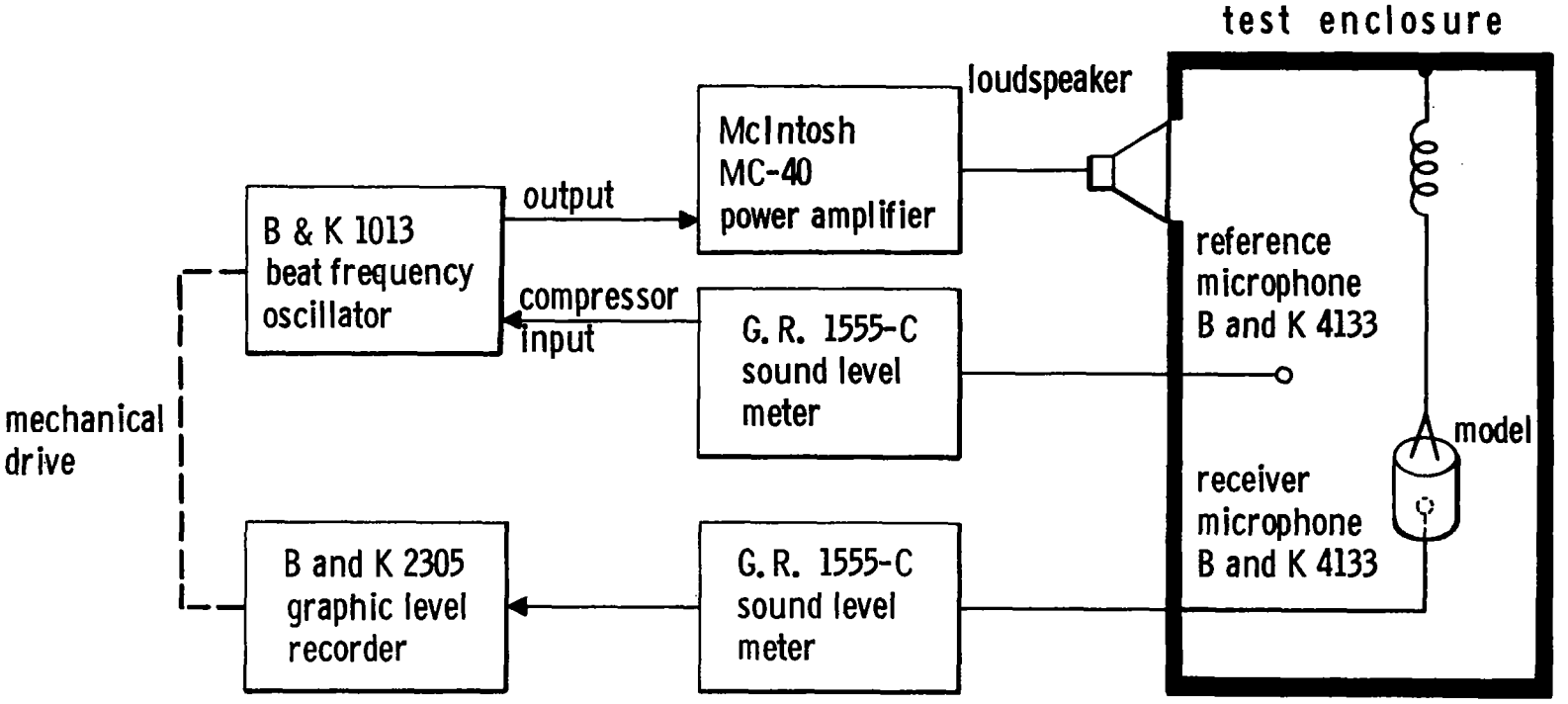

FIG. 32 EXPERIMENTAL APPARATUS

Constructed Models and Test Results

The cylindrical models that we shall examine are:

1) Cylindrical shell, scaling membrane (extensional) stiffness.

2) Cylindrical shell as above, with one end piece scaling the bending stiffness of the hatch cover.

   a) Set-in hatch (Fig. 33)

   b) Overlapping hatch (Fig. 34)

1) A cylinder with 1/2-in. thick end plates held rigidly apart by 1-in. diameter posts, as sketched in Fig. 35, was built with an 0.005-in. aluminum wall. Care was taken to ensure that the cylindrical wall was kept smooth and wrinkle-free. The

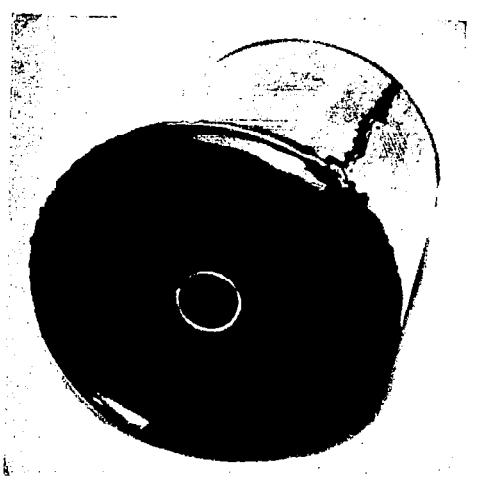

FIG. 33 SCALE MODEL OF SECTIONS 4 AND 5 OF APOLLO CM. THIS MODEL HAS A 7.0"-DIA. SET-IN END PLATE AND 0.005" WALL THICKNESS

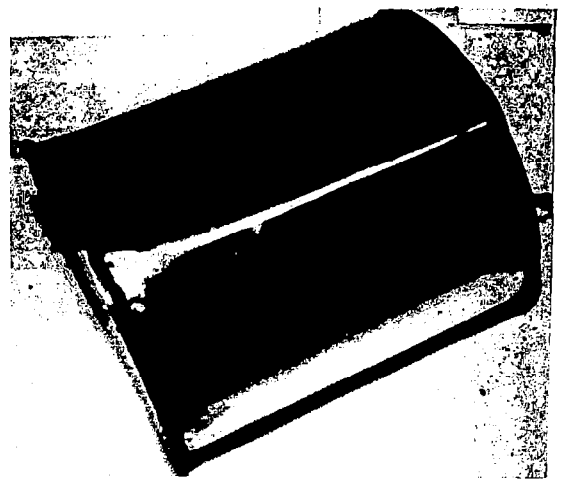

FIG. 34 SCALE MODEL AS IN FIG. 33 EXCEPT WITH 7.2"-DIA. END PLATE

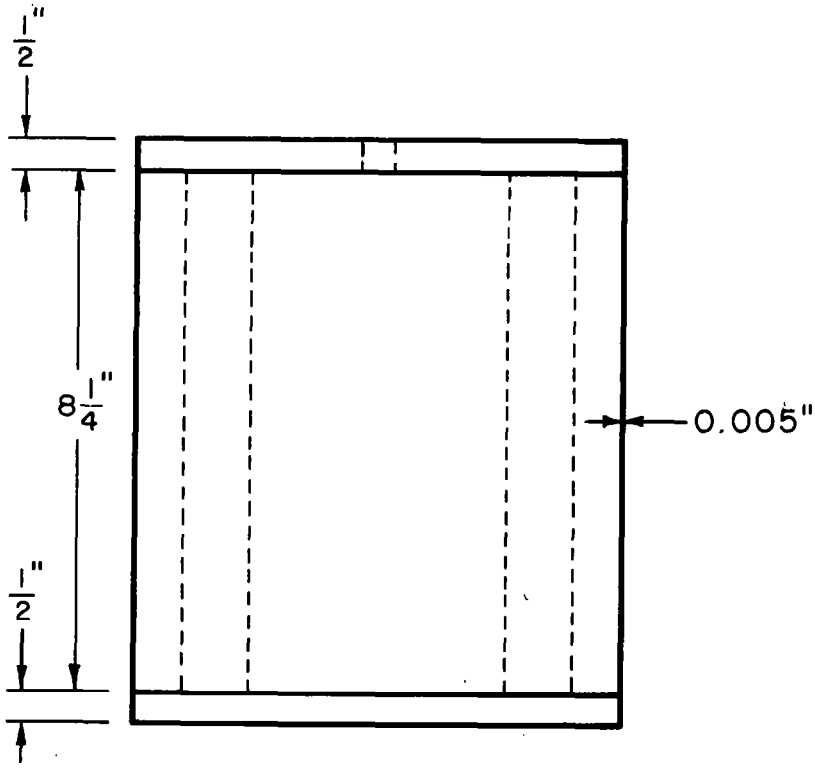

FIG. 35 1/4 SCALE MODEL, SECTION 5 OF APOLLO CM

performance of this cylinder, which models only the membrane-stiffness-controlled wall, is shown in Fig. 36. Modifying Eq. (18) by a factor of $4/(5 - 4\nu)$, to correspond to the assumption that the end plates do not move axially, gives a calculated value of 50 dB NR.

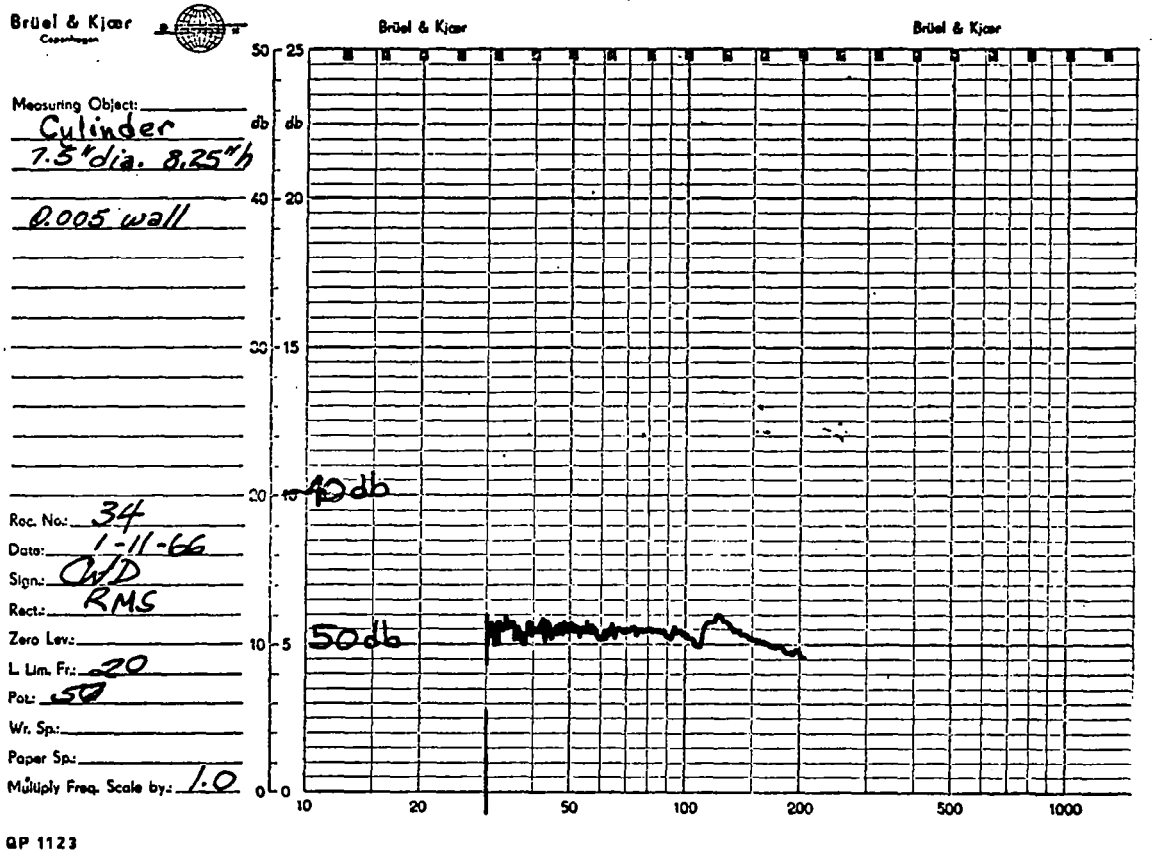

FIG. 36 NR DATA, 1/4 SCALE MODEL, SECTION 5 OF APOLLO CM

2) A second cylindrical shell made of 0.004-in. thick T6 tempered aluminum was rolled into a 7.0-in. diameter cylinder 7.5 in. high with a single 1/8-in. overlap seam sealed with epoxy. A 3/8-in. thick aluminum disc was set into one end of the cylinder and a bead of epoxy run around the joint. A 1/2-in. diameter hole provides receiver microphone access. For the first test, a similar 3/8-in. thick disc was sealed into the opposite end. The entire assembly was pressure-tested in a water bath to

detect small leaks. The NR of this cylinder with 3/8-in. end plates is shown in Fig. 37(a). The calculated NR, based on the membrane compliance of the shell and the flexural compliance of the end plates, is shown by the heavy dashed line at 44 dB NR.

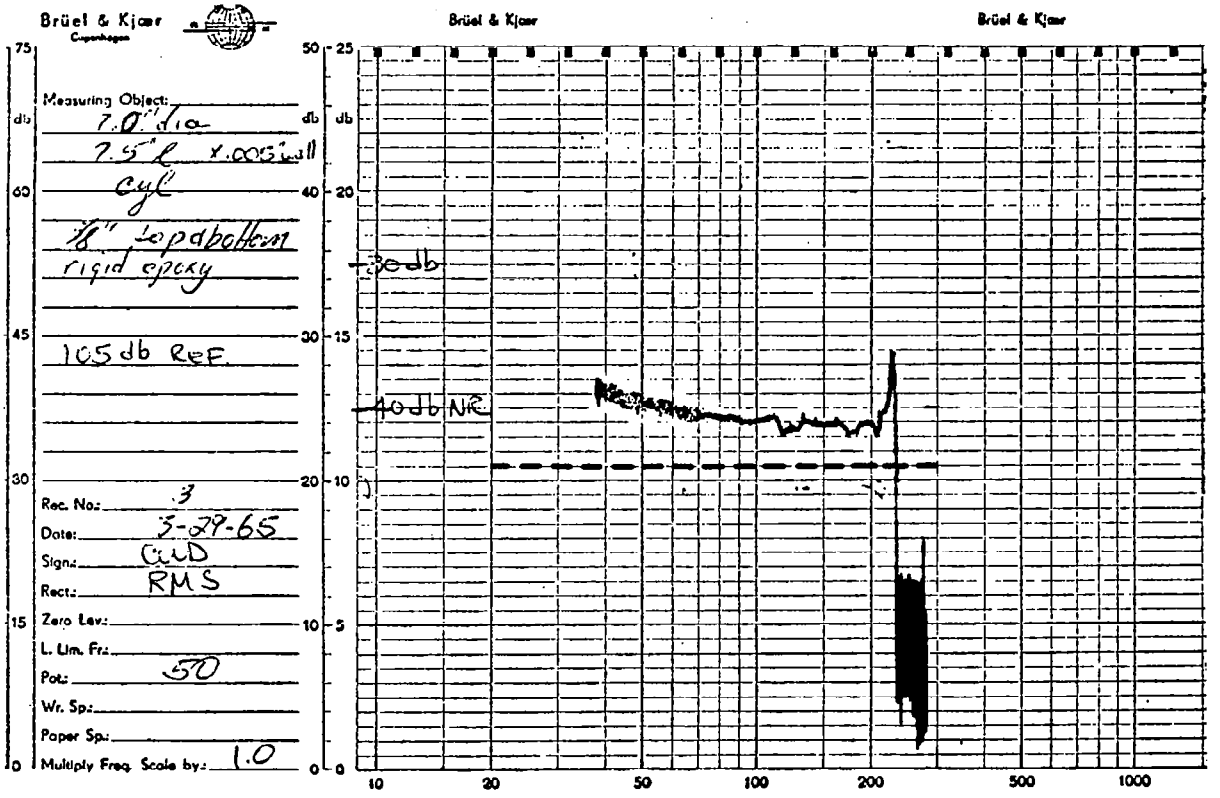

FIG. 37(a) NR DATA. 1/4 SCALE MODEL, SECTION 5 OF APOLLO CM

One 3/8"-thick end disc was then replaced with a 1/8"-thick disc installed in the same manner as before. The NR curve for this arrangement is shown in Fig. 37(b). The calculated NR is 40 dB, determined almost entirely by flexural compliance of the 1/8-in. disc. A different joint was tried by using a 1/8-in. thick disc that overlapped the cylinder with an epoxy-filled seam, as shown in Fig. 34. The performance curve is shown in Fig. 37(c). Figs. 37(b) and 37(c) show that the edge conditions of the hatch cover can have an effect on its compliance and, consequently, the NR obtained.

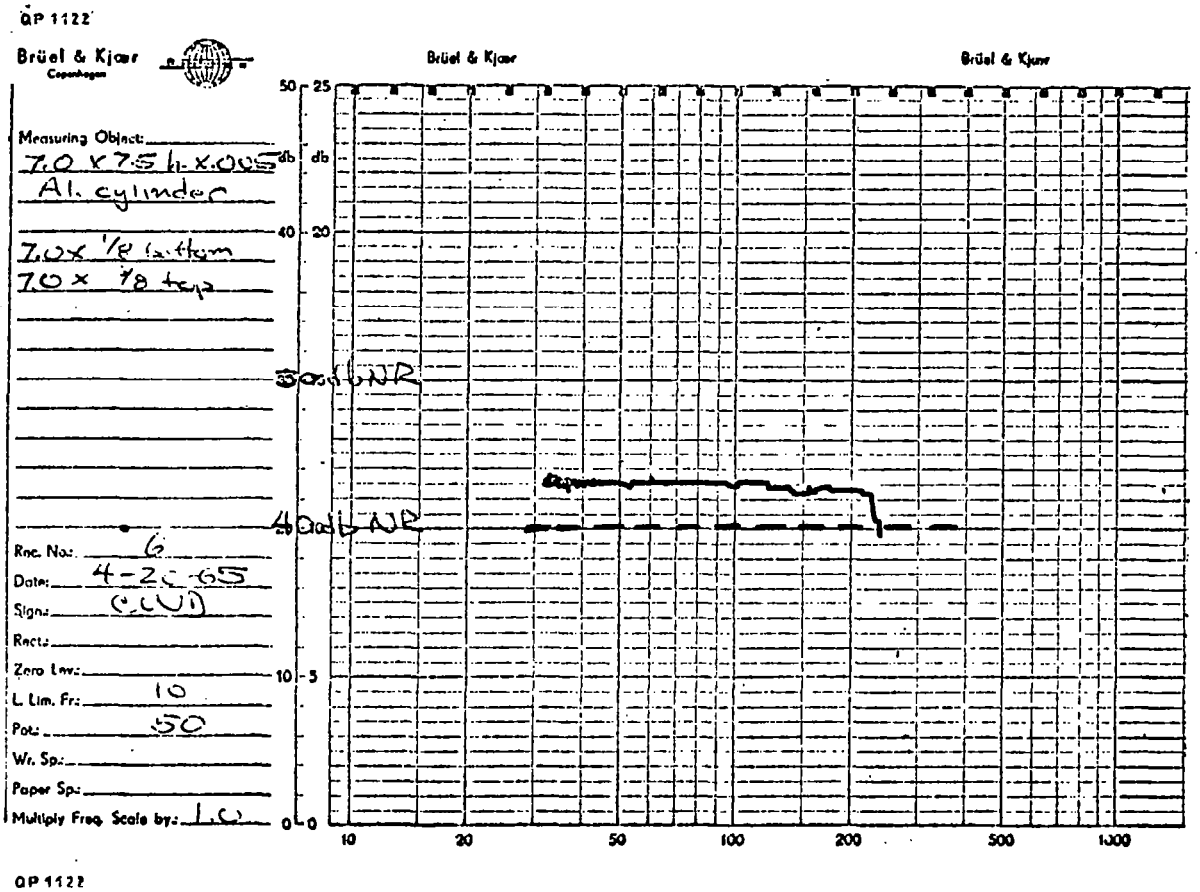

FIG. 37(b) NR DATA, 1/4 SCALE MODEL, SECTIONS 5 AND 6 OF APOLLO CM

We conclude from the lack of frequency-dependence in the NR experimental data that the quasistatic analysis is sufficient to predict the NR of the structural elements tested here. The disagreement between theory and experiment (3 - 6 dB in Fig. 37) points out the considerable influence minor wrinkles have on the ability of such a shell to follow membrane-stiffness control. This effect will be more pronounced in the next section, where experiments with a larger model of a conical shape

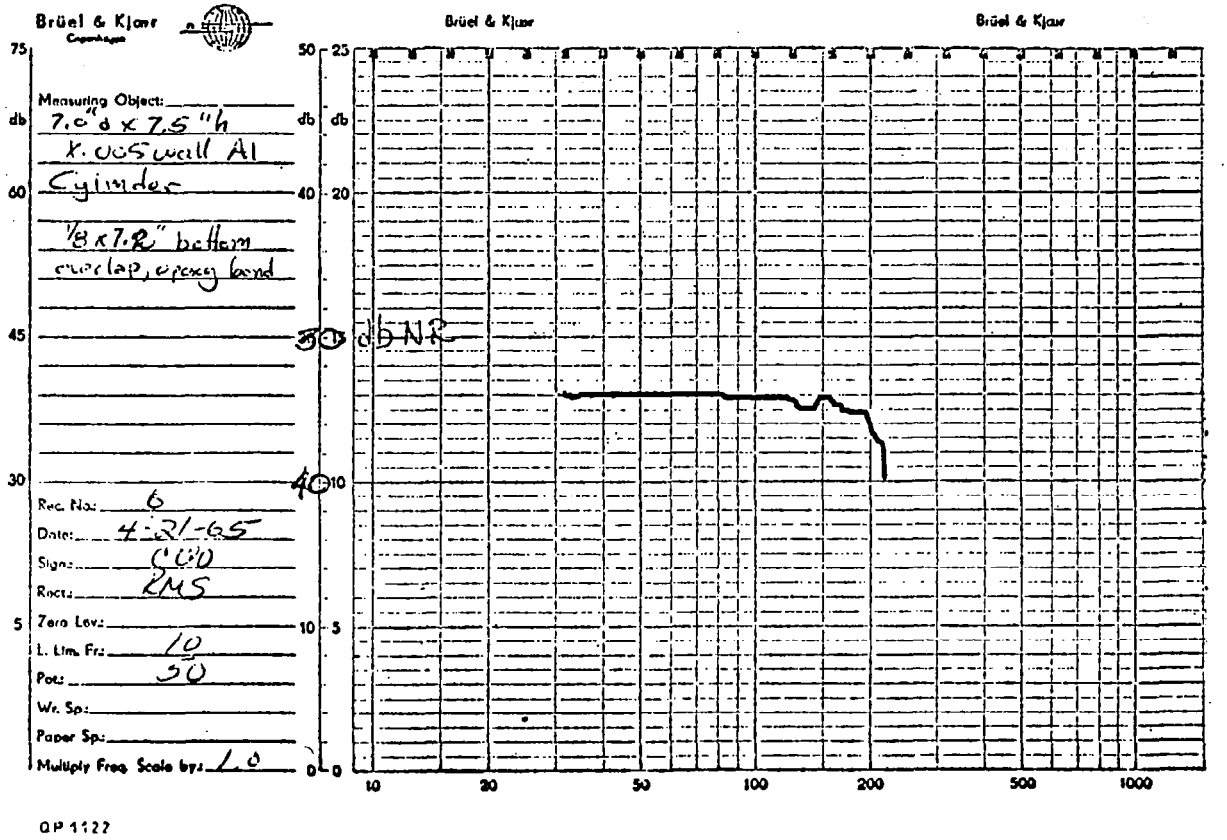

FIG. 37(c) NR DATA, 1/4 SCALE MODEL, SECTIONS 5 AND 6 OF APOLLO CM

are described. The reduction in the NR obtained by changing from a set-in end plate to a lap joint should be attributed to the numerous small wrinkles seen in Fig. 34 that were permitted by the lack of inner support when the set-in end plate was removed. When the model was constructed with considerable care to avoid these wrinkles, excellent agreement was obtained between the theory and the experiment.

Vibration Tests

We would now like to examine the vibration of the cylinder wall. The wall is supposedly membrane-rigidity-controlled. It is not clear that we can ignore the effects on the vibration levels caused by nonuniformities or discontinuities such as ribs, supports, or seams.

Equipment.—Vibration-measuring equipment was added to the pressure test equipment shown in Fig. 32. A small piezoelectric accelerometer weighing about 1 gm is attached to the wall at various positions, and the output is amplified and filtered in the same way as the receiver microphone signal for NR tests. The accelerometer channel is calibrated so that the absolute vibration level can be recorded as a function of the frequency of the applied acoustic excitation. The low-pass filter between the receiver microphone preamplifier and the level recorder passes only those signals below 300 Hz. This filter eliminates false responses to high-frequency excitation generated by nonlinearities in the loudspeaker or mechanical rattles in the test chamber or model.

The first cylindrical model described under section 3 is now instrumented for acceleration at three positions as shown in Fig. 38. Using the same test chamber and a uniform 105 dB SPL acoustic excitation, a plot of the wall vibration vs frequency was obtained. Such a plot is shown in Fig. 39. The corresponding NR measurement was shown in Fig. 37(a).

The cylinder was then modified by adding internal axial stiffening ribs at different positions on the outer circumference. Each rib was 3/4-in. deep and 1/8-in. wide aluminum beam fastened to the cylinder wall by epoxy. The beam length gave a 1/4-in. overlap support from the end plates, as shown in Fig. 38.

Adding two ribs spaced 120° apart produced no change in the measured NR, as illustrated in Fig. 40. The point vibration levels were somewhat affected, as a comparison of Figs. 38 and 42 shows. The data in Figs. 38 and 41 were taken at the same position, away from a rib, while the data in Fig. 42 was taken near a rib.

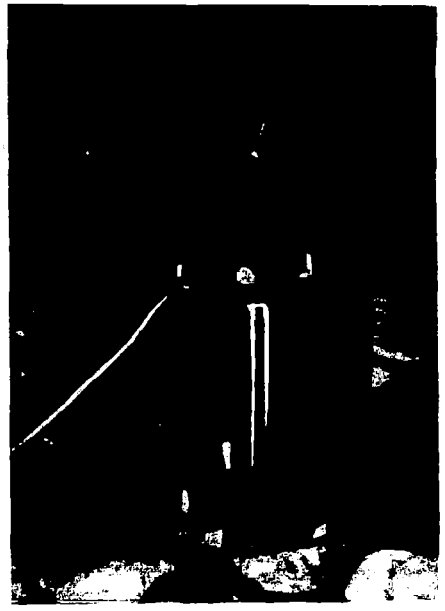

FIG. 38 SCALE MODEL OF SECTION 5, APOLLO CM IN TEST CHAMBER

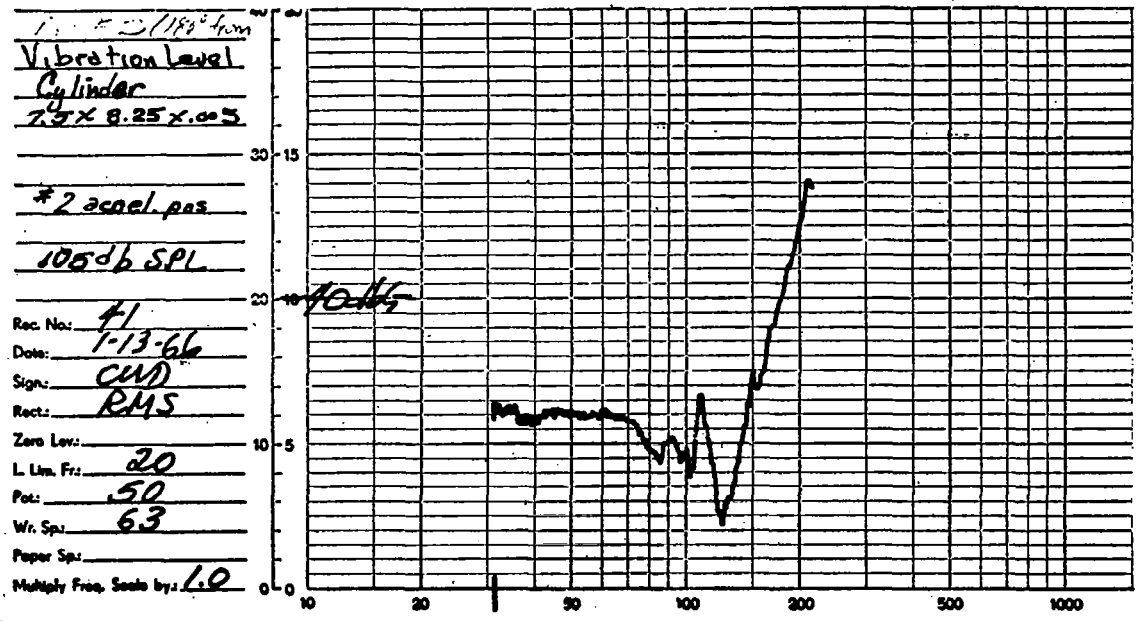

FIG. 39 VIBRATION LEVEL, 1/4 SCALE MODEL; SECTION 5 OF APOLLO CM (NO RIBS)

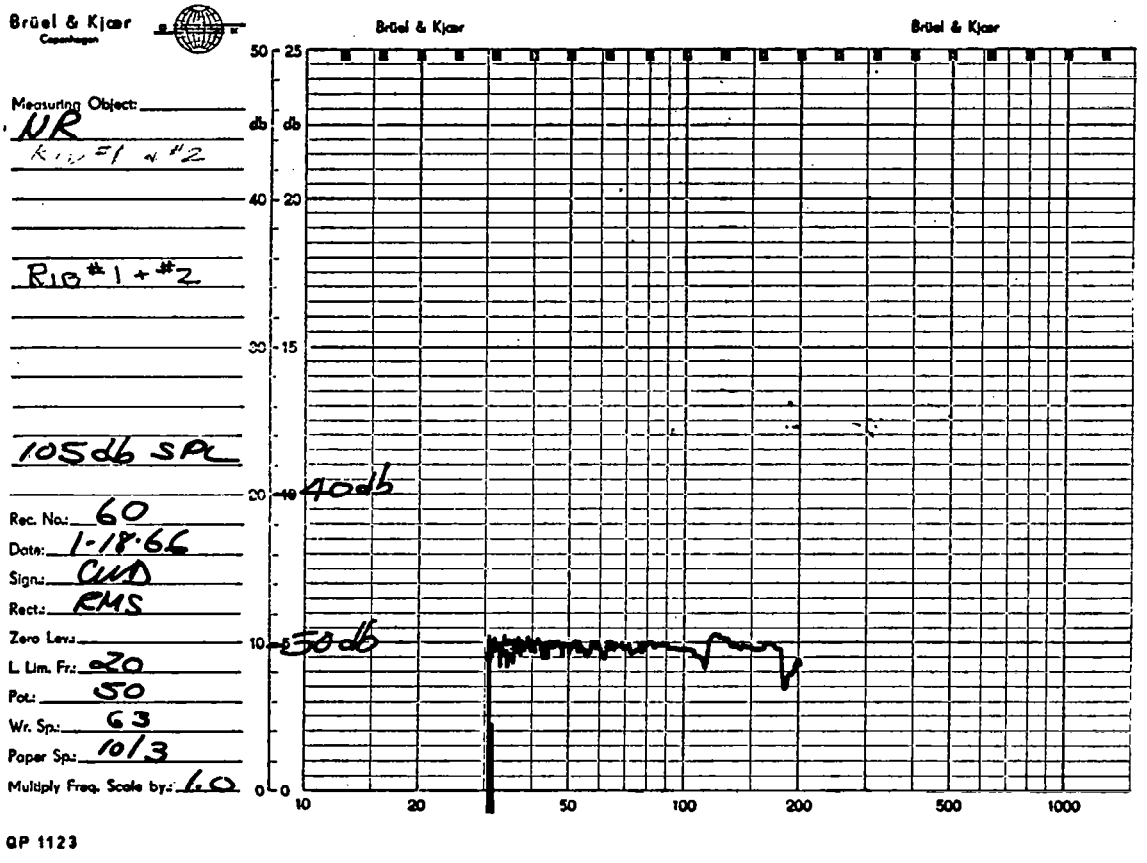

FIG. 40 NR DATA, 1/4 SCALE MODEL, SECTION 5 OF APOLLO CM, WITH 2 RIBS

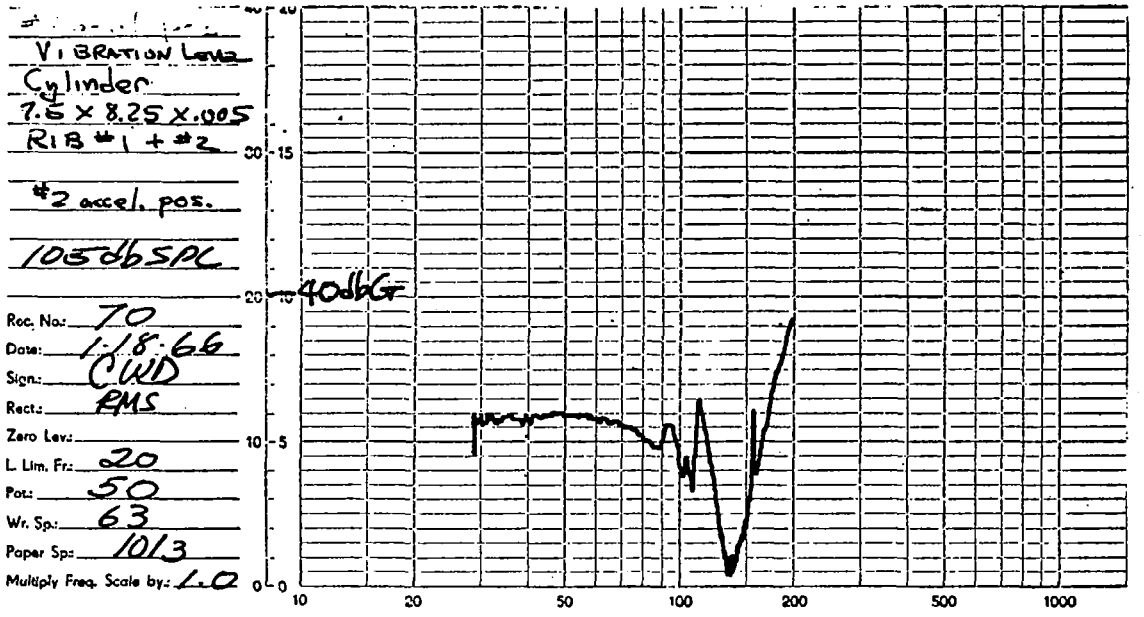

FIG. 41 VIBRATION LEVEL, 1/4 SCALE MODEL, SECTION 5 OF APOLLO CM (TWO RIBS, MEASURED AWAY FROM A RIB)

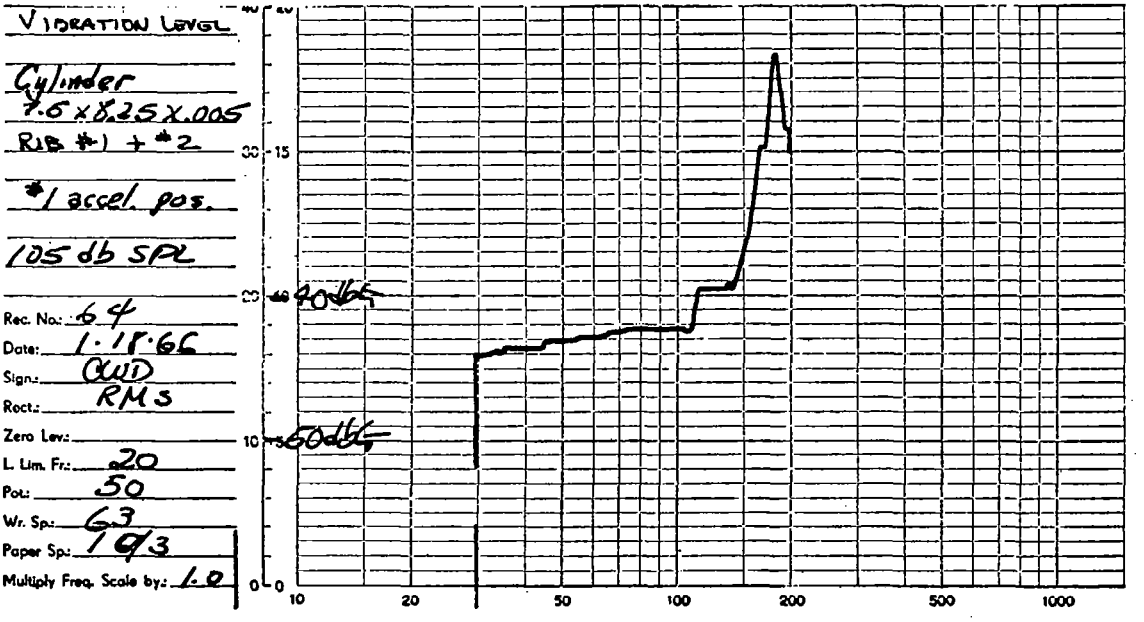

FIG. 42 VIBRATION LEVEL, 1/4 SCALE MODEL, SECTION 5 OF APOLLO CM (TWO RIBS, MEASURED AT A RIB)

EXPERIMENTAL STUDIES OF CONICAL OUTER SHELL OF THE CM

Scaling the Outer Shell

The second portion of the Apollo CM to be modeled is the entire outer shell. This consists of the sections numbered 1, 2 and 3 in Fig. 14. For our purposes, this complex shape can be simplified and represented by only two surfaces, a spherical segment (dish) representing 3 and a cone representing 1 and 2. A 1:8 dimension scale was selected to fit the model in the existing test chamber.

In contrast with the cylindrical model, both the conical sidewall and the dish bottom are hypothesized to be controlled by membrane stiffness, and thus the appropriate quantity to scale for both segments is the membrane compliance. Since the in-plane stresses are carried in the inner and outer faces of the steel sandwich structure, the scaled cone and scaled dish are 1/8 the total face thicknesses. The hypothesis of membrane-stiffness control was subject to some doubt in the case of the bottom dish, and one result of the experimental analyses has been to resolve this point.

The scale model described above should simulate the NR behavior of the original structure when exposed to pressure fluctuations below structural resonances of either the original or the scale model. An estimate of the lowest structural resonance will define the upper frequency limit to the model's usefulness.

Concentrating our attention on the larger and thinner cone structure, we might consider bending waves along the slant height and the circumference. As in the case of a cylinder, we see that only integral numbers of wavelengths are allowed around any circumference lying in a plane perpendicular to the axis, and thus no net volume displacement is expected inside from such resonant motion. The first radial expansion mode may be estimated by the ring frequency of the largest circumference; this would occur at 3200 Hz in the model and 1/8 this, or 400 Hz in the original.

We can estimate the lowest flexural resonance frequency of the conical shell by replacing it with a cylinder of the same average radius. Thus, for the 1:8 scale model, the height of the cylinder is 16 in., and its average diameter is 5 in. The lowest internal acoustic resonance is f_a = 425 Hz. From Eq. (90),

$$\frac{f_{min}}{f_a} = 15\sqrt{\frac{2 \times 10^{-3}}{\sqrt{3}\cdot 5}} = 0.18 \qquad (161)$$

or, $f_{min} = 76$ Hz. This resonance, which is presumably non-volume-pumping, will occur in the frequency range of the experiment. The asymptotic frequency separation between structural modes is

$$\delta_f = \frac{2\kappa c_\ell}{A} = \frac{2 \times 10^{-3} \times 2 \times 10^5}{2\pi\cdot 5\cdot 16} \approx 0.8 \text{ Hz} \qquad (162)$$

Thus, in the region of structural resonance, we can expect many resonances to be observed in the vibration response.

NR Measurement Apparatus

Quasistatic pressure testing was carried out in the same test chamber as described above. In order to accommodate the larger size of the proposed model, the 15-in. diameter loudspeaker was removed to the outside of the chamber. For a later part of this experiment, a source of adjustable low-pressure air was brought into the chamber. No significant change was noted in the frequency range over which a uniform pressure field could be generated; the new scale factor makes the test range of 20 to 200 Hz correspond with 2.5 to 25 Hz in a full-scale experiment. Uniform sound pressure levels of 105 dB were developed inside the test chamber.

Construction of Outer Shell Model

The cone portion of the model was constructed of steel 0.002 in. thick. Since such thin steel is not available in a sheet large enough (20 in. x 40 in.), the surface was constructed by joining together a number of triangular pieces, each having a height of 20 in. and a base of 6 in. Eleven such pieces were joined by spot-welding a narrow (1/16 in.) overlap seam as shown in Fig. 43. A strip of tape seals each seam air-tight.

The validity of substituting a pieced construction for a homogeneous sheet was investigated by tensile-testing sample 2-mil steel strips 6 in. long and 1/2 in. wide, and comparing the force-elongation curves with those of strips having spot-welded joints and also epoxy joints.

FIG. 43
SPOT-WELDED SEAM
(SPACING IS 1/8 IN.)

It was observed that, after a short region of creep of the sample in the test machine jaws, a long linear region follows where all samples, both without and with joints, behave alike. In each case two samples were tested, and the results are identical until the point of rupture is reached. It is concluded that the use of the spot-welded seams has no effect on the membrane compliance.

The bottom dish of the model was constructed from a steel pan sold as a child's winter toy. Its radius of curvature and overall diameter were suitable, but its thickness was 0.032 in., or approximately twice the thickness required in the model. However, it was used for the first assembly to check the behavior of the cone wall, and to investigate the hypothesis of membrane-stiffness control of such a large-radius spherical segment. Although the thickness of 0.032 in. is double that for a scale model based on plane stress, it is less than 1/4 the required thickness (0.14 in.) if bending rigidity is assumed to control the behavior. This would scale bending stiffness by 1:64, and give an extremely low NR in the tests.

The steel bottom dish is shown in Fig. 44 with the ring used to align the rather flexible cone during the application of the final epoxy joint. A rubber insert in the joint of the ring keeps it from contributing to the compressional stiffness of the cone. The assembled cone is shown in Fig. 45. The top of the cone is truncated, and a 1/2 in. thick disc of aluminum 1 in. in diameter is epoxied in place. This allows fitting of the two support pins and the 1/2 in. receiver microphone access hole. The model is shown in the test chamber in Fig. 46.

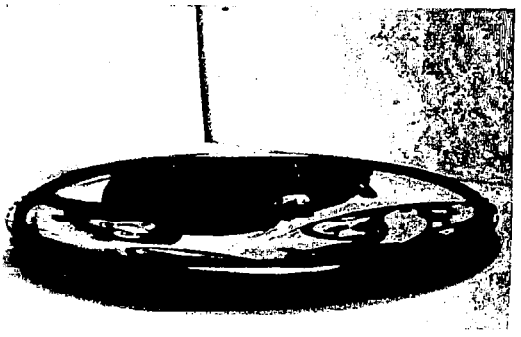

FIG. 44
BOTTOM DISH AND RING

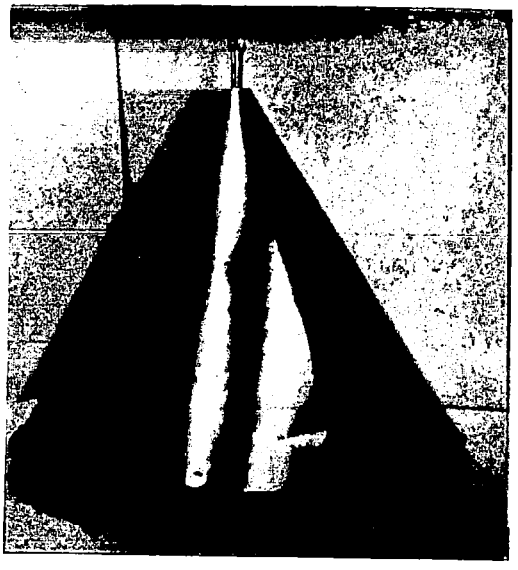

FIG. 45
ASSEMBLED CONE
(1:8 SCALE)

FIG. 46
SURFACES SMOOTHED BY 2.5 CM Hg INTERNAL PRESSURE

The results of the NR tests are presented in Fig. 47(a). The curve shows the measured NR. The results shown in this Figure are surprisingly low, and a number of resonances are observed starting at 80 Hz. Inspection of the cone showed a number of wrinkles in the skin caused by distortions during the spot-welding of the seams. To investigate the possibility that these corrugations do not stiffen, but actually may act as small bending-rigidity controlled areas, a plastic tube carrying air at low pressure (not above 5 cm Hg) was introduced into the model. This pressurization served to smooth the skin in many places (Fig. 46), and the results shown in Fig. 47(b) show quite a significant difference in the measured NR. About 20 dB of NR is obtained, and resonant effects below 100 Hz are eliminated

While these results are not close to the 40 dB NR predicted by quasistatic analysis, it is safe to conclude that the compliance of the bottom dish is not bending-rigidity-controlled, and that a cone constructed without wrinkles or corrugations may well follow the membrane-rigidity hypothesis better than the model tested here.

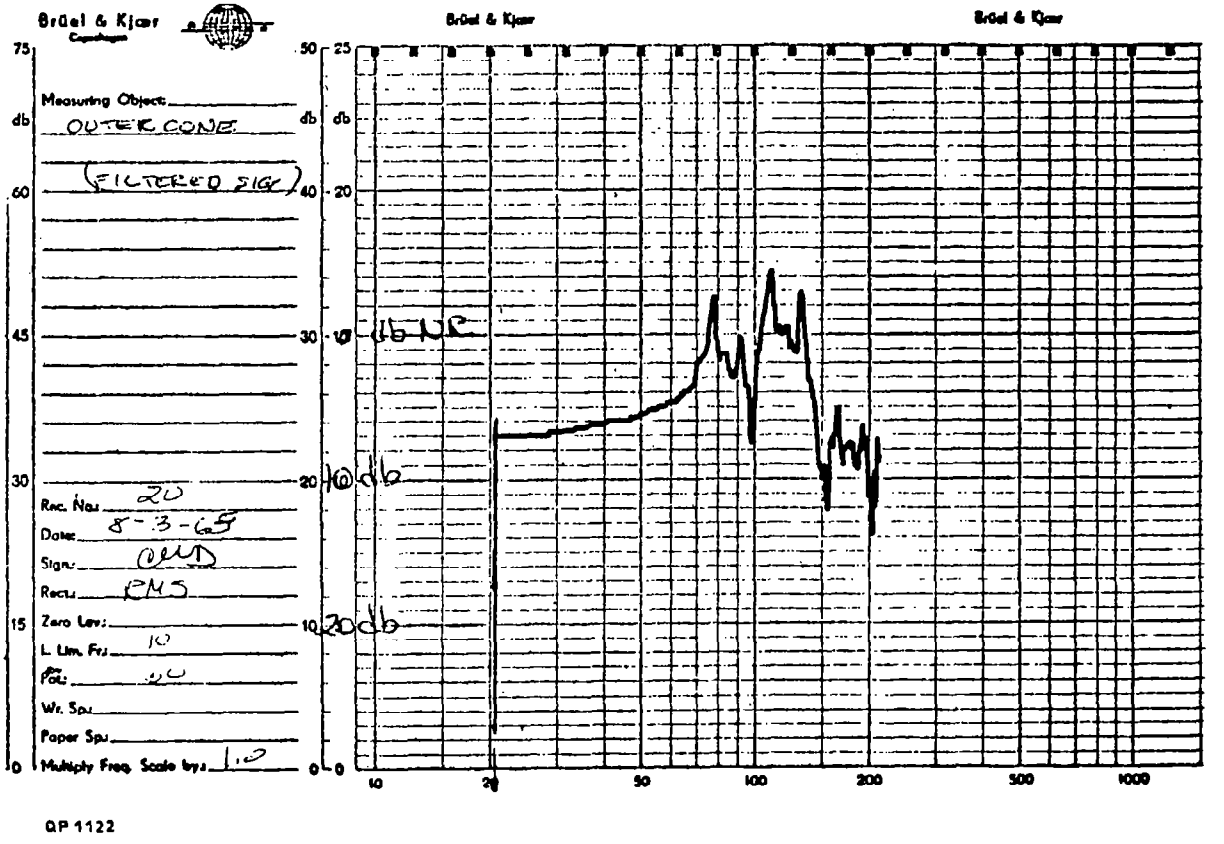

FIG. 47(a) NR DATA 1/8 SCALE MODEL SECTIONS 1 AND 2 OF APOLLO CM. (NOT PRESSURIZED)

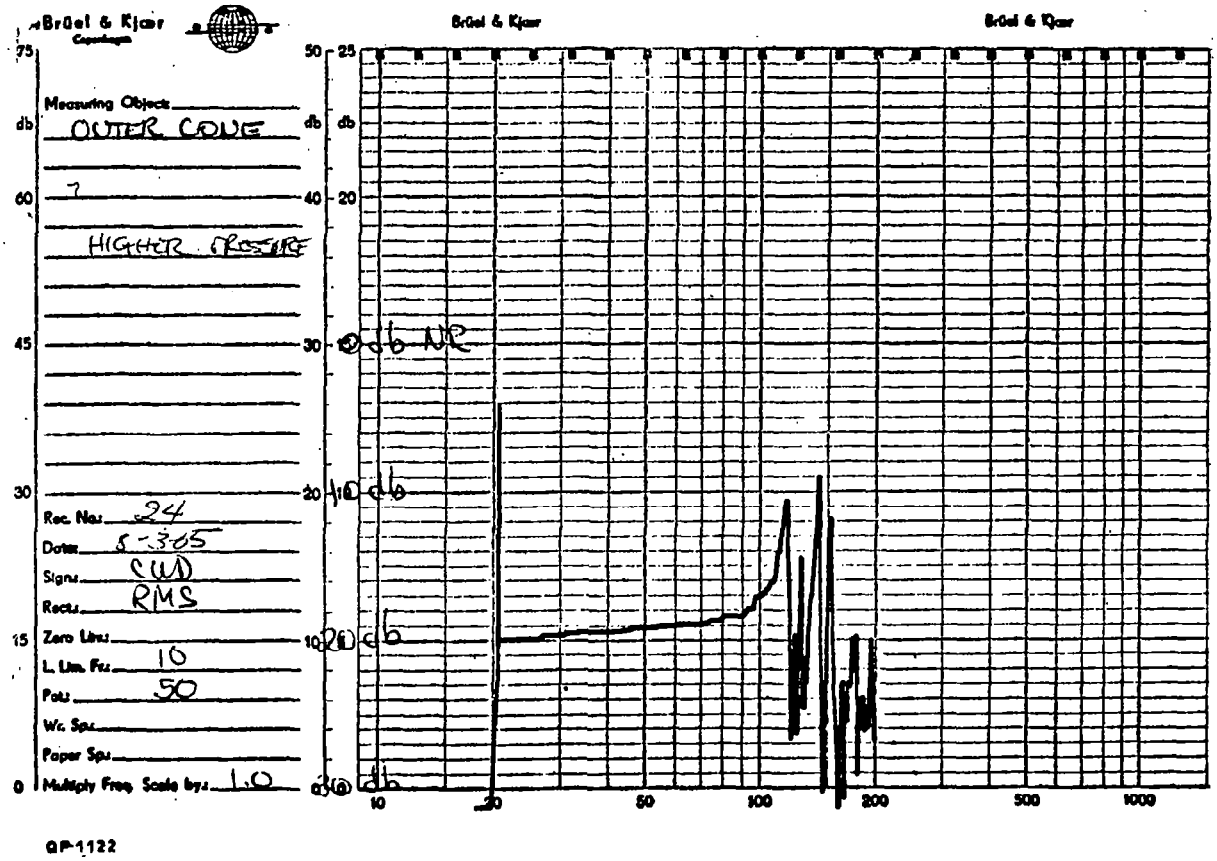

FIG. 47(b) NR DATA 1/8 SCALE MODEL SECTIONS 1 AND 2 OF APOLLO CM (PRESSURIZED)

Membrane-Stiffness-Controlled Walls

Considerable disagreement was reported between theoretical and experimental values of NR for the outer-shell model in the preceding paragraphs. Not only was the experimental NR much less than predicted by membrane-stiffness-controlled shell theory, but resonant dips in the NR were seen (Fig. 47(a)) at frequencies between 80 and 200 Hz. This is quite far below any radial-expansion mode, which would allow net volume displacement to occur. It was suggested that, in the case of the conical outer shell, wrinkles in the 0.002-inch steel skin affect the NR. To investigate this, a second outer-shell model was constructed. A 1:10 dimension scale was used instead of 1:8.

Construction and NR Tests of Aluminum Outer-Shell Model

The second outer-shell model to be constructed, shown in Fig. 48, reproduces only sections 1 and 2 of Fig. 14. The conical shell described above was constructed from 0.002-in. thick steel, the proper thickness for a 1:8 scale model. The present 1:10 scale would require 0.0016-in. steel, which would also require a pieced-together construction. Since such construction was suspected of affecting the membrane-stiffness control through the dimpling, aluminum sheet was used instead. The appropriate thickness, 0.0048 in., is three times as great, since the ratio of the Young's modulus of steel to that of aluminum is 1:3. Such aluminum sheet 0.005 in. thick was available in a size large enough to construct the model from a single piece.

The single seam used to fabricate the model could not be welded successfully in aluminum with the available equipment. A cemented seam was used instead, with a strip of tape to insure against small air leaks. Such cement or epoxy seams were previously found to have no effect on the elastic modulus of the steel test strips. It would be expected that this would also apply to aluminum three times as thick.

The cone was terminated with a 1-in. thick aluminum plug at the top, and was sealed to a thick wooden base. The assembly is shown in the test chamber in Fig. 48. The comparative smoothness of this model is evident in a comparison with Fig. 46 showing the earlier model. Access for the receiver microphone was provided through the wooden base.

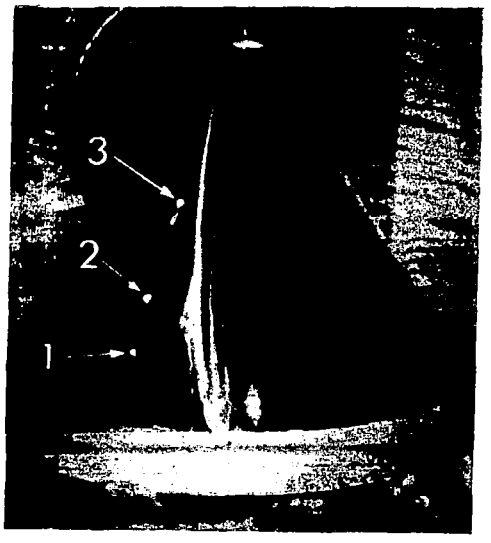

FIG. 48
VIBRATION PICKUP POINTS ON OUTER CONE ONE-TENTH SCALE MODEL

The results of the NR tests are shown in Fig. 49. The curve shows the measured NR. It is quite flat and shows higher NR than the curves taken for the 1:8 model. The new 1:10 scale makes the test range of 20 to 200 Hz correspond with 2 to 20 Hz in the full-scale structure. Uniform sound pressure levels of 108 dB were obtained inside the test chamber.

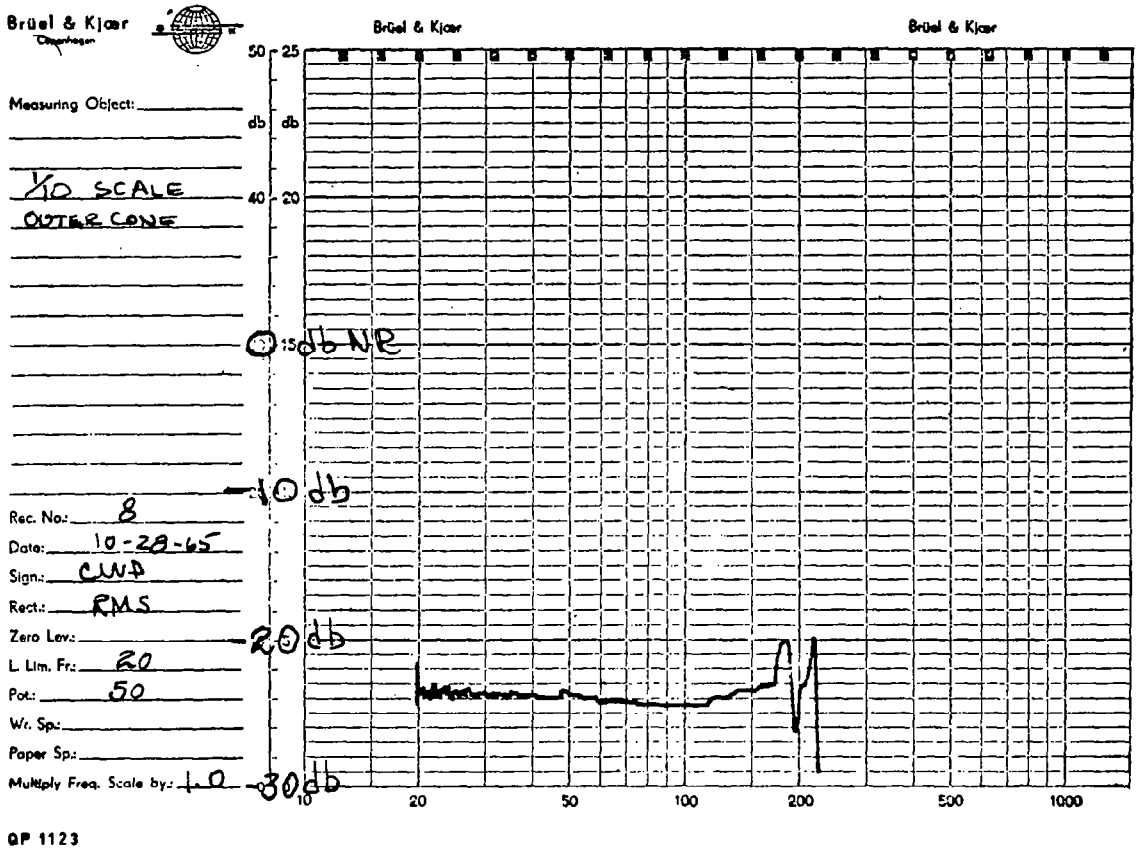

FIG. 49 NR DATA 1/10 SCALE MODEL SECTIONS 1 AND 2 OF APOLLO CM

To check the possible connection between lower NR values and wrinkles, a single dimple was temporarily made in the model wall, and a 6-dB reduction in the NR was observed at 90 Hz. Removing the pressure allowed the wall to return to its previous shape, and the NR rose to its previous value.

Vibration Measurements

A small piezoelectric accelerometer was then mounted at three positions on the model, as shown in Fig. 48. Applying the same uniform 108 dB SPL acoustic excitation as used to measure the NR, a plot of the wall vibration versus frequency was obtained. Such plots are shown in Figs. 50 and 51. The lower curve in Fig. 50 is the background vibration level, measured with no acoustic excitation. Sufficient signal-to-noise ratio exists at all measurement frequencies to determine the actual vibration levels without narrow-band filtering. These plots show a number of distinct resonances below 80 Hz, and then a quite uniform increase in vibration level of approximately 24 dB/octave.

This is in sharp contrast with the accelerations to be expected from the NR curve of Fig. 49. Since it shows a constant NR, corresponding to a constant volume displacement, we would expect a slower 12 dB/octave increase in the wall accelerations. The resonances observed are not necessarily unexpected, but they are not capable of producing net volume displacement inside, and thus would not affect the observed NR.

The preceding discussions have shown the usefulness of detailed examination of wall structures supposedly controlled by membrane-rigidity alone. The results for the 1:10-scale smooth cone have demonstrated that quite different behavior is observed, depending on whether or not wrinkles or corrugations are present. The validity of the simple quasistatic analysis for cone structures is supported by the data, although the absolute levels are not so high as predicted.

Vibration measurements have verified the presence of resonant modes in the wall structure, which, as predicted, are not associated with corresponding fluctuations of NR.

RESONANCES OF INTERSPACE CONTAINED BETWEEN AXISYMMETRIC SHELLS

Recap of Theoretical Study

Chapter V presents a theoretical study of the acoustics of the interspace between axisymmetric shells. An approximation technique, the Rayleigh-Ritz method, was adopted to predict the upper limit to the acoustic resonances in the interspace when this region is not geometrically simple enough to handle analytically. After illustrating and verifying this method, both with a simple problem which could be handled analytically and with approximation technique, an acoustic model of the

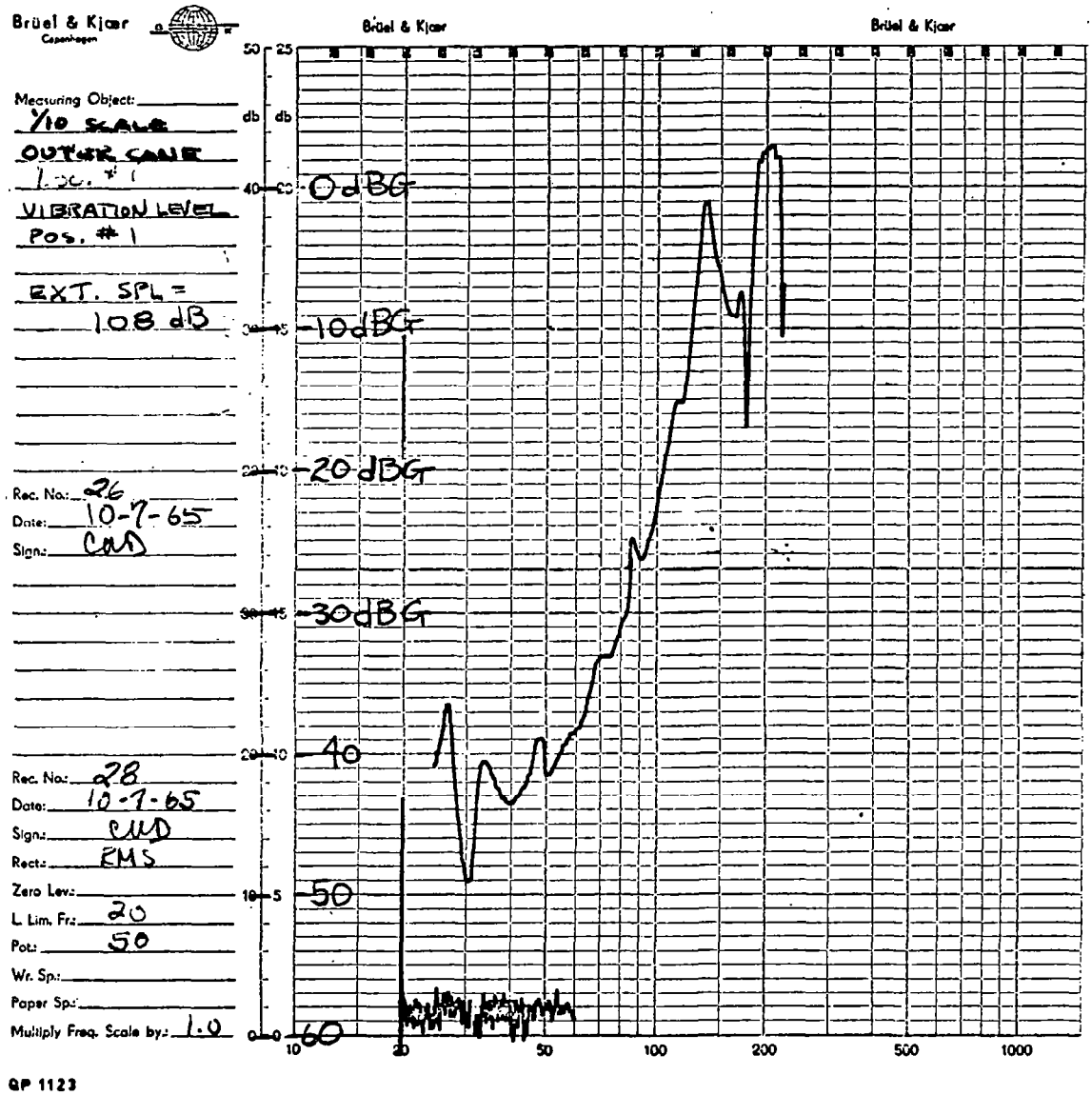

FIG. 50 POSITION 1, VIBRATION LEVEL, 1/10 SCALE MODEL SECTIONS 1 AND 2 OF APOLLO CM

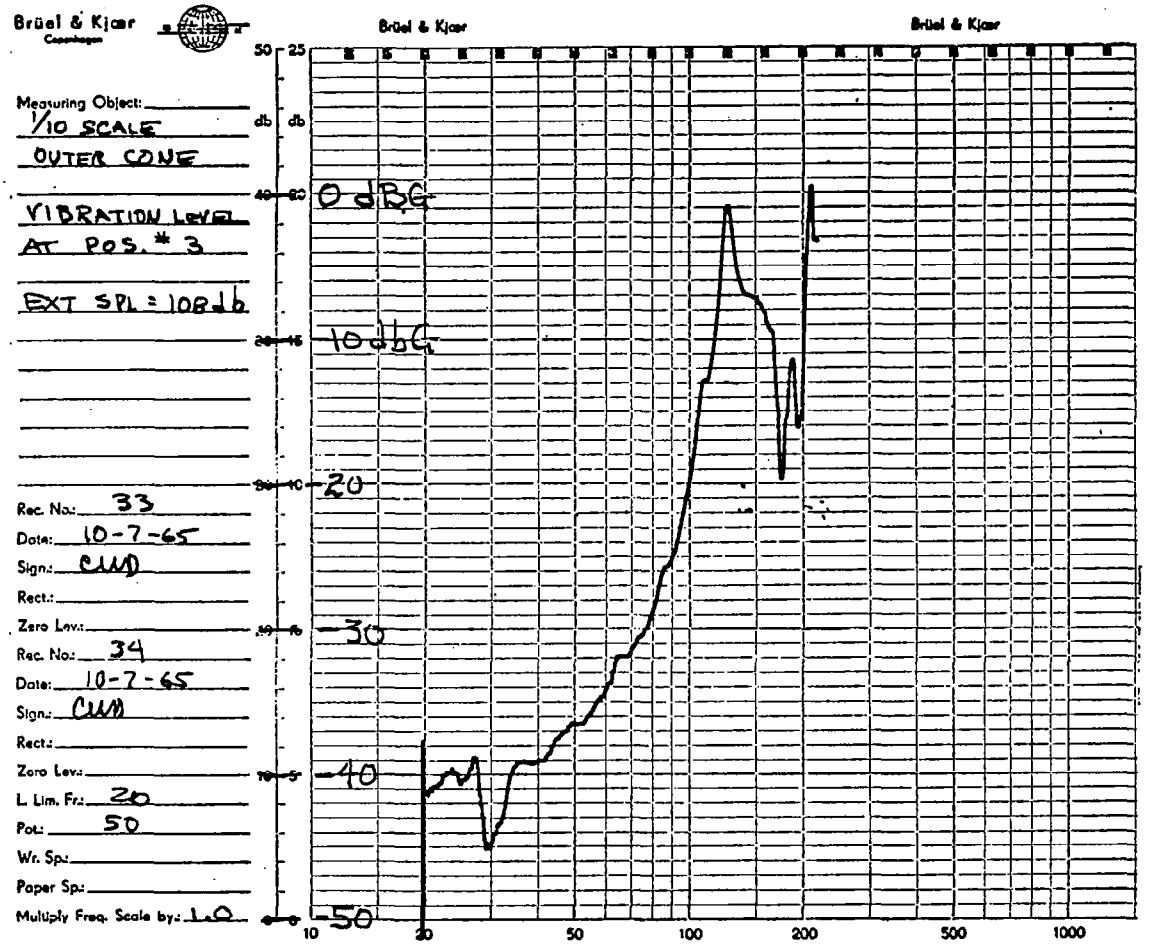

FIG. 51 POSITION 3, VIBRATION LEVEL, 1/10 SCALE MODEL SECTIONS 1 AND 2 OF APOLLO CM

Apollo CM was analyzed. Two of the resonances calculated fall into the range below 50 Hz. These two resonances are characterized by:

Mode Shape	Frequency	Type of Resonance
$\psi = \left[\cos\left(\frac{\pi s}{S}\right) - 0.361 \cos\left(\frac{2\pi s}{S}\right)\right] \cos m\phi$	40 Hz	m=0, longitudinal mode
$\psi = \left[\sin\left(\frac{\pi s}{S}\right) + 0.476 \sin\left(\frac{2\pi s}{S}\right)\right] \cos m\phi$	43 Hz	m=1, azimuthal mode

This section describes the experimental analysis of the acoustic resonances. The purpose of the experiments was to locate resonances, especially below 50 Hz in the interspace, and to identify these resonances as to their "longitudinal" or "azimuthal" character.

Experimental Model and Apparatus

Model.—The acoustic model of the Apollo CM was constructed to a 1:10 scale. Frequencies measured, therefore, will be ten times those of the full-scale model. The model consists of three basic parts, as illustrated in Figs. 52 and 53.

1. A wooden carved-out base plate (used in an earlier experiment)
2. A truncated aluminum cone
3. A wooden inner piece separated from the base plate and cone by dowel spacers

The dimensions of the model are shown in Fig. 54. The truncation of the small curved surface that would exist atop the CM has negligible effect on the acoustics of the interspace. The base plate was fitted with rubber tubing along its bottom edge to assist in allowing a tight fit. Any potential air leaks at the bottom were eliminated by applying tape and clay.

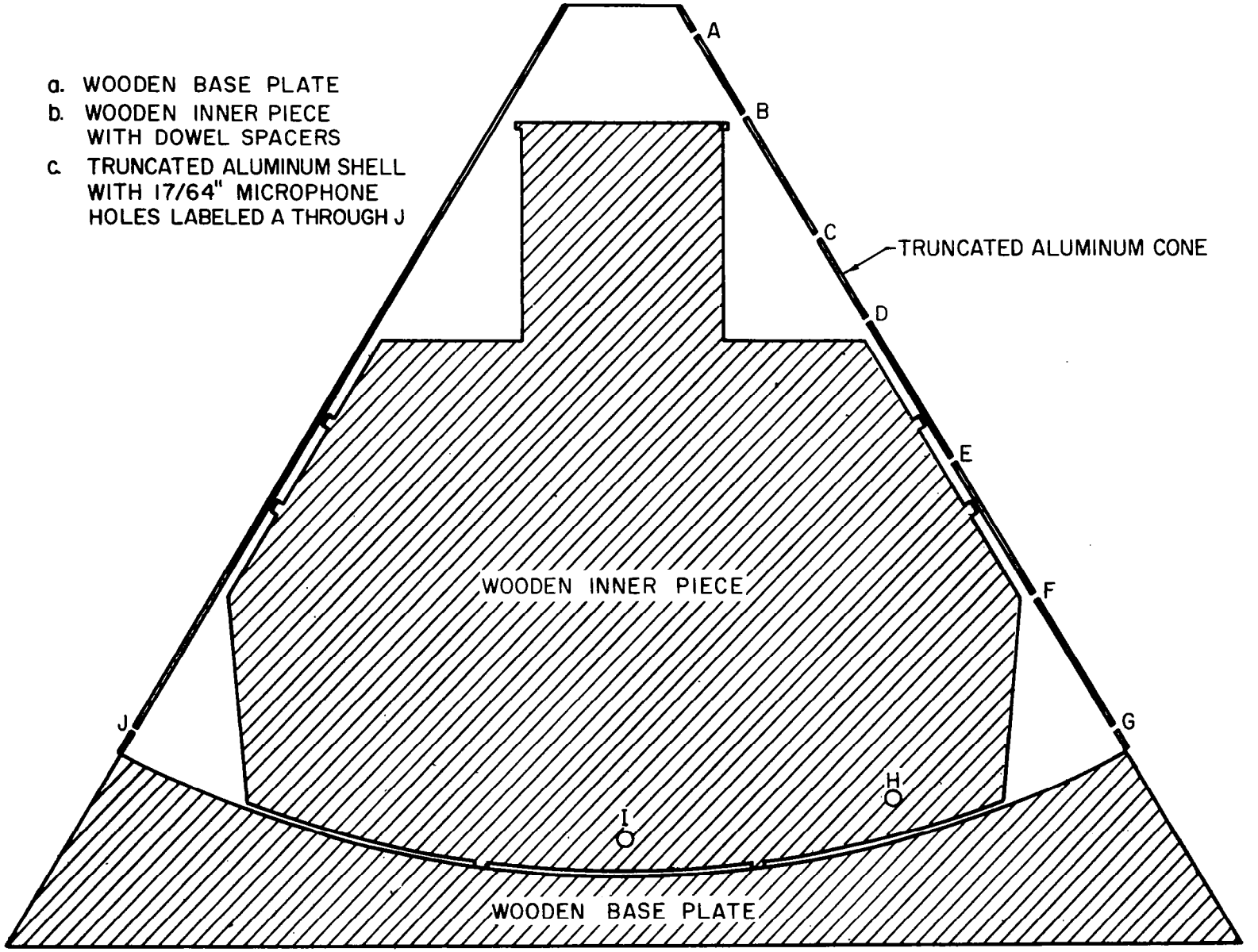

FIG. 52 1/10 SCALE MODEL OF APOLLO CM

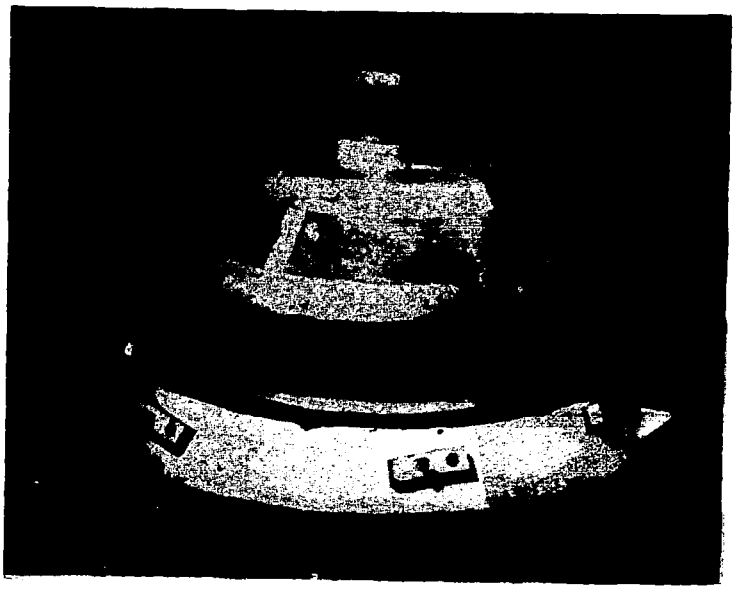

FIG. 53 PHOTOGRAPH OF INNER WOODEN PIECE AND WOODEN BASE PLATE

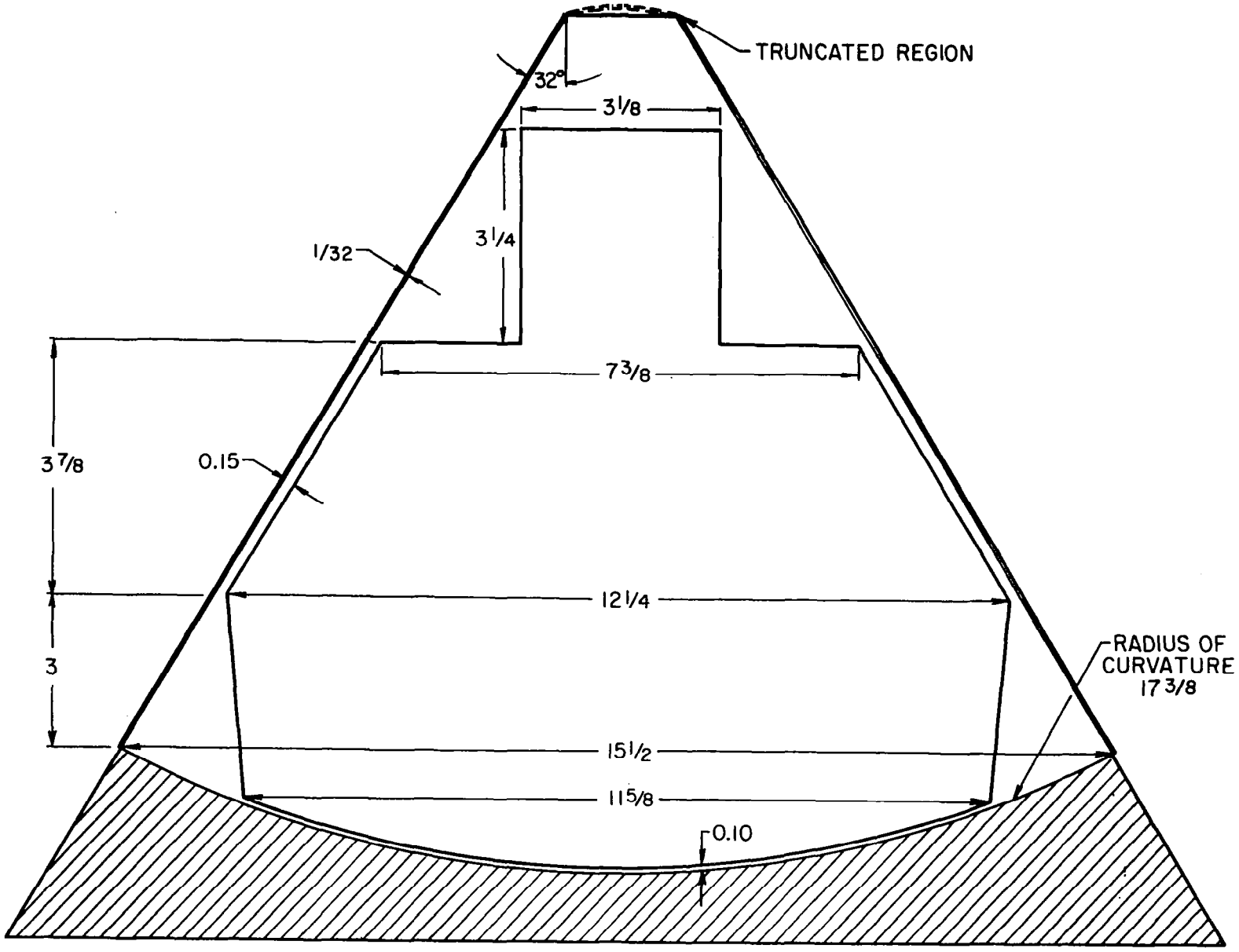

FIG. 54 DIMENSIONING OF 1/10 SCALE MODEL OF APOLLO CM

Apparatus.—The two problems encountered in measuring the resonances are:

1. How to excite the acoustic resonances while maintaining "rigid" boundaries.

2. How to measure the acoustic signal at various positions in the interspace without perturbing the sound field.

The first problem is solved by using a horn driver with a high-impedance "snout." A high-impedance source is desired because the driver is replacing a solid, high-impedance surface. In source position 1 (see Fig. 55) the snout consists of a small amount of packed steel wool followed by a wire-filled tube of 13/16 in. inner diameter. In position 2 (see Figs. 54 and 55) the wire-filled tube is followed by a 1/2-in. diameter, 2-in. length tube of tightly packed steel wool. The frequency response of these sources in the free field was measured and found to be fairly constant below 1000 Hz. Since the source of position 1 excites the model symmetrically, only axially symmetric (m = 0) modes are excited. The m refers to $e^{im\phi}$ dependence. The asymmetrically placed source in position 2 excited both m=0 and m$\neq$ 0 modes.

The measurement of interspace pressures is accomplished by using a 1/4-in. Bruel and Kjaer condenser microphone. Holes of 17/64-in. diameter are drilled in the side of the cone in positions labeled A through J in Figure 52. When not in use, these holes are filled with shallow wooden caps. When the relative phase between signals at two different positions in the model was desired, a second 1/4-in. Bruel and Kjaer condenser microphone was used.

A schematic of the apparatus is illustrated in Fig. 55. The frequency response of the interspace is plotted by a General Radio Graphic Level Recorder. The relative phase is measured by feeding the two microphone signals into the horizontal and vertical inputs of the oscilloscope, and observing the Lissajous pattern.

Characterizing the Resonant Modes

Symmetric m = 0 modes are characterized by a mode shape function ψ that depends only on s. This entails measurements in microphone positions A through G. The lowest m = 0, n = 1 mode is characterized by maxima at positions A and near G, and by a minimum somewhere near E. Asymmetric modes, especially m = 1 and m = 2 modes, are determined by finding from Lissajous patterns the relative phase between signals received at microphone positions G, H, I and J.

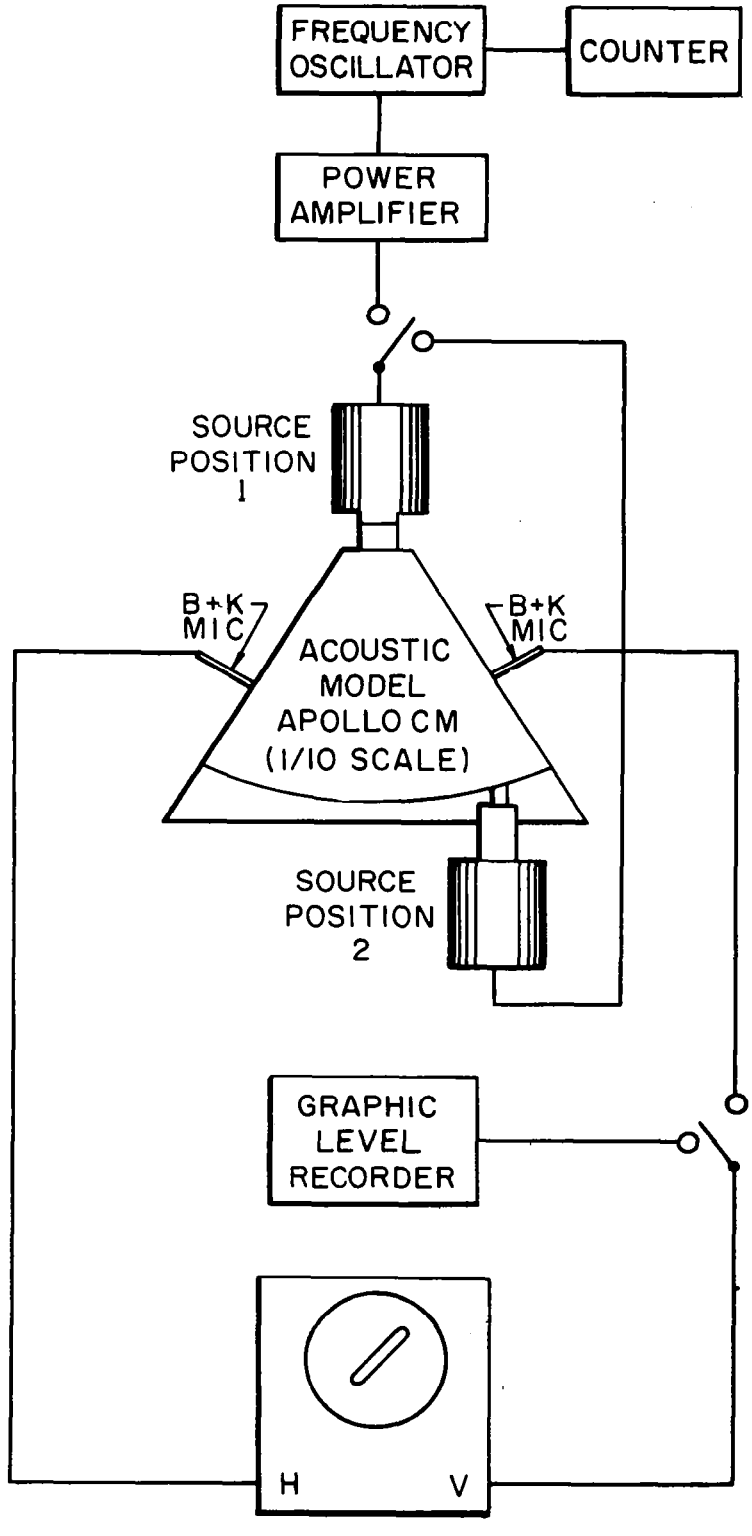

FIG. 55 SCHEMATIC OF EXPERIMENTAL SET-UP

Experimental Results

In the 1:10 scale model, we are primarily concerned with resonances below 500 Hz (50 Hz full-scale). Two such resonances are observed: one at 315 $\pm$ 20 Hz and one at 415 $\pm$ 10 Hz. The $\pm$ 10 and $\pm$ 20 Hz tolerances correspond to small changes in the model set-up. It is to be noted that these resonances are fairly sensitive to changes in the bottom and side spacing (especially for the m = 0 mode). The smaller the spacing, the higher the kinetic energy and, therefore, the lower the frequency.

The lower resonance is found to be the lowest m = 0 mode; the resonance at 415 Hz was identified as the lowest m = 1 mode. Another resonance, identified as the m = 2 mode, was located at 745 $\pm$ 10 Hz. Note that the reading from the graphic level recorder does not give the resonance frequency precisely (especially at higher frequencies). The numbers given for the resonances are found more exactly with an oscilloscope and frequency counter.

Sample frequency-response plots are displayed in Fig. 56. The three plot segments correspond to different microphone positions.

Comparison with Theory - Conclusions

The table below shows the important theoretical calculations and experimental results. The experimental data is adjusted to full scale (frequencies are divided by 10).

Mode	Resonance Frequency	
	Experimental	Theoretical (upper limit)
m = 0	31.5 $\pm$ 2 Hz	40.5 Hz
m = 1	41.5 $\pm$ 1 Hz	43.2 Hz
m = 2	74.5 $\pm$ 1 Hz	80.5 Hz

Not only does the theory furnish an upper limit to the actual resonance frequency, but it also provides a result which is fairly close to the upper limit. Moreover, careful analysis of the frequency plots with the microphone in positions A through G indicates that the experimental mode shape is in good qualitative agreement with the theoretical prediction.

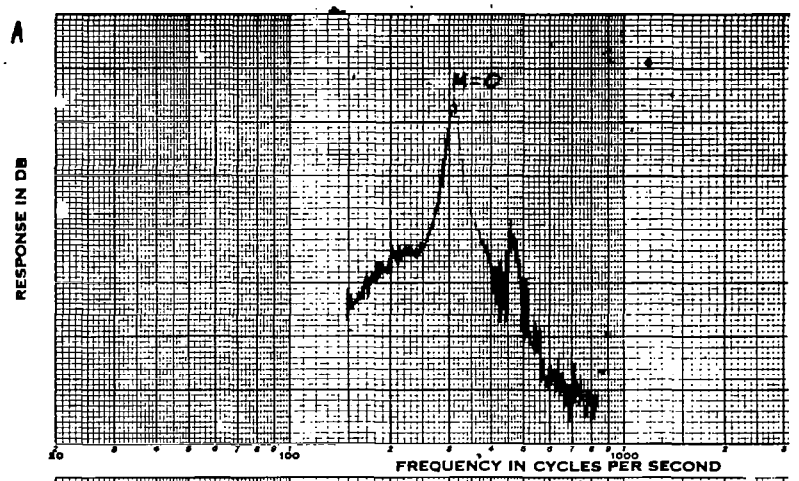

(a)

FREQUENCY PLOT, MICROPHONE AT POSITION A

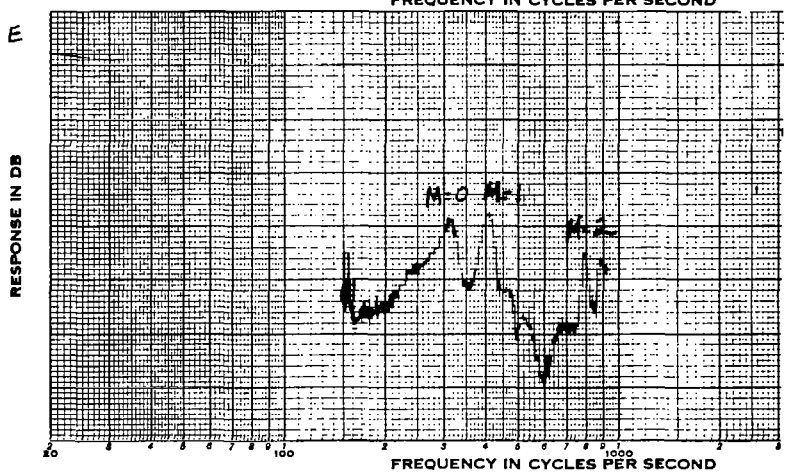

(b)

FREQUENCY PLOT, MICROPHONE AT POSITION E

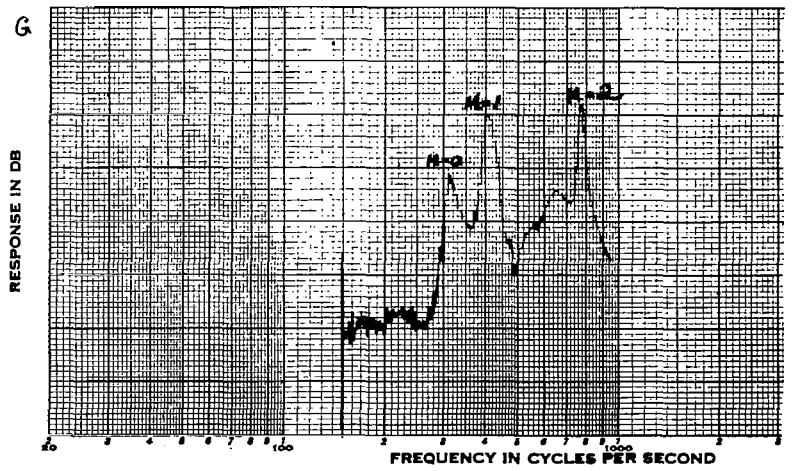

(c)

FREQUENCY PLOT, MICROPHONE AT POSITION G

FIG. 56 FREQUENCY - RESPONSE PLOTS OF INTERSPACE PRESSURE

The above provides reasonably conclusive evidence that there exist two natural acoustic resonance frequencies below 50 Hz in the interspace region of the acoustic model of the Apollo CM. One of these is of "longitudinal" character; the other is an azimuthal resonance. If excited, these resonances may not be damped out. There exists, therefore, the possibility of noise-reduction problems at these frequencies unless effective methods of low-frequency sound absorption are employed.

RECOMMENDATIONS FOR THE DESIGN AND CONSTRUCTION OF AN ACOUSTIC MODEL OF THE APOLLO CM

Introductory Remarks

The preceding analyses have provided a basis for suggesting the primary modes of sound transmission in the Apollo CM at low frequencies. In this section, we describe a simplified model of the Apollo CM that will simulate its acoustical performance. Its detailed construction and structural configuration is quite different from the actual CM. The purposes of the deviations from the original are:

1. to make it simpler to change certain structural and acoustical features of the model
2. insofar as possible, to make the model lighter and easier to fabricate
3. to allow a testing of the conclusions of this report with regard to the relative importance of flexural vs membrane rigidity and resonance effects
4. to reduce the cost of model construction

Selection of the Skin Thicknesses

A simplified diagram of the Apollo CM is shown in Fig. 13. It is formed of sandwich panels with dimensions and materials as indicated in Table I. We believe that this structure can be modeled with homogeneous steel and aluminum panels applying the following principles:

1. Steel sandwiches are replaced by steel plates, aluminum sandwiches are replaced by aluminum plates, except as noted below.

2. Membrane-rigidity-controlled elements are replaced by homogeneous plates of thickness 2t = H. In this case, steel (aluminum) plates may be replaced by aluminum (steel) plates if the thicknesses are changed inversely as the ratio of Young's modulus.

3. Bending-rigidity-controlled elements are replaced by homogeneous plates of thickness $H = h\,(6t/h)^{1/3}$. In this case, steel (aluminum) plates may be replaced by aluminum (steel) plates if the thicknesses are changed inversely as the ratio of Young's modulus.

4. Resonant effects in the structure are not modeled; it is not possible to model simultaneously flexural rigidity and wavespeed of a sandwich with a homogeneous plate. This makes properties such as core density and ablating material density and damping unimportant.

5. Resonant effects in the acoustic spaces, particularly in the space between the shells, are probably affected by the "Q-felt." The model should be designed so that this space can be filled with a material of similar flow resistance.

Our analyses in Chapter III suggest that sections 4 and 6 display flexural rigidity control in their NR behavior while sections 1, 2, 3, 5, 6, 7, 8 and 9 are membrane-controlled. They are to be modeled, therefore, according to the rules in items 2 and 3 above. A list of appropriate homogeneous panels corresponding to the sandwich panels in Table I is given in Table VI.

Inter-Shell Connections

The connections between the shells of the model should be made between rigid joining sections. A suggested arrangement is shown in Fig. 57. A rigid frustrated conical plug "A" is used as a structural termination at the apex of the outer canister. This mounts to a supporting ring on the hatch section of the inner canister by three vibration mounts. The combined stiffness of these mounts should be less than that of the ledge-hatch combination;

$$3K_m < \pi a^2/c_{4,6} \qquad (163)$$

TABLE VI

HOMOGENEOUS PANELS CORRESPONDING TO SANDWICH PANELS IN TABLE I

Section	Material	Thickness H (mils)	Controlling Behavior
1	steel*	16	membrane
2	"	16	"
3	"	120	"
4	aluminum	780	bending
5	"	20	membrane
6	"	397	bending
7	"	40	membrane
8	"	32	"
9	"	66	"

*If aluminum skins are substituted for steel, increase thickness H by factor of 3.

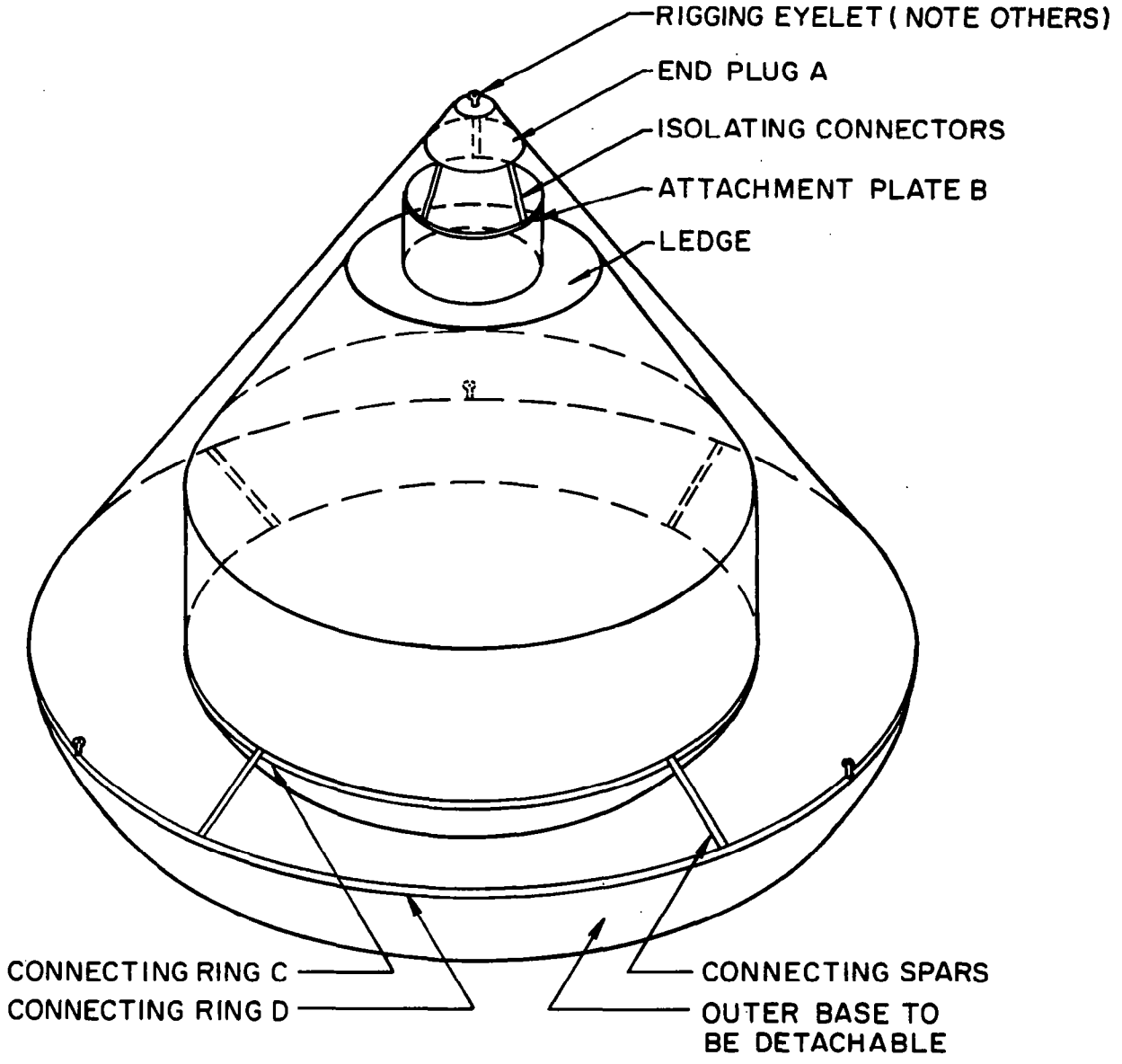

FIG. 57 ATTACHMENT POINTS AND STRUCTURAL CONNECTIONS IN CM ACOUSTIC MODEL

where K_m is the individual mount stiffness, a is the ledge radius (17.8 in.) and $C_{4,6}$ is the acoustic compliance of the ledge-hatch combination as determined in Chapter III. This requires

$$K_m \lesssim 0.25 \text{ lb/in.} \qquad (164)$$

This is a very soft mount, and cannot be relied on to support any weight of the inner canister. It is essentially a guide rod that keeps the inner canister from rocking.

The lower connection is made between mounting rings C and D on the inner and outer shells. These rings can be fairly heavy. Ring C is placed at the junction of the spherical segment base of the inner shell and its lower cylindrical segment. Ring D is placed where the spherical segment base of the outer shell joins its conical section. They can be jointed by relativel stiff spars, sufficiently rigid so as not to have resonances below 100 Hz or so.

Modeling the Q-Felt

The prototype Apollo CM uses a dense glass fiber blanket for thermal insulation within the space between the two shells. We have investigated the possible acoustic effects that such a blanket would have. As presently envisioned, the blanket is formed from Owens Corning PF-105-700 Fiberglas. It has an 0.00005 in. diam. fiber and is compressed to a density of 6 lb/ft^3. Glass fiber of this fiber diameter and density has a flow resistance of approximately 3000 rayls/in. (Ref. 34). Since this is much larger than the acoustic impedance of the sound wave, any material that can be placed in the space between the shells that will occupy the same volume that the Q-felt does, will probably be an acceptable substitute. Some candidates are balsa wood and closed-cell polystyrene foam.

RECOMMENDATIONS FOR ADDITIONAL STRUCTURAL MODELS FOR TESTING NR PREDICTION METHODS

Introduction

In developing the methods for predicting low-frequency NR presented in this report, we have sought to delineate classes or primary forms of structural and acoustic behavior. Our hope is to assign sound transmission characteristics to each, and to treat a complex structural configuration by reducing its behavior to the appropriate set of forms. Some of these forms of behavior (quasi-static deflection, interspace resonances and vent-shell-internal volume resonance) have been examined theoretically and experimentally. Others, such as structural resonance, and the effect of bridging elements between the shells, have not been so fully examined. The purpose of the models described here is to suggest ways of analyzing experimentally other potentially significant forms of behavior.

In this section we shall specify wall constructions which should be useful for studying noise transmission due to structural discontinuities and bridging connections between shells. Appropriate structural parameters, such as wall thicknesses, dimensions, etc., are suggested on the basis of analytical studies of these effects.

Non-Uniform Wall Structures

The quasi-static compliance calculations derived in Chapter III assume that the shells have uniform properties throughout. Actual structures have hatches, stiffeners, bulkheads, etc., which locally stiffen or weaken the shell.

The first recommended test structure is shown in Fig. 58. This structure, which is very much like the cylinder discussed earlier in this chapter, would be designed, however, to have a fundamental acoustic resonance at 100 Hz. This resonance frequency requires that the cylinder be 5 ft long. Let us choose a 3-ft diameter and a skin thickness of 0.032 in. The fundamental structural resonance will be

$$f_{min} = 13.5\ (H/a)^{1/2}\ f_a = 57\ \text{Hz} \qquad (166)$$

if the cylindrical shell edges are simply supported.

If the cylindrical skin is attached to rigid end pieces by a suitable clamping arrangement, there should be no noticeable effect on tne NR of this cylinder due to resonance as stiffening ribs are added.

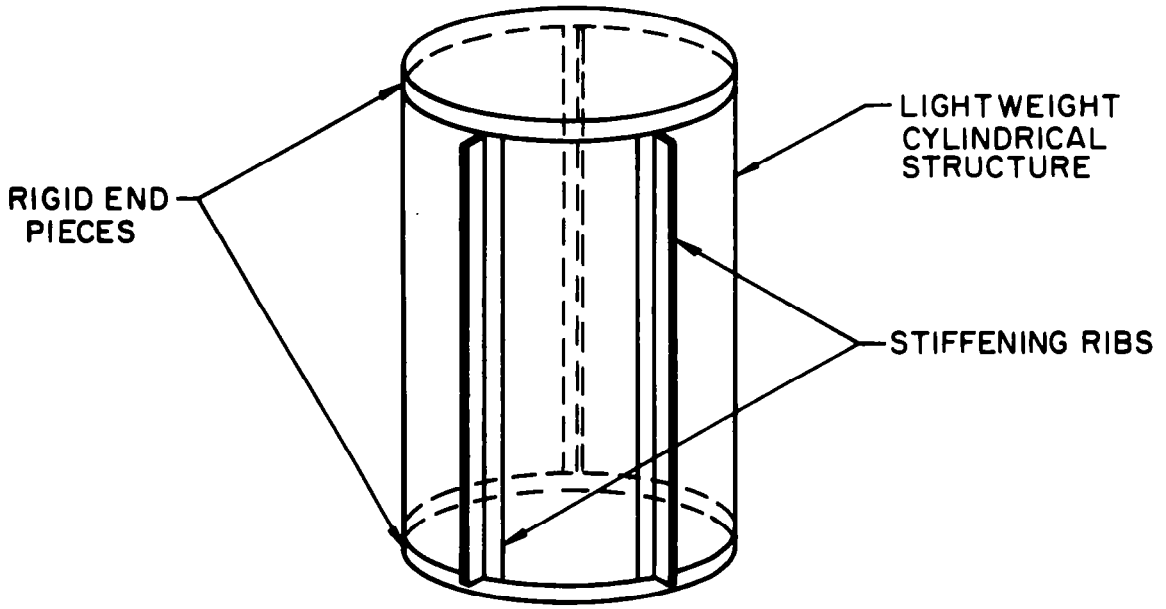

FIG. 58 CYLINDER WITH AXIAL STIFFENERS TO TEST EFFECT OF STRUCTURAL INHOMOGENEITY

Let us now suppose that the cylinder wall is not connected to the end pieces. However, the edges must be sealed, e.g. with heavy tape, to keep air from entering the contained volume. The lowest resonance of the cylinder now corresponds to the condition where the circumference is a complete bending wavelength, or to $\lambda = 2\pi a$. The lowest structural resonance in this case is

$$f_{min} = \frac{2500}{\lambda^2(ft)} H \text{ (in.)} \approx 1 \text{ Hz} \qquad (166)$$

The lowest structural resonance frequency is greatly reduced by removing the restraint at the end pieces. The addition of ribs will cause some of these low-frequency modes to become volume-pumpers and reduce the NR. The added ribs should be sufficiently rigid so that their first resonance is 100 Hz or higher.

Effect of Bridging Connections

When direct mechanical connections are made in double-shell structures, an additional path for sound transmission is available. In Fig. 59, an experimental arrangement is shown that illustrates a method of demonstrating these effects. Three connecting spars are suggested: "A" is a connection between points on the curved sections, "B" is a connection between "resistive" positions, and "C" is a spar between positions of very high impedance. Only one spar would be involved in a single experiment.

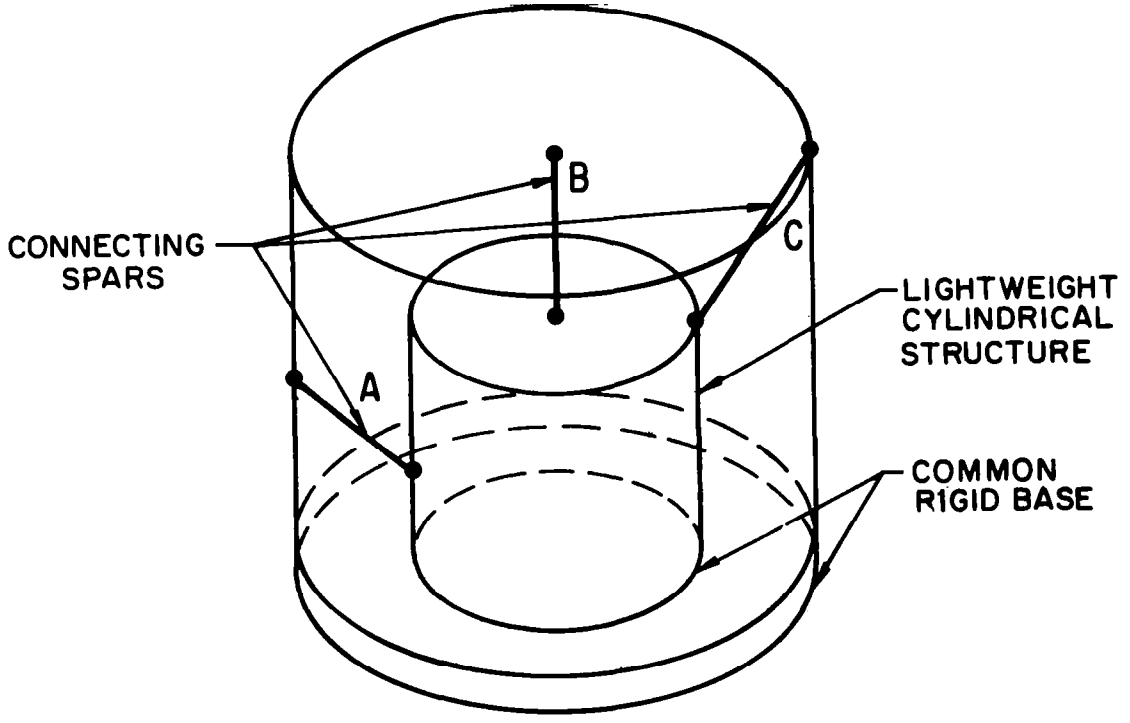

FIG. 59 DOUBLE CANISTER STRUCTURE WITH CONNECTING SPARS AT LOCATIONS OF VARYING MECHANICAL IMPEDANCE TO TEST EFFECT OF BRIDGING ELEMENTS

In Fig. 60 we show an equivalent circuit that aids us in evaluating the effect of connections on NR. The source velocity v_s is the unloaded skin vibration amplitude on the outer shell in the absence of the spar. The point impedance of this shell is Z_{oc}, compliant for spar "A," and resistive for spar "B." Z_{ic} is a similar impedance for the inner cylinder. The translational impedance of the spar, Z_{spar}, will probably be its mass reactance at frequencies below any resonance of the spar itself. The appropriate impedances are:

$$\left.\begin{aligned} Z &= 0.12 \frac{EH^3}{a^2 f} i \quad \text{(curved cylinder) (Ref. 34)} \\ Z &= 2.2 \frac{EH^2}{c_\ell} \quad \text{(flat panels) (Ref. 23)} \end{aligned}\right\} \quad (167)$$

$$Z_{spar} = - i\omega M_{spar}$$

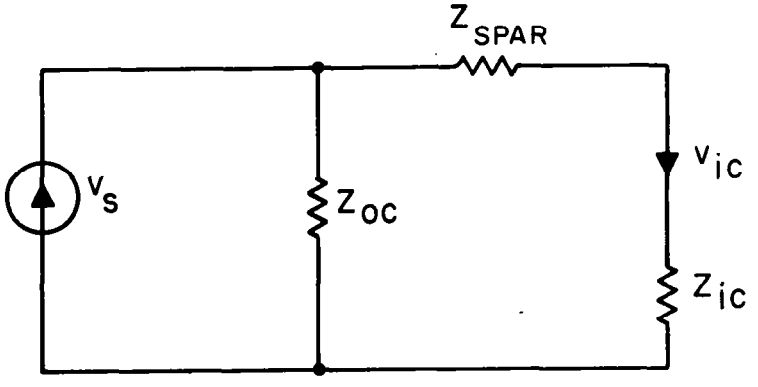

FIG. 60 EQUIVALENT CIRCUIT FOR DERIVING SPAR MOTION

Using the general relation

$$v_{ic} = \frac{Z_{oc}}{Z_{oc} + Z_{ic} + Z_{spar}} \qquad (168)$$

and the relations above for the impedances, the velocity can be computed. The point motion v_{ic} of the attachment to the inner cylinder can be converted to volume velocity from Heckl's analysis (Ref. 33) for flat plates, and from Roark (Ref. 31) for the curved section. It must be remembered that this volume velocity will be coherent with that existing in the absence of the spar. The combined effect of both components of volume velocity must be considered to evaluate the NR.

Some suggested experimental parameters are:

Outer cylinder: ℓ = 48 in., a = 18 in., H = 0.032 in.

Inner cylinder: ℓ = 42 in., a = 15 in., H = 0.032 in.

The spar should be long enough to reach between the shells and heavy enough to satisfy the condition $Z_{spar} > Z_{oc}$, Z_{ic} at the upper range of the frequency of interest (50 Hz in this case). At lower frequencies for which $Z_{spar} \approx Z_{oc}$, Z_{ic} interesting effects should develop.

CHAPTER VII

IMPLICATIONS FOR DESIGN

CHOICE OF STRUCTURAL GEOMETRY

We saw in Chapters III and VI that the choice of structural geometry can have a very significant effect on the low-frequency noise reduction. The flat structural segments have a compliance which is controlled by flexural stiffness, whereas membrane stresses tend to dominate the behavior of curved structural segments. Generally speaking, membrane-controlled compliances are significantly more resistant to volume deflection than are flexural elements. In the case of the Command Module, the inner-shell sound transmission was primarily dominated by the flat ledge section of the hatch. As a result, only 10 dB of NR was achieved by the inner shell, whereas the outer shell, which had no flat segments, had a noise reduction of 40 dB.

In Chapter III analyses are given which suggest when membrane control of curved structures will be obtained. In the case of the cylinder, the length must be somewhat greater than the geometric mean of the radius and the wall thickness of the cylinder. For the case of a spherical shell segment, the depth of the segment must be sufficiently large in comparison with the radius of curvature. These criteria are only general, however, and the detailed behavior will depend on the particular situation. In cases where doubt is anticipated, an experimental analysis of typical systems is likely to be more effective in leading one to an appropriate conclusion than a complex series of detailed calculations.

The general axisymmetric shape of space vehicles is chosen, of course, for constructional and aerodynamic reasons. It happens, however, that this geometry also favors high values of low-frequency NR. As we have discussed, this geometry tends to discriminate against volume-pumping modes.

DISCRIMINATION AGAINST STRUCTURAL RESONANCES

We have seen in Chapters III and VI the deleterious effects that structural resonances can have on the low-frequency noise reduction. Flat segments can have structural volume-pumping resonances at relatively low frequencies. If a conical or cylindrical shell is interrupted by longitudinal ribs, some of its lower-frequency resonances can also become volume-pumpers. Volume-pumping is important as long as the inner contained volumes are stiff — i.e., below their first acoustical resonance.

There are two methods by which one can avoid such structural resonance effects. One way is to select structural configurations and parameters so that the lowest resonance frequencies occur above the first acoustic mode of the contained space. This can be done by selecting panel sizes and thicknesses so that the lowest panel mode of the structure is shifted to higher frequencies.

The other way consists of adding damping to the structures, but this has marginal practical utility. An increase in the structural damping by a factor of 10 can result in an increase in the noise reduction by 10 dB in a band near the offending resonance. Increases in damping of this order, however, are not usually achieved easily. If the structure is formed from sandwich panels, then additional applied damping usually involves a substantial weight penalty. It is conceivable that the structural panels could incorporate the damping, using a core material that has a high loss factor. This is perhaps the best hope for useful amounts of structural damping, but may involve considerable development effort.

Other kinds of structural resonances that can occur at low frequencies include the resonances of mass elements attached to curved sections of structure. The point load impedance of a curved structure at low frequencies is a stiffness reactance (as given in Chapter IV). This stiffness can act with an attached mass to result in a volume-displacing resonant vibration.

COMBATTING THE EFFECTS OF ACOUSTIC RESONANCE

The procedures used to minimize the effects of acoustic resonance on sound transmission at low frequencies generally parallel those for combatting structural resonance. They include changing the geometry so that the undesirable resonances occur at higher frequencies and adding damping material (acoustic absorption) so that the resonance is attenuated.

Roughly speaking, the condition for critical damping of acoustic modes is that the total flow resistance in the acoustic path be ρc, the characteristic impedance of the acoustic medium. If the resistance is substantially smaller than this, the absorption will not be so effective as it could be. If it is substantially larger than this, the fluid will avoid the absorption material by flowing around it, if alternate paths are available.

We saw in Chapter III that double-walled shell structures can have low-frequency resonances if long path lengths are allowed. These resonances should be avoided, either by blocking the flow path so that the resonances are moved to higher frequencies, or by providing appropriate acoustic absorption in the interspace so that resonant modes are damped out. We saw that the thermal-insulating Q-felt is not a good acoustic absorber, since its flow resistance is very high compared with the acoustic impedance of the medium. However, in the Apollo CM the Q-felt may block the flow path sufficiently so that the low-frequency modes do not occur.

We also saw in Chapter III that low-frequency resonances may be associated with the venting system, in combination with portions of or all of the interspace volume. The effect of this resonance can be eliminated by designing the vent so that it has sufficient acoustic mass (constriction) for its resonances to occur at very low frequencies. A second approach is to introduce a flow resistance in the path, so that the resonance is critically damped. Vent damping should not cause significant vent operation problems, since the periods of the resonances of concern are of the order of one-tenth of a second, and this generally is much shorter than the time which the venting system needs to readjust the interspace pressure.

GENERAL COMMENTS

In a sense, design for good low-frequency noise reduction involves much the same considerations as design to contain the pressure in the spacecraft. The basic compliance analysis presented in Chapter III is closely related to the pressure vessel analysis that is required for predicting the structural integrity of the vehicle. There are subtleties in the acoustic design, however, that are not present in the mechanical structure design. These have to do primarily with the occurrence of structural and acoustic resonances that can severely diminish the NR provided by the structure. It is these resonances and their associated effects that we have tried to catalog and analyze in the discussions of this report.

The transmission of sound is a complex problem. At all times, it is worth reconsidering the inclusion of experimental analyses of potential designs in any spacecraft development program. Acousticians, faced with the problems of predicting the acoustical behavior of rooms and the sound transmission properties of walls, learned long ago to couple their calculations with model studies and well-thought-out experiments. A similar development in the field of space vehicle design would result in a great improvement of our understanding of the basic processes at work in such structures and perhaps result in a significant improvement of the acoustical and vibrational behavior of these systems.

NOTES AND REFERENCES

1. Goldman, D. E.; and von Gierke, H. E.: Effects of Shock and Vibration on Man. Chapter 44 of Shock and Vibration Handbook, Vol. III. McGraw-Hill Book Co., Inc., 1961. Also J. M. Pickett: Low-Frequency Noise and Methods for Calculating Speech Intelligibility. J. Acoust. Soc. Am., Vol. 31, No. 9, Sept. 1959, pp. 1259 ff.

2. Carter, N. L.; and Kryter, K. D.: Masking of Pure Tones and Speech. Journ. Aud. Res., Vol. 2, No. 1, January 1962, pp. 66-98.

3. Wiener, F. M.: Rocket Noise of Large Space Vehicles. Paper presented at 4th ICA Congress (Copenhagen, Denmark), August 1962.

4. Beranek, L. L.: Acoustics. McGraw-Hill Book Co., Inc., 1954, p. 324.

5. Morse, P. M.: Vibration and Sound, 2nd Ed., McGraw-Hill Book Co., Inc., 1948, p. 384.

6. Beranek, L. L.: The Transmission and Radiation of Acoustic Waves by Solid Structures. Noise Reduction, L. L. Beranek, Ed., McGraw-Hill Book Co., Inc., 1960, p. 287.

7. Lyon, R. H.: Noise Reduction of Rectangular Enclosures with One Flexible Wall. J. Acoust. Soc. Am., Vol. 35, No. 11, November 1963, pp. 1791-1797.

8. Eichler, E.: Thermal Circuit Approach to Vibrations in Coupled Systems and the Noise Reduction of a Rectangular Box. J. Acoust. Soc. Am., Vol. 37, No. 6, June 1965, pp. 995-1007.

9. Reference 4, p. 129.

10. Reasonably rapid pressure variations are assumed so that the gas compression occurs essentially isentropically. A somewhat different constant applies for other compression processes. If the compression were isothermal, γ would be replaced by unity.

11. Roark, R. J.: Formulas for Stress and Strain. McGraw-Hill Book Co., Inc., 1954, p. 194, Case 1.

12. Reference 11, p. 195, Case 6.

NOTES AND REFERENCES (continued)

13. Timoshenko, S.: Theory of Plates and Shells. McGraw-Hill Book Co., Inc., 1940, pp. 399 ff.

14. Reference 13, pp. 476 ff.

15. Shaffer, B. W.: Supplementary Notes on Discontinuity Analysis of Shells. Allegany Ballistics Laboratory, Cumberland, Maryland, August 1958.

16. Reference 13, pp. 370 ff.

17. Wang, C. T.: Applied Elasticity. McGraw-Hill Book Co., Inc., 1953, pp. 326 ff.

18. Reference 13, p. 371.

19. Reference 11, p. 194, No. 1, and p. 197, No. 12.

20. Reference 13, pp. 393, 399.

21. Reference 7, Equation (2.1).

22. Reference 4, p. 93.

23. Smith, P. W., Jr.; and Lyon, R. H.: Sound and Structural Vibration. NASA CR-160, prepared under Contract NASw-788 by Bolt Beranek and Newman Inc., March 1965.

24. Analytical Procedure for Determining Random Load Acting on a Spacecraft Due to a Primary Random Load Acting on an Exterior Structure. First Quarterly Report, Contract NAS5-9601. Bolt Beranek and Newman Inc., 14 June - 31 August, 1965.

25. Maidanik, G.: Response of Ribbed Panels to Reverberant Acoustic Fields. J. Acoust. Soc. Am., Vol. 34, No. 6, June 1962, pp. 809-826.

26. Macduff, J. N.; and R. P. Felgar: Vibration Design Charts. Paper No. 56-A-75, Amer. Soc. Mech. Engrs., November 1956; also, Vibration Frequency Charts, Machine Design, February 7, 1957.

27. Heckl, M.: Vibrations of Point Driven Cylindrical Shells. J. Acoust. Soc. Am., Vol. 34, No. 10, October 1962, pp. 1553-1557.

NOTES AND REFERENCES (continued)

28. The authors are indebted to Dr. J. E. Manning for the essentials of the following discussion.

29. Reference 4, p. 132.

30. Salmon, V.: A New Family of Horns. J. Acoust. Soc. Am., Vol. 17, No. 3, January 1946, pp. 212-218.

31. Temple, G.; and Bickley, W. G.: Rayleigh's Principle. Dover Publications, Inc., 1956.

32. Reference 31, pp. 46-47.

33. Reference 6, Fig. 12.5, p. 253.

34. Reference 11, p. 270.

35. Heckl, M.; and Rathe, E. J.: Relationship Between the Transmission Loss and the Impact-Noise Isolation of Floor Structures. J. Acoust. Soc. Am., Vol. 35, No. 11, November 1963, p. 1825.

"The aeronautical and space activities of the United States shall be conducted so as to contribute . . . to the expansion of human knowledge of phenomena in the atmosphere and space. The Administration shall provide for the widest practicable and appropriate dissemination of information concerning its activities and the results thereof."

—NATIONAL AERONAUTICS AND SPACE ACT OF 1958

NASA SCIENTIFIC AND TECHNICAL PUBLICATIONS

TECHNICAL REPORTS: Scientific and technical information considered important, complete, and a lasting contribution to existing knowledge.

TECHNICAL NOTES: Information less broad in scope but nevertheless of importance as a contribution to existing knowledge.

TECHNICAL MEMORANDUMS: Information receiving limited distribution because of preliminary data, security classification, or other reasons.

CONTRACTOR REPORTS: Technical information generated in connection with a NASA contract or grant and released under NASA auspices.

TECHNICAL TRANSLATIONS: Information published in a foreign language considered to merit NASA distribution in English.

SPECIAL PUBLICATIONS: Information derived from or of value to NASA activities. Publications include conference proceedings, monographs, data compilations, handbooks, sourcebooks, and special bibliographies.

TECHNOLOGY UTILIZATION PUBLICATIONS: Information on technology used by NASA that may be of particular interest in commercial and other nonaerospace applications. Publications include Tech Briefs; Technology Utilization Reports and Notes; and Technology Surveys.

Details on the availability of these publications may be obtained from:

SCIENTIFIC AND TECHNICAL INFORMATION DIVISION

NATIONAL AERONAUTICS AND SPACE ADMINISTRATION

Washington, D.C. 20546